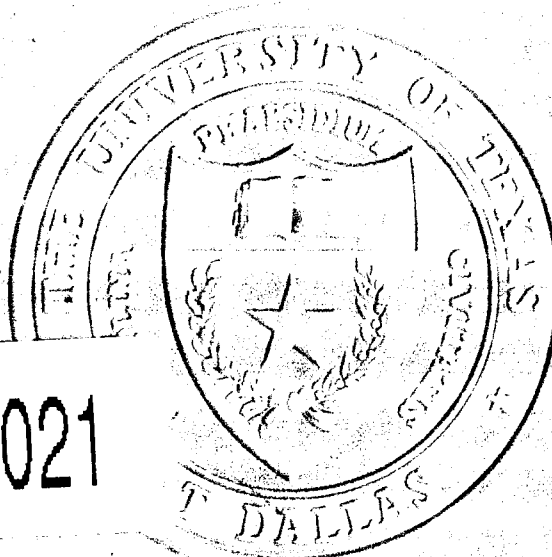# CENTER FOR APPLIED OPTICS

Spectral Inverse Scattering Theory for Dielectric Media: Application to Optical Devices

Final Report 1991–94
submitted to

Office of Naval Research

Lakshman S. Tamil
Principal Investigator

DTIC QUALITY INSPECTED 1

THE UNIVERSITY OF TEXAS AT DALLAS

Spectral Inverse Scattering Theory for Dielectric Media: Application to Optical Devices

Final Report 1991–94
submitted to

Office of Naval Research

Lakshman S. Tamil
Principal Investigator

Erik Jonsson School of Engineering and Computer Science

and

Center for Applied Optics

University of Texas at Dallas, Richardson, TX

December 1994

REPORT DOCUMENTATION PAGE

Public reporting burden for this collection of information is estimated to average 1 hour per response, including the time for reviewing instructions, searching existing data sources, gathering and maintaining the data needed, and completing and reviewing the collection of information. Send comments regarding this burden estimate or any other aspect of this collection of information, including suggestions for reducing this burden, to Washington Headquarters Services, Directorate for Information Operations and Reports, 1215 Jefferson Davis Highway, Suite 1204, Arlington, VA 22202-4302, and to the Office of Management and Budget, Paperwork Reduction Project (0704-0188), Washington, DC 20503.

1. AGENCY USE ONLY (Leave blank)	2. REPORT DATE December 10, 1995	3. REPORT TYPE AND DATES COVERED Final Report 1991–1994

4. TITLE AND SUBTITLE Spectral Inverse Scattering Theory for Dielectric Media: Application to Optical Devices	5. FUNDING NUMBERS N0014-92-J-1030
6. AUTHOR(S) Lakshman S. Tamil	

7. PERFORMING ORGANIZATION NAME(S) AND ADDRESS(ES) University of Texas at Dallas 2601 North Floyd Road Richardson, TX 75083-0688	8. PERFORMING ORGANIZATION REPORT NUMBER UTD/CAO/35

9. SPONSORING/MONITORING AGENCY NAME(S) AND ADDRESS(ES) Office of the Naval Research 800 N. Quincy Street Arlington, VA 22217-5000	10. SPONSORING/MONITORING AGENCY REPORT NUMBER

11. SUPPLEMENTARY NOTES

12a. DISTRIBUTION/AVAILABILITY STATEMENT UNLIMITED	12b. DISTRIBUTION CODE

13. ABSTRACT (Maximum 200 words)

Optical devices and circuits can be synthesized from specified transmission characteristics using the methods of inverse scattering. Both analytical and numerical inverse scattering techniques that have been developed to synthesize optical devices and circuits are discussed. Large-scale guided-wave structures such as optical logic gates and optical interconnects can be synthesized using the techniques discussed here. Finite difference based frequency-domain analysis technique has been used to verify the results obtained by these inverse scattering techniques.

14. SUBJECT TERMS optical waveguides, EM theory, inverse scattering theory, optical interconnects, multi-layer optical integrated circuits	15. NUMBER OF PAGES 108
	16. PRICE CODE

17. SECURITY CLASSIFICATION OF REPORT Unclassified	18. SECURITY CLASSIFICATION OF THIS PAGE. Unclassified	19. SECURITY CLASSIFICATION OF ABSTRACT Unclassified	20. LIMITATION OF ABSTRACT UL

Table of Contents

Name and Address of the Institution	**University of Texas at Dallas** 2601, N. Floyd Road Richardson, TX 75080 (non-profit educational institution)
Title of the Proposal	**Spectral Inverse Scattering Theory for Dielectric Media: Application to Optical Devices**
Fund Number	N0014-92-J-1030
Duration	Oct. 1991- Sept. 1994
Principal Investigator	**Dr. Lakshman S. Tamil** Erik Jonsson School of Engineering P.O. Box 830688, BE 28 Richardson, TX 75083-0688 (214) 690-2197 (phone) (214) 690-2813 (fax) laxman@utdallas.edu (email)
Contact Person	Dr. Marianne Woods University of Texas at Dallas P.O. Box 830688, FN 3.1 (214) 690-2313
Date of Submission	December 1994

PREFACE

This report summarizes the research carried out under the Office of the Naval Research grant # N0014–92–J–1030 during the period 1991–94.

The tasks accomplished are: (1) Synthesis and Analysis of optical waveguides with prescribed TE and TM modes; (2) development of computer program based on Darboux transform to create refractive index for waveguides with prescribed propagation constants; (3) development and testing of direct scattering solver to analyze optical waveguides; (4) analysis of truncated permittivity profile to form optical guiding structures; (5) development of inverse scattering theory for the design of planar optical waveguides with same propagation constants for different frequencies; (6) Analysis of coupling in multilayered waveguides using inverse scattering techniques; (7) modeling and developing inverse scattering theory for guided wave optical interconnects; and (8) studies on Levinson's theorem to estimate the number of propagating modes in a waveguide.

Seventeen journal articles have been published during the period 1991–1994 based on the research carried out on this project. Two Ph.D. dissertations and three M.S. theses were carried out under this grant. Reprint and Preprint of selected research articles are attached in the appendix.

The award of this grant has been of great help to me and my students in carrying out our research and is gratefully acknowledged.

Richardson, TX

Dec. 10, 1994

Lakshman S. Tamil

Principal Investigator

1

DESCRIPTION OF RESEARCH CARRIED OUT

1. Introduction

The conventional method of designing optical guided-wave devices or structures is to assume a refractive index profile and solve the governing differential equation to find the various propagating modes and their propagation characteristics. If the propagation characteristics do not meet the expected behavior, the refractive index is changed and the propagation characteristics are again evaluated; this is repeated until the expected propagation behavior of the modes are obtained. This being an iterative procedure, it is time consuming. Also, to obtain certain arbitrary transmission characteristics, one may not be able to guess the correct initial refractive index profile.

The procedure discussed in this report as opposed to the direct method, starts with the required propagation characteristics of the guided-wave device and obtains the refractive index profile as the end result. We achieved this by transforming the wave equation for both the TE and TM modes in the planar waveguide to a Schrodinger type equation and then applying the inverse scattering theory as formulated by Gelfand, Levitan and Marchenko [1–2]. The inverse scattering problem encountered here has a direct analogy to the inverse scattering problem of the quantum mechanics. The refractive index profile of the planar waveguide is contained in the potential of the Schrodinger type equation and the propagating modes are the bound states of the quantum mechanics [3]. In general the guided-wave devices are based on channel waveguides, however we have considered here planar waveguides for mathematical simplicity. The theory presented here can be extended to channel waveguide structures though it is non-trivial.

2. Physical Model of a Planar Waveguide

The wave equations for the inhomogeneous planar optical waveguides can be derived from the Maxwell's equations. If we take z as the propagation direction and let ω represent the frequency of laser radiation, we have the following wave equations for one dimensional inhomogeneous planar waveguides [4]

$$\frac{d^2}{dx^2} E_y(x) + \left[k_0^2 \epsilon(x) - \beta^2 \right] E_y(x) = 0 \tag{1}$$

for TE modes and

$$\frac{d^2}{dx^2} E_x(x) + \frac{d}{dx} \left[\frac{1}{\epsilon(x)} \frac{d\epsilon(x)}{dx} E_x(x) \right] + \left[k_0^2 \epsilon(x) - \beta^2 \right] E_x(x) = 0 \tag{2}$$

for TM modes. The planar waveguide we are considering here has a refractive index which varies continuously in the x direction. For the planar optical waveguide shown in Fig. 1, our problem is to find the refractive index profile function in the core for a set of specified propagation constants.

2

We assume that this planar waveguide has a refractive index profile guiding N modes. The propagation constants $\{\beta_n\}$ are $k_0 n_1 > \beta_1 > \beta_2 > ...\beta_N \geq k_0 n_\infty$, in which n_∞ is the value of $n(x)$ as $x \to \infty$ and $n_1 = \sup n(x)$. Designing an optical waveguide is analogous to the inverse problem encountered in quantum mechanics. We are trying to get the potential function from the given bound states and scattering data. The wave equation for the TE modes can be easily transformed to an equivalent Schrodinger equation

$$\frac{d^2}{dx^2} E_y(x) + \left[k^2 - V(x)\right] E_y(x) = 0 \tag{3}$$

by letting

$$V(x) = -k_0^2 \left[n^2(x) - n_\infty^2\right] \tag{4}$$

and

$$k^2 = -\kappa_n^2 = -\left(\beta_n^2 - k_0^2 n_\infty^2\right) . \tag{5}$$

We can see in our case the potential function $V(x)$ is continuous and $V(x) \to 0$ as $\mid x \mid \to \infty$. The TE mode cases have been solved by Yukon and Bendow [5] and Jordan and Lakshmanasamy [6].

We now need to transfer the wave equation for the TM modes to Schrodinger type equation to apply the inverse scattering method. In Eq. (2), the first derivative of E_x can be eliminated if we let $E_x(x) = \epsilon^{-1/2}(x)\Phi(x)$. The wave equation then becomes

$$\frac{d\Phi^2}{dx^2} + \left[\frac{1}{2\epsilon(x)}\frac{d^2\epsilon(x)}{dx^2} - \frac{3}{4\epsilon^2(x)}\left(\frac{d\epsilon(x)}{dx}\right)^2\right]\Phi + \left(k_0^2\epsilon(x) - \beta^2\right)\Phi = 0 . \tag{6}$$

We are now able to obtain the equivalent Schrodinger equation

$$\frac{d^2\Phi(x)}{dx^2} + \left[k^2 - V(x)\right]\Phi(x) = 0 \tag{7}$$

by setting the potential function as

$$V(x) = \frac{3}{4\epsilon^2(x)}\left(\frac{d\epsilon(x)}{dx}\right)^2 - \frac{1}{2\epsilon(x)}\frac{d^2\epsilon(x)}{dx^2} - k_0^2\left(\epsilon(x) - n_\infty^2\right) \tag{8}$$

and letting

$$k^2 = -\kappa_n^2 = k_0^2 n_\infty^2 - \beta_n^2 . \tag{9}$$

The TM mode case has been solved by Tamil and Lin [7].

3. Inverse Scattering Theory

The inverse scattering theory of Kay and Moses [8] provides us a way to obtain the potential from the reflection coefficient which characterizes the propagation properties of the planar waveguide. As the potential we defined vanishes at infinity, we can apply the Gelfand-Levitan-Marchenko (GLM) equation to solve our problem. Let us consider a time-dependent formulation of the scattering. We take the Fourier transform of Eq. (7) [the transform pairs are $\Phi(x,k) \Leftrightarrow \Psi(x,t)$ and $k \Leftrightarrow t$] to obtain

$$\frac{\partial^2}{\partial x^2}\Psi(x,t) - \frac{\partial^2}{\partial t^2}\Psi(x,t) - V(x)\Psi(x,t) = 0 \ , \tag{10}$$

in which t is the time variable with the velocity of light $c \equiv 1$. The incident plane wave is represented by the unit impulse

$$\Psi(x,t) = \delta(x-t) \ , \qquad x < 0 \ , \qquad t < 0 \ , \tag{11}$$

which will produce the reflected transient wave function

$$R(x+t) = \frac{1}{2\pi}\int\limits_{-\infty}^{\infty} r(k)e^{-ik(x+t)}dk + \sum_{n=1}^{N}A_n e^{-ik_n(x+t)} \ , \tag{12}$$

where $k^2 = -\kappa_n^2$ are the discrete eigenvalues of Schrodinger-type [Eq. (7)], $r(k)$ is the complex reflection coefficient, A_n are arbitrary constants normalizing the wave equation such that

$$\int\limits_{-\infty}^{+\infty} \Phi(x)\Phi^*(x)dx = 1 \ . \tag{13}$$

The reflected transient is produced only after the incident unit impulse has interacted with the inhomogeneous core of the optical waveguide and therefore

$$R(x+t) = 0 \qquad \text{for} \quad x+t \leq 0 \ . \tag{14}$$

A linear transform independent of k can now relate the wave amplitude $\Psi(x,t)$ in the core region with the wave amplitude $\Psi_0(x,t)$ in the exterior region

$$\Psi(x,t) = \begin{cases} \Psi_0(x,t) + \int\limits_{-x}^{x} K\left(x,\xi'\right)\Psi_0\left(\xi',t\right)d\xi' & x > 0 \\ \Psi_0(x,t) & x \leq 0 \end{cases} \ . \tag{15}$$

Here the exterior field is

$$\Psi_0(x,t) = \delta(x-t) + R(x+t) \ . \tag{16}$$

4

From physical consideration, since $\Psi(x,t)$ is a rightward moving transient

$$\Psi(x,t) = 0 \quad \text{for} \quad t < x \ . \tag{17}$$

Thus the kernel $K(x,t) = 0$, for $t > x$ and $K(x,t) = 0$ for $t \leq -x$. We substitute Eq. (16) into Eq. (15) and using Eqs. (14) and (17) yield the integral equation

$$K(x,t) + R(x+t) + \int_{-x}^{x} K\left(x,\xi'\right) R\left(\xi'+t\right) d\xi' = 0 \quad t < x \ . \tag{18}$$

By substituting Eqs. (15) into Eq. (10) the kernel $K(x,t)$ satisfies a differential equation of the same form as Eq. (10) provided the following conditions are imposed

$$K(x,-x) = 0 \ , \tag{19}$$

and

$$2\frac{d}{dx}K(x,x) = V(x) \ . \tag{20}$$

We now could see how the solution of the integral Eq. (18) for the function $K(x,t)$ can lead to the synthesis of optical waveguides.

4. Design Example 1: Zero Reflection Coefficient

The reflection coefficient characterizes the propagation properties of the guided-wave optical devices. The zero reflection coefficient characterizes a system with propagating modes only, whereas a non-zero reflection coefficient characterizes a system with both guided and non-guided modes. Let us first consider the special case of zero reflection coefficient [9]. We substitute Eq. (12) for $r(k) = 0$ in Gel'fand-Levitan-Marchenko equation [Eq. (18)] to obtain

$$K(x,t) + \sum_{n=1}^{N} A_n e^{\kappa_n(x+t)} + \sum_{n=1}^{N} A_n \int_{-\infty}^{x} K(x,\xi) e^{\kappa_n(t+\xi)} d\xi = 0 \ . \tag{21}$$

It is clear from the above equation that the solution for $K(x,t)$ should have the form [9]

$$K(x,t) = \sum_{n=1}^{N} f_n(x) e^{\kappa_n t} \ . \tag{22}$$

We substitute Eq. (22) into Eq. (21) produces a system of equations for $f_n(x)$:

$$A_n \sum_{\nu=1}^{N} \left(\frac{e^{(\kappa_\nu + \kappa_n)x}}{\kappa_n + \kappa_\nu} \right) f_\nu(x) + f_n(x) + A_n e^{\kappa_n x} = 0 \tag{23}$$

5

where $n = 1, 2, ...N$. This system can be conveniently written as

$$[A][f] + [B] = 0 \tag{24}$$

where [f] and [B] are column vectors with f_n, and $B_n = A_n \exp(\kappa_n x)$ respectively, and A is a square matrix with elements

$$A_{\nu n} = \delta_{\nu n} + A_\nu \left(\frac{e^{(\kappa_\nu + \kappa_n)x}}{\kappa_\nu + \kappa_n} \right) \tag{25}$$

in which $\delta_{\nu n}$ is a Kronecker delta. The solution for f is $f = -A^{-1}B$ and then from Eq. (22) $K(x, x) = E^T f$ where E is the column vectors with element $E_n = \exp(\kappa_n x)$ and T denotes transpose. Now,

$$\frac{d}{dx} A_{\nu n} = A_\nu e^{(\kappa_\nu + \kappa_n)x} = B_n E_n \tag{26}$$

and so

$$K(x, x) = E_n f_n = -E_n A_{\nu n}^{-1} B_\nu = A_{\nu n}^{-1} \frac{d}{dx} A_{n\nu} \tag{27}$$

when written with subscript notation and the summation convention. The $K(x, x)$ given by Eq. (22) can be recognized in the form

$$K(x, x) = \text{tr} \left(A^{-1} \frac{dA}{dx} \right) = \frac{d}{dx} \ln(\det A) \tag{28}$$

and therefore the potential $V(x)$ according to Eq. (20) is

$$V(x) = -2 \frac{d^2}{dx^2} \ln(\det A) . \tag{29}$$

Given N modes with desired propagation constants, we can obtain a potential function as given by Eq. (29). Here we have N degrees of freedom due to N arbitrary constants $\{A_n \mid n = 1, 2...N\}$.

For TE modes the refractive index profiles is simply given by

$$n^2(x) = n_\infty^2 - \frac{V(x)}{k_0^2} \tag{30}$$

in which k_0 is the free space wave number. Where as for TM modes, obtaining the refractive index profile is more complicated because it is a solution to a nonlinear differential equation [Eq.(8)]. The nonlinear differential equation can only be solved numerically. First we transform Eq. (8) in to a convenient form by setting $\epsilon(x) = e^{y(x)}$, we then obtain,

$$\frac{1}{2} \frac{d^2 y(x)}{dx^2} - \frac{1}{4} \left[\frac{dy(x)}{dx} \right]^2 + k_0 e^{y(x)} + \left[V(x) - k_0^2 n_\infty^2 \right] = 0 . \tag{31}$$

This is a constant coefficient equation which yields the refractive index profile $\sqrt{\epsilon(x)}$ provided the potential $V(x)$ is given.

6

5. Design Example 2: Non-Zero Reflection Coefficient

In the previous section, we took advantage of assuming that the reflection coefficient is zero, which simplified the problem a lot. Now we are going to solve the problem with non-zero reflection coefficient.

We take the rational function approximation for our scattering data. We represent our reflection coefficient using a three-pole rational function of transverse wave number k [6], the three poles are: one pole on the upper imaginary axis of the complex k plane, which represents discrete spectrum of function $R(x + t)$ [Eq. (12)] characterizing the propagating mode. Two symmetric poles lie in the lower half of the k plane, which represent the continuous spectrum of $R(x + t)$ characterizing the unguided modes. The three-pole reflection coefficient can be written as

$$r(k) = \frac{r_0}{(k - k_1)(k - k_2)(k - k_3)} \ , \tag{32}$$

where r_0 can be determined by the normalization condition $r(0) = -1$, this condition ensure total reflection at $k = 0$. k_1, k_2 have following forms: $k_1 = -c_1 - ic_2$ and $k_2 = c_1 - ic_2$. The third pole on the positive imaginary axis is $k_3 = ia$.

The pole positions are confined to certain "allowed regions" that are determined by the law of conservation of energy, which can be represented by $|r(k)|^2 \leq 1$ for all real k; see Fig. 2 and refer to Ref. [6] for details.

It has been shown that the reconstructed potential function $V(x)$ has following form:

$$V(x) = 2 \left[\frac{d\left(a^T(x)\right)}{dx} - a^T(x)A^{-1}(x)\frac{d(A(x))}{dx} \right] A^{-1}(x)b \ , \tag{33}$$

in which, a and b are column vectors, and are given by

$$a^T(x) = \begin{bmatrix} 1 & x & e^{\eta_1 x} & e^{-\eta_1 x} & e^{\eta_2 x} & e^{-\eta_2 x} \end{bmatrix} \tag{34}$$

$$b^T = \begin{bmatrix} 0 & 0 & 0 & 0 & 0 & -a(c_1^2 + c_{2^2}) \end{bmatrix} \ , \tag{35}$$

where

$$\eta_1 = \left[\frac{1}{2}a^2 + c_2^2 - c_1^2 + \frac{1}{2}(a^2 - 4c_2^2)^{1/2}(a^2 + 4c_1^2)^{1/2} \right]^{1/2} \tag{36}$$

$$\eta_2 = \left[\frac{1}{2}a^2 + c_2^2 - c_1^2 - \frac{1}{2}(a^2 - 4c_2^2)^{1/2}(a^2 + 4c_1^2)^{1/2} \right]^{1/2} . \tag{37}$$

7

Matrix $A(x)$ is given by

$$\begin{bmatrix} 0 & 1 & 0 & 0 & 0 & 0 \\ 0 & 0 & f(\eta_1) & a(c_1^2 + c_2^2) & 0 & 0 \\ 0 & 0 & 0 & 0 & f(\eta_2) & a(c_1^2 + c_2^2) \\ 1 & -x & e^{-\eta_1 x} & e^{\eta_1 x} & e^{-\eta_2 x} & e^{\eta_2 x} \\ 0 & -1 & -\eta_1 e^{-\eta_1 x} & \eta_1 e^{\eta_1 x} & \eta_2 e^{-\eta_2 x} & \eta_2 e^{\eta_2 x} \\ 0 & 0 & \eta_1^2 e^{-\eta_1 x} & \eta_1^2 e^{\eta_1 x} & \eta_2^2 e^{-\eta_2 x} & \eta_2^2 e^{\eta_2 x} \end{bmatrix} , \qquad (38)$$

where

$$f(x) = x^3 + (2c_2 - a)x^2 + [c_1^2 + c_2^2 - 2ac_2]x - a(c_1^2 + c_2^2) . \qquad (39)$$

So, it is possible to construct the potential from the three poles of reflection coefficient using the above equations.

6. Design Example 3: Non-rational Reflection Coefficient

The refractive index profiles reconstructed for the cases discussed above go to zero asymptotically and they approximately model the actual refractive index profiles used in practice. The refractive index profiles used in practice are truncated and the truncations form the core-cladding boundary. For a doubly truncated refractive index profile modeling a planar optical waveguide, the reflection coefficient is not a rational function of the complex wavenumber, but a more complicated form [10–12]. Reconstructing refractive index profiles for non-rational reflection coefficients is not possible in analytical closed forms and so numerical techniques must be used.

A. Discretization of G-L-M equation

To solve the G-L-M equation (18) by numerical methods, the space-time diagram is discretized into square grids rotated by 45° with respect to abscissa, as shown in Fig. 3. The interval $\Delta t = 2\Delta x$ and $x = m\Delta x$, $m = 0, 1, ...N$, where N is the total number of grid points along the x direction, and $t = n\Delta t - (m/2)\Delta t$, $n = 0, 1, ..., m$. The G-L-M integral equation can then be discretized as

$$K_m(n) + R_m(n) + \sum_{l=m-n}^{m} C(l)K_m(l)R_m(l)\Delta t = 0 , \quad n = 0, 1, ..., m \qquad (40)$$

where $y = l\Delta t - (m/2)\Delta t$. The subscript m in $K_m(n)$ represents the grid position along the x direction and the argument n represents the grid position along the t direction. $C(l)$ is the coefficient for numerical integration; if the trapezoidal rule is used,

$$C(l) = \begin{cases} 1/2 & l = m - n \text{ and } m \\ 1 & \text{elsewhere} \end{cases} . \qquad (41)$$

8

B. Iteration scheme with relaxation

The Gel'fand-Levitan-Marchenko equation is an integral equation of the second kind and can be solved numerically in an iterative manner. We rewrite Eq.(40) as

$$K_m^i(n) = -R_m(n) - \sum_{l=m-n}^{m} C(l)K_m^{i-1}(l)R_m(l)\Delta t,$$ (42)

where the superscript i in $K_m^i(n)$ represents the i-th iteration result. It is worth pointing out that the iterative process involves only the grid points on the m-th column in Fig. 3.

In Eq. (12) the poles on the positive imaginary axis $k_n = i\kappa_n$, $\kappa_n > 0$, are in the discrete spectrum and correspond to the guided modes. The exponential term in Eq.(12) then grows rapidly as $(x + t)$ increases and in order to improve the convergence, the relaxation technique is used [13], so that Eq.(42) is revised as

$$\begin{aligned} K_m^i(n) =& (1-\omega)K_m^{i-1}(n) \\ &+ \omega\left[-R_m(n) - \sum_{l=m-n}^{m} C(l)K_m^{i-1}(l)R_m(l)\Delta t\right], \end{aligned}$$ (43)

where ω is the relaxation factor. If ω lies between 0 and 1.0, it is called the under–relaxation method; if ω lies between 1.0 and 2.0, it is called the over-relaxation method. In our computations, $\omega < 0.7$ provides the desired results.

C. Initial values for K(x,t)

The convergence of analytical solution to the G-L-M equation has been proved [14]. However, the convergence of its discretized form cannot be ascertained, because of the additional errors due to truncation and discretization. Good initial values for $K(x,t)$ are important for the numerical iterative scheme, in particular when a bound state corresponding to the propagating mode exists. The Born approximation has been used by other authors to provide initial trial values for $K(x,t)$ for cases where there are no bound states. However, for cases discussed here, where there are bound states, the Born approximation when used to provide the initial values for $K(x,t)$ fails to reconstruct the potential correctly. Although for shorter lengths of the potential the reconstruction is in agreement with the actual value, the method fails for larger lengths. The leap-frogging algorithm [15] provides an effective initial value for $K(x,t)$.

To obtain the leap-frogging algorithm, we substitute Eq.(20) into (10) where $\psi(x,t)$ has been replaced by $K(x,t)$ yielding

$$\frac{\partial^2 K(x,t)}{\partial x^2} - \frac{\partial^2 K(x,t)}{\partial t^2} - 2\frac{dK(x,x)}{dx}K(x,t) = 0$$ (44)

9

and introduce new variables u and v, defined as

$$u = \frac{x - t}{\sqrt{2}} \tag{45}$$

and

$$v = \frac{x + t}{\sqrt{2}} \tag{46}$$

(see Fig. 3). With this coordinate transformation, the partial differential equation (44) can be rewritten as

$$\frac{\partial^2 K(u,v)}{\partial u \, \partial v} - \sqrt{2} \frac{\partial K(u,v)}{\partial v} K(u,v) = 0 \tag{47}$$

so that its discretization gives the following equation [15],

$$\begin{aligned} K_m(n) =&K_{m-1}(n) + K_{m-1}(n - 1) \\ &+ \{2\Delta x[K_n(n) - K_{n-1}(n - 1)] - 1\}K_{m-2}(n - 1); n > 0, m > 0, n = m, \end{aligned} \tag{48}$$

which relates the grid point $K_m(n)$ with the other five grid points, as shown in Fig. 3. Note that $K_m(n)$ on the LHS of Eq. (48) is at the "current" reconstruction column m, while the remaining five grid points on the RHS are all located within its left region, which are either on the boundary whose values are provided by $K(x, -x) = -R(0)$ or grid points that have already been reconstructed by the step-by-step marching algorithm marching in the x direction. Equation (48) does not provide values for $K_m(m), m = 1, 2, ...N$ and a different procedure should be adopted to find those values.

Solving Eq.(42) for $K_m(m)$ yields

$$K_m(m) = \frac{-R_m(m) - \sum\limits_{l=0}^{m-1} C(l)K_m(l)R_m(l)\Delta t}{1 + C(m)R_m(m)\Delta t}, \quad m > 0, m = n \tag{49}$$

which provides initial trial values for $K_m(m)$. Furthermore, we obtain

$$K_m(0) = -R(0). \tag{50}$$

To summarize, Eqs. (48), (49), and (50) can provide the initial trial values for $K(x, t)$ necessary for the iterative numerical solution of the G-L-M equation.

D. Reconstruction of the potential v(x)

The potential in its discretized form can be expressed using Eq.(20) as

$$v(m-1) = \frac{K_m(m) - K_{m-2}(m-2)}{\Delta x}, \quad m \geq 2. \tag{51}$$

This expression can be used to reconstruct the potential when the values of $K_m(m); m = 0, 1, ...N$ are already evaluated. This reconstructs the potential at every point in x except at $x = 0$; corresponding to the grid point $m = 0$.

To evaluate the potential at the origin we substitute Eq.(18) into Eq. (20), yielding

$$v(x) = -2\frac{dR(2x)}{dx} - K(x,x)R(2x) + \int\limits_{-t}^{x} \frac{\partial}{\partial x}[K(x,y)R(y+x)]dy. \tag{52}$$

Because $R(t) = 0$ for $t \leq 0$, we obtain at the origin

$$v(0) = -2\frac{dR(2x)}{dx}\Big|_{x=0} = -4R'(0), \tag{53}$$

which is an exact formula for recovering the potential at the origin. It is interesting to note that the perturbation expansion theory derives the approximate solutions [16]

$$v(x) = -2\frac{dR(2x)}{dx} \tag{54}$$

and

$$v(x) = -2\frac{dR(2x)}{dx} + 4[R(2x)]^2, \tag{55}$$

which are called the Born and the modified Born approximation respectively. At the origin, the Born expression provides an approximate reconstruction, even though there exists a discontinuity at the boundary.

The numerical inverse scattering theory can now be summarized in the following steps:

(a)   Compute the potential at the origin, $v(0)$ using Eq.(53) ;

(b)   Set the initial trial values for $K_m(n)$, $n = 0, 1, ... m$ on the current column m using Eqs.(48), (49) and (50) ;

(c)   Iteratively calculate $K_m(n)$, $n = 1, 2, ... m$ for each value of n on the current column m using Eq.(42) with an appropriate choice of relaxation factor ω ;

(d)   Evaluate potential $v(m-1)$ using Eq.(51) ;

(e)   Move the current column from m to $m+1$, and repeat the steps (b) to (d).

11

7. Discussion

We have developed a method based on inverse scattering theory that can be used to design planar optical waveguides that transmit a prescribed number of TE or TM modes with prescribed propagation constants. To demonstrate some practical examples for the zero reflection case, let us compute the refractive index profiles for two cases: the single mode case and the N mode case.

For the single mode case, Eq.(23) becomes

$$A_1 e^{\kappa_1 x} + f_1(x) + \left(\frac{A_1 e^{2\kappa_1 x}}{2\kappa_1} \right) f_1(x) = 0 \ . \tag{56}$$

Then, the potential has the form

$$V(x) = \frac{-4\kappa_1 A_1 e^{2\kappa_1 x}}{\left(1 + A_1 e^{2\kappa_1 x}/2\kappa_1\right)^2} \ , \tag{57}$$

where A_1 is an arbitrary constant and note that κ_1 can be obtained from

$$\kappa_1^2 = \beta_1^2 - k_0^2 n_\infty^2 \ . \tag{58}$$

For a desired propagation constant β_1, we can get a set of refractive index profiles corresponding to different arbitrary choice of A_1; see Fig. 4. We use the following data relating to waveguide: $n(\infty) = n_s = 2.177$, wavelength $\lambda = 0.8\mu m$ and $\beta_1 = 17.20 \ (\mu m)^{-1}$. We obtained the refractive index profiles by solving Eq. (31) using the potential $V(x)$ obtained from Eq. (57). Runge-Kutta's fourth order approximation is applied in solving the differential equation (31) [17]. We can see from Fig. 4 that the maximum value of refractive index lies on the positive side of $x = 0$ when $A_1 < 2\kappa_1$; on the negative side of $x = 0$ when $A_1 > 2\kappa_1$ and at $x = 0$ when $A_1 = 2\kappa_1$.

On substituting $A_1 = 2\kappa_1$ into Eq. (57) yields

$$V(x) = -2\kappa_1^2 sech^2 \kappa_1 x \ . \tag{59}$$

This potential is everywhere negative and goes to zero as x goes to infinity. Also the potential is symmetric about its minimum point. We can truncate the potential at the point where the potential is 1% of its maximum value to find the width of the core d. The refractive index profile corresponding to this potential is shown by continuous line in Fig. 4.

Similarly, for the N mode case, we need to construct the potential first using Eq. (25) and then solve the nonlinear differential equation (31) for the refractive index profiles. For a set of prescribed propagation constants, every arbitrary choice of normalization constants will produce a different potential and a corresponding refractive index profile. In order to construct a symmetric refractive index profile

12

with single peak, we found that the normalization constants $\{A_n \mid n = 1, 2 ... N\}$ must satisfy the following equation [18]

$$A_n = \sqrt{2\kappa_n P_n} \, , \tag{60}$$

where

$$P_n = (-1)^{n-1} \prod_{\nu=1\,(\nu \neq n)}^{N} \frac{\kappa_\nu + \kappa_n}{\kappa_\nu - \kappa_n} \qquad n = 1, 2, ... N \tag{61}$$

for the reflectionless case. Here N is the number of guided modes in the planar waveguide. For the case $N = 5$, using sets of arbitrary normalization constants $\{A_n \mid n = 1, 2 ... N\}$ we have computed the refractive index profiles and these are shown in Fig. 5. The symmetric profile obtained using the condition (60) is shown by continuous line in the figure.

To demonstrate the reconstruction of the potential from a three poles reflection coefficient; a case of non zero rational reflection coefficients, we have chosen here two examples. In example 1, the poles are determined by the following parameters: $a = 1.0$, $c_1 = 0.8$, and $c_2 = 0.499$; example 2 has different unguided modes characterized by $c_1 = 0.05$, $c_2 = 0.1$ and the same propagating mode characterized by $a = 1.0$. Figure 6 shows the plots of potential functions for examples 1 and 2. In the example 2, we see that the potential is everywhere negative.

Figure 7 shows the refractive index profiles for TM mode in both the above discussed examples obtained by substituting the potentials into the nonlinear differential equation (31) and solving for $\sqrt{\epsilon(x)}$. We notice that a depressed cladding is obtained in example 1 and we also see that the profiles we found here resemble the profiles we normally find in practical optical waveguides [19].

Introducing a truncated potential to model the planar waveguide [11], it can be shown that both propagating and non-propagating modes appear when the reflectionless potential $v(x) = -2 \operatorname{sech}^2(x)$ is truncated at a point on the left $x = x_1$. Based on the Jost solutions corresponding to the untruncated potential $v_0 = -2 \operatorname{sech}^2(x)$, the reflection coefficient from the left for the truncated potential can be derived [11] as

$$r(k) = -\exp\left(i2kx_1\right)\frac{\operatorname{sech}^2(x_1)}{k^2 + 1 + \left(k + i \tanh(x_1)\right)^2}, \tag{62}$$

which has two poles in the complex k–plane located at

$$k_1 = -\frac{i}{2}\left[\sqrt{2 - \tanh^2(x_1)} + \tanh(x_1)\right] \tag{63}$$

and

$$k_2 = \frac{i}{2}\left[\sqrt{2 - \tanh^2(x_1)} - \tanh(x_1)\right]. \tag{64}$$

13

Since $\sqrt{2 - \tanh^2(x_1)} > |\tanh(x_1)|$, both poles are located on the imaginary axis, so that $k_2 = i\kappa$ corresponds to the guided mode. The exponential factor $\exp(i\, 2kx_1)$ in Eq.(62) represents a shift x_1 on the x axis relative to the corresponding untruncated potential. Equation (62) can then be rewritten as

$$r_0(k) = \frac{-\operatorname{sech}^2(x_1)}{k^2 + 1 + (k + i\tanh(x_1))^2} \tag{65}$$

in which the phase shift factor has been excluded. The characteristic function is

$$R_0(t) = \frac{\operatorname{sech}^2(x_1)}{2\sqrt{2 - \tanh^2(x_1)}} \Big\{ -\exp\Big[-0.5\Big(\sqrt{2 - \tanh^2(x_1)} + \tanh(x_1)\Big)t\Big]$$
$$+ \exp\Big[0.5\Big(\sqrt{2 - \tanh^2(x_1)} - \tanh(x_1)\Big)t\Big]\Big\}. \tag{66}$$

Using Eq.(53), the potential at the truncation location is

$$v_0(0) = -2\operatorname{sech}^2(x_1). \tag{67}$$

This is a case of non-rational reflection coefficient. Figure 8 gives the potential, assuming $x_1 = -1.0$, where the asterisks show the potential obtained by numerical reconstruction, and the exact potential

$$v_0(x) = -2\operatorname{sech}^2(x + x_1) \tag{68}$$

is plotted in solid line for comparison, again good agreement is achieved.

The results obtained by inverse scattering theory can be verified by a finite difference based analysis scheme. Using this method we find the propagation constants of guided modes of an optical waveguide with arbitrary refractive index profile. Owing to its simplicity and flexibility, this method is proved to be very effective. For demonstration purpose we consider here a symmetric planar waveguide. We have compared in table 1 the propagation constants of various modes that we used in reconstructing the refractive index profile of the waveguide against the propagation constants obtained by analysis for the normalized frequency at which the propagation constants are prescribed. We see that last two columns of the table agree very well. This shows that the inverse technique outlined here can be used to synthesize waveguides with prescribed modes.

The method demonstrated here can be extended to the synthesis of optical devices [20]-[21] with specified transmission characteristics. The details are provided in the appendices.

8. References

1. I. M. Gel'fand and B. M. Levitan, "On the determination of a differential equation by its spectral function," Transl. AM. Math. Soc. Ser. **21**, 253–304. (1955).

2. V. A. Marchenko, "Concerning the theory of a differential operator of second order," Dokl. Akad. Nauk SSSR **T2**, 457–463. (1950).

3. D. Marcuse, *Light Transmission Optics* (Van Nostrand Reinhold, Princeton, N. J., 1972), 100–105.

4. T. Tamir, *Guided-Wave Optoelectronics*, (Springer-Verlag press 1990), Chap. 2.

5. S. P. Yukon and B. Bendow, "Design of waveguides with prescribed propagation constants," J. Opt. Soc. Am. **70**, 172–179. (1980).

6. A. K. Jordan and S. Lakshmanasamy , "Inverse scattering theory applied to the design of single-mode planar optical waveguides," J. Opt. Soc. Am. A, **6,** 1206–1212 (1989)

7. L. Tamil and Y. Lin, " Synthesis and analysis of optical planar waveguides with prescribed TM modes," J. opt. Soc. Am. A., **9** 1953–1962 (1993).

8. I. Kay, "The inverse scattering problem," Rep. **EM**-74 (New York university, New York, N. Y., 1955)

9. I. Kay and H. Moses, "Reflectionless transmission through dielectrics and scattering potentials," J. Appl. Phys. **27**, 1503–1508 (1956).

10. D. W. Mills and L. S. Tamil, " A new approach to the design of graded-index guided wave devices," IEEE Microwave Guided Wave Lett. **1**, 87–88 (1991).

11. D. W. Mills and L. S. Tamil, " Analysis of planar waveguides using scattering data," J. Opt. Soc. Am. A. **9**, 1769–1778 (1992).

12. G. L. Lamb, Jr., Elements of Soliton Theory (Wiley, New York, 1980)

13. W. H. Press, B. P. Flannery, S. A. Teukolsky, and W. T. Vetterling, Numerical Recipes (Cambridge University Press, New York, 1989)

14. H. H. Szu, C. E. Caroll, C. C. Yang, and S. Ahn, " A new functional equation in the plasma inverse scattering problem and its analytical properties," J. Math. Phy. **17**, 1236–1247 (1976).

15. A. K. Jordan and H. Ladoucer, "A renormalized inverse scattering theory for discontinuous profiles," Phy. Rev. A, **36**, 4245–4253 (1987).

16. H. N. Kritikos, D. L. Jaggard and D. B. Ge, " Numeric reconstruction of smooth dielectric profiles," Proc. IEEE, **70**, 295–297 (1982).

17. H. Levy and E. A. Baggott, " Numerical Solution of Differential Equations (Springer-Verlag, New York, 1976)

18. P. Deift and E. Trubowitz, "Inverse scattering on the line," Commn. Pure Appl. math., **32**, 121–251 (1979).

19. T. Okoshi, Optical Fibers (Academic Press, New York, 1976)

20. D.W. Mills and L.S. Tamil, " Synthesis of Guided wave optical interconnects," IEEE J. Quantum Electron, **29**, 2825–2834 (1993).

21. D. W. Mills and L. S. Tamil, "Coupling in multilayer optical waveguides: An Approach based on scattering data," **9**, 1560–1568 (1994).

9. List of Tables

Table 1. Prescribed TM mode spectra used in reconstructing refractive index of planar waveguide and spectra obtained by analysis using finite difference scheme. .
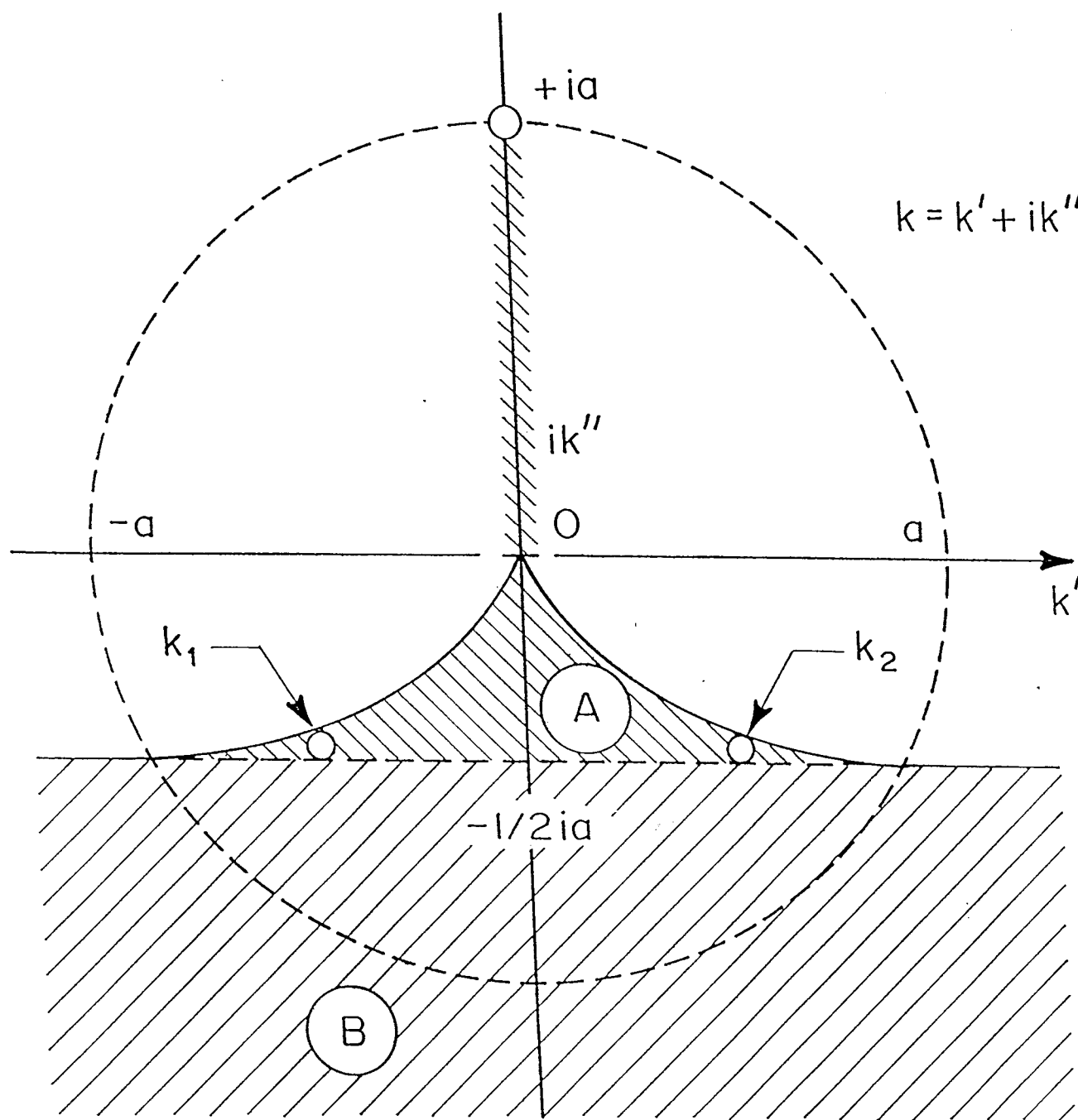
Table 1

number of modes	mode number γ	prescribed mode spectra β_γ/k_0	β_γ/k_0 obtained by our analysis
N=1	0	2.18997	2.18995
N=2	0	2.20556	2.20553
	1	2.18417	2.18398
N=3	0	2.20926	2.20916
	1	2.19140	2.19100
	2	2.18061	2.18036
N=5	0	2.21288	2.21266
	1	2.20003	2.19968
	2	2.18998	2.18968
	3	2.18278	2.18254
	4	2.17845	2.17797
N=7	0	2.21466	2.21452
	1	2.20473	2.20449
	2	2.19630	2.19606
	3	2.18927	2.18915
	4	2.18397	2.18379
	5	2.18010	2.17997
	6	2.17778	2.17753

10. List of Figures

CLADDING

n_2

CORE

$n(x)$

n_2

0

d

e^{ikx}

$r(k)e^{-ikx}$

$t(k)e^{ikx}$

$+ia$

$k = k' + ik''$

ik''

$-a$ O a

k'

k_1 A k_2

$-1/2\,ia$

B

v

$t=x$

$K_m(m)$

$\sqrt{2}\,\Delta x$

$K_n(n)$

$K_{n-1}(n-1)$

$K_{m-1}(n)$

$K_{m-2}(n-1)$

$K_m(n)$

$K_{m-1}(n-1)$

$K_{m-2}(n-2)$

$K_m(n-1)$

$K_0(0)$

x

O

$dt=2dx$

$K_m(1)$

$K_m(0)$

$K_m(0)$

dx

$t=x$
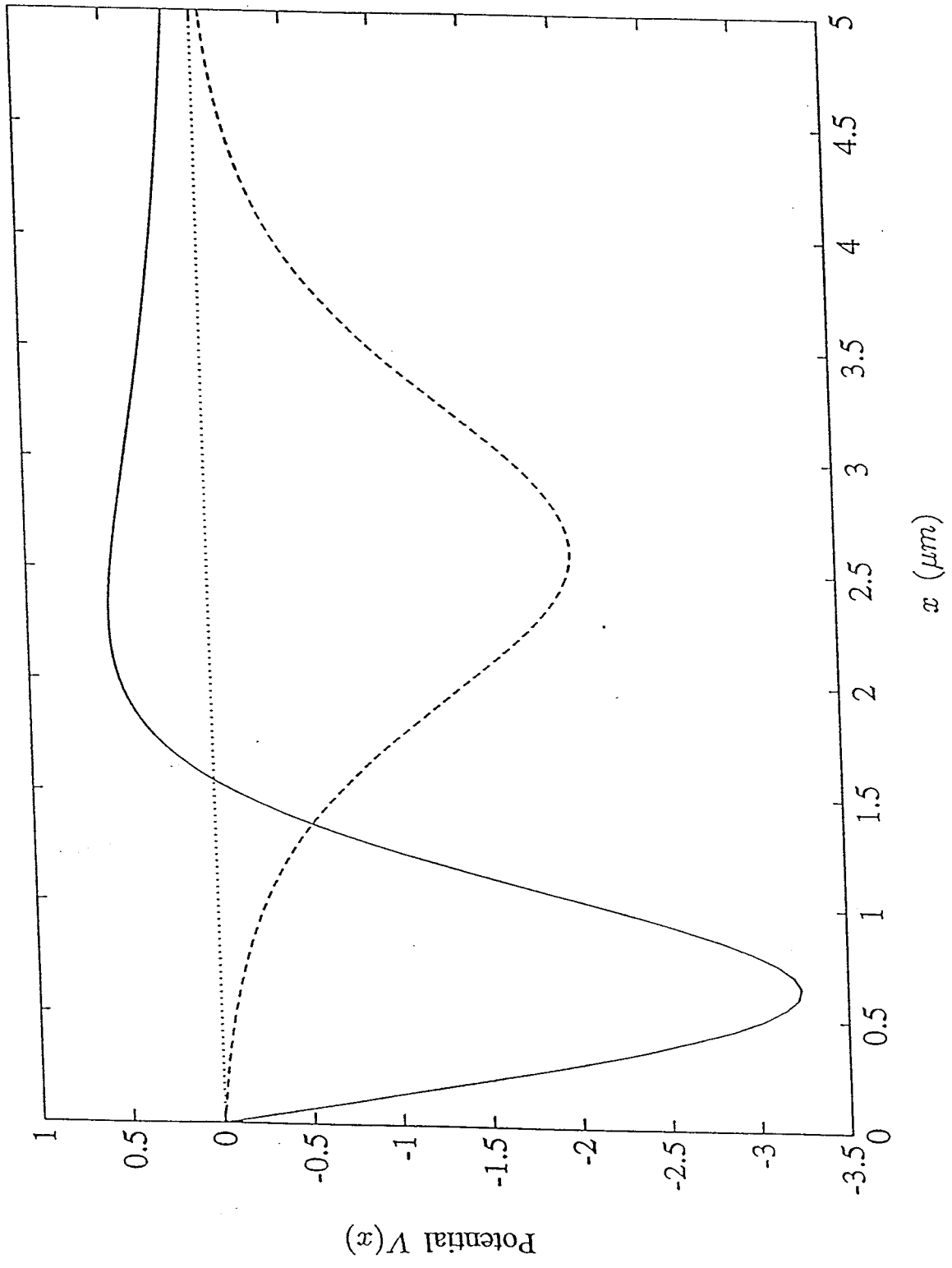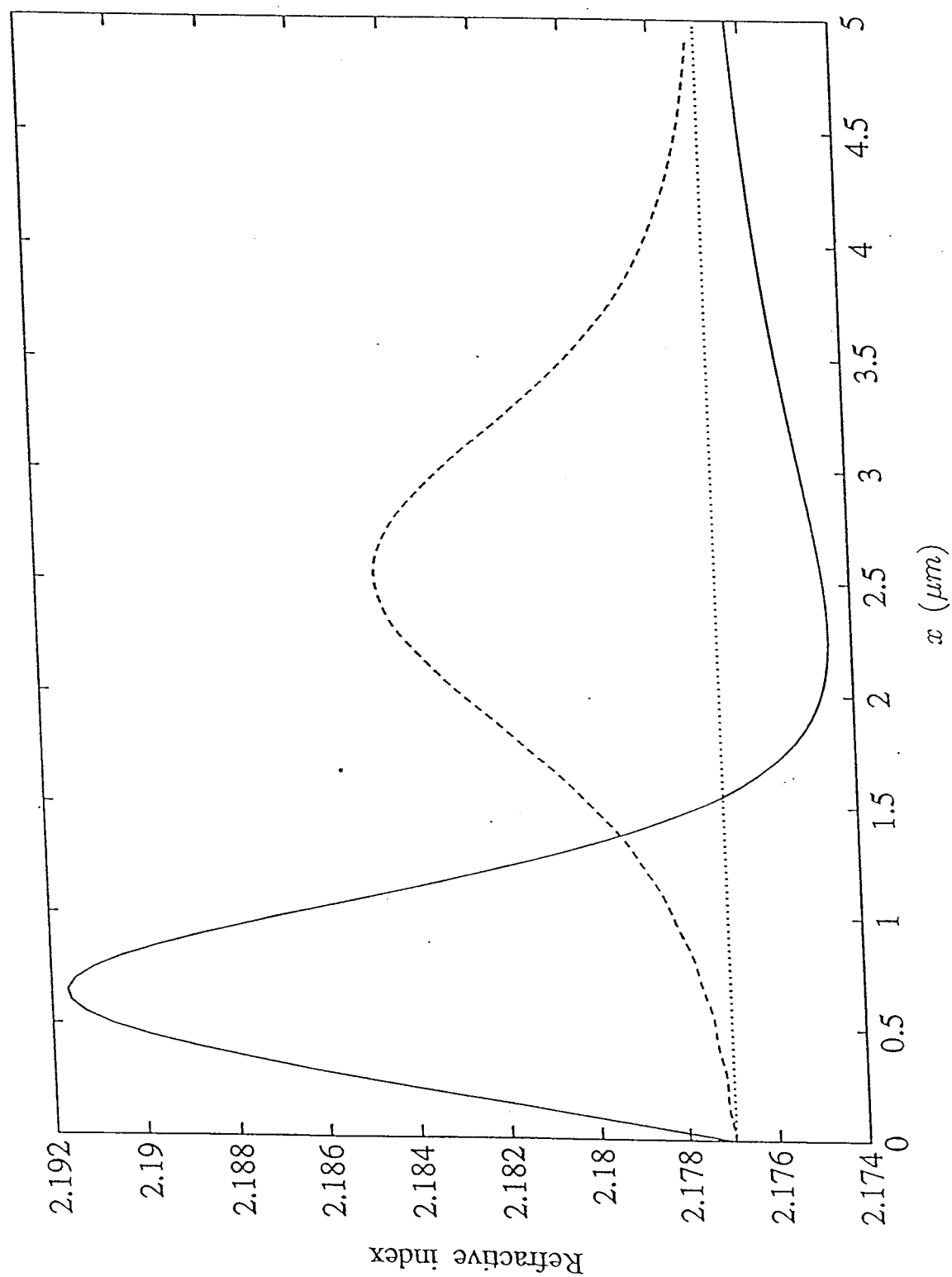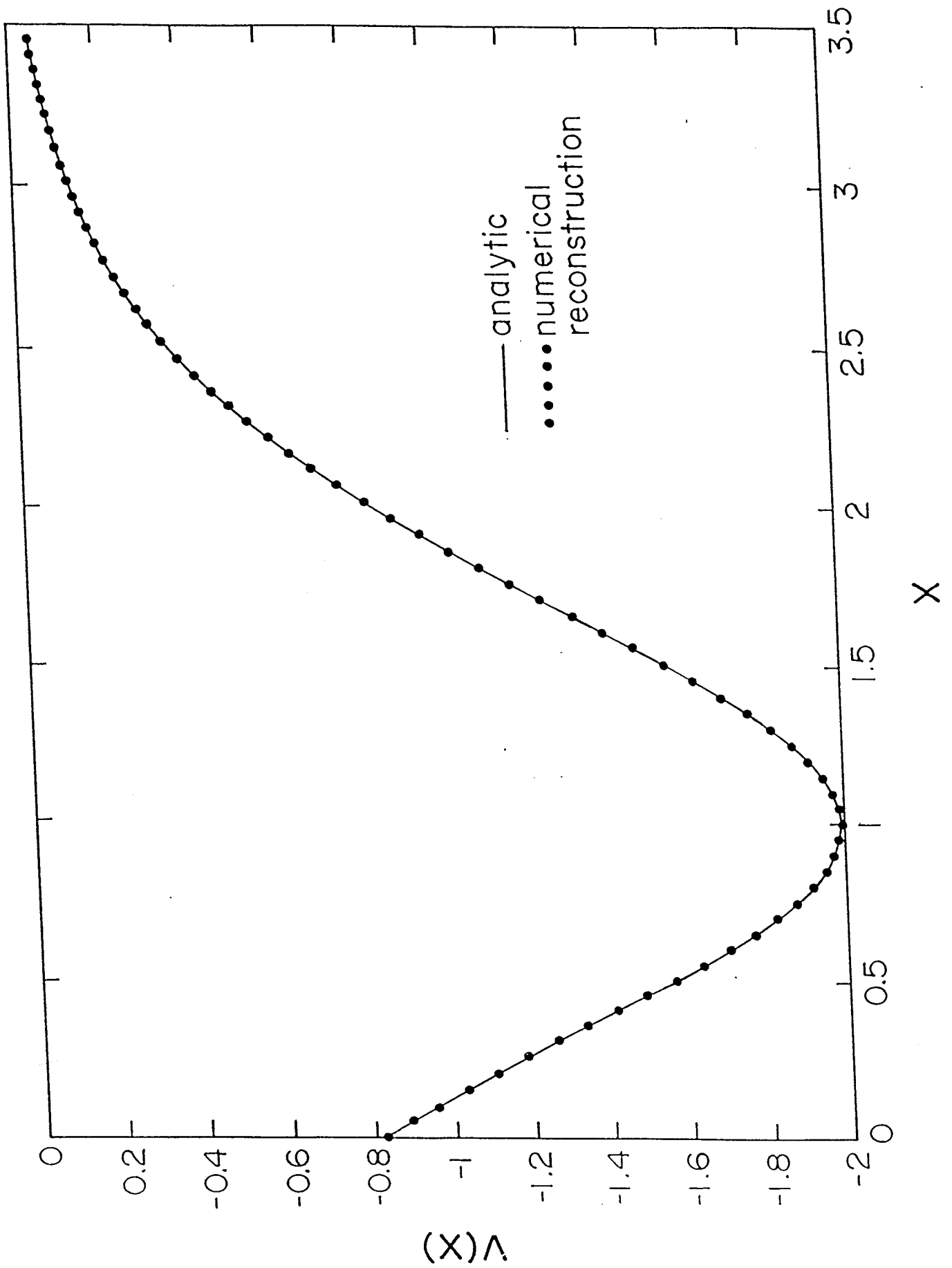
u

Potential $V(x)$

x (μm)

LIST OF PUBLICATIONS RELATED TO THE PROJECT

1. L. S. Tamil and A. K. Jordan, "Spectral Inverse Scattering Theory for Inhomogeneous Dielectric Waveguides and Devices," Proceedings of the IEEE, Special issue on electromagnetic, Vol. 79, No. 10, pp. 1519–1528, October 1991.

2. L. S. Tamil and A. K. Jordan, "Optical Waveguides for Imaging Applications: Design by an Inverse Scattering Approach," International Journal of Imaging Systems and Technology, Vol. 3, pp. 18–26, 1991.

3. L. S. Tamil and A. K. Jordan, "Inverse Scattering Model for an All-optical Logic Gate," Journal of Applied Physics, Vol. 70, No. 3, pp. 1882–1884, August 01, 1991..

4. D. W. Mills and L. S. Tamil, "A New Approach to the Design of Graded-Index Guided Wave Devices," IEEE Microwave and Guided Wave Letters, Vol. 1, No. 4, pp. 87–89, Apr. 1991.

5. M. A. Hooshyar and L. S. Tamil, "Inverse Scattering Theory at Fixed Energy and the Design of Circular Optical Waveguides", Journal of Mathematical Physics, Vol. 33, No. 2, pp. 663–669, Feb. 1992..

6. L. S. Tamil, "An Inverse Scattering Model for Optical Binary Switches," Optics Communications, Vol. 91, No. 3, 4, pp. 197–202, July 15, 1992.

7. D. W. Mills and L. S. Tamil, "Analysis of Planar Optical Waveguides Using Scattering Data," Journal of the Optical Society of America A, Vol. 9, No. 10, pp. 1769-1778, Oct. 1992..

8. L. S. Tamil and Y. Yu, "A Beam Propagation Technique to Analyze Integrated Photonic Circuits," Microwave and Optical Technology Letters, Vol.5, No. 12, pp. 617–621, Nov. 1992.

9. M. A. Hooshyar and L. S. Tamil, "Inverse Scattering Theory and the Design of Planar Optical Waveguides with same Propagation Constant for Different Frequencies," Inverse Problems, (published by the Institute of Physics, London) Vol. 9, pp. 69–80, 1993.

10. L. S. Tamil and G. H. Aicklen, "Analysis of Optical Fibers with Arbitrary Refractive Index Profiles: Accuracy, Convergence, and Effects of Finite Cladding," Optics Communications, Vol. 99, pp. 393–404, 1993. .

11. G. H. Aicklen and L. S. Tamil, "Interactive Analysis of Propagation in Optical Fibers," Computer Applications in Engineering Education, Vol. 1, No. 3, pp. 197–204, 1993.

12. L. S. Tamil and Y. Lin, "Synthesis and Analysis of Optical Planar Waveguides with Prescribed TM Modes," Journal of the Optical Society of America A, Vol. 10. No. 9, pp. 1953–1962, 1993..

13. D. W. Mills and L. S. Tamil, "Synthesis of Guided wave Optical Interconnects: An Inverse Scattering Approach," IEEE Journal of Quantum Electronics, Vol.29, No. 11, pp. 2825–2834, 1993..

14. L. S> Tamil, Y. Li, J. M. Dugan and K. A. Dugan,"Dispersion Compensation for High Bit Rate Fiber Optics Communication Using a Dynamically Tunable Optical Filter," Applied Optics, Vol.33, No.9 , pp. 1697–1706, 1993.

15. D. W. Mills and L. S. Tamil, "Coupling in multilayer optical waveguides: an approach based on scattering data," IEEE/OSA Journal of Lightwave Technology, Vol.12 , No. 9, pp. 1560–1568, 1994.

16. D. B. Ge, A. K. Jordan and L. S. Tamil, "Numerical Inverse Scattering Theory for the Design of Planar Optical Waveguides," J. Optical Soc. Am. A, Vol. 11. No. 11, pp. 2809–2815, 1994.

17. A. K. Jordan and L. S. Tamil, "An Inverse Scattering Approach to the Design of Multimode Optical Waveguides for Image Transmission,"Inverse Problem in Scattering and Imaging, Edited by M. Bertero and E. R. Pike, pp. 228–245, Adam Hilgar, New York, 1992, Proc. of the NATO advanced research workshop, Cape Code, MA, April 15–19, 1991. .

18. L. S. Tamil and A. K. Jordan, "Synthesis and Analysis of Large Scale Integrated Photonic Devices and Circuits," National Academy of Sciences, Proceedings of the National Research Council Synposium on Large Scale Electromagnetics and Acoustic Structures held on September 26–27, 1994, Washington, DC.

19. L. S. Tamil and A. K. Jordan, "Synthesis of Optical Interconnects and Logic Gates,"in Guided-Wave Optoelectronics: Device Characterization, Analysis, and Design, T. Tamir, H. Bertoni and G. Griffel, Eds., Plenum Press, New York, 1994.

20. L. S. Tamil, M. A. Hooshyar, Y. Lin and G. H. Aicklen, "Inverse Problem in Fiber Design," Inverse Problems in Scattering and Imaging, Society of the Photo Instrumentation Engineers' 1992 Symposium on Optical Applied Sciences and Engineering, 19–24 July 1992, San Dieago, CA..

21. L. S. Tamil, "Synthesis of Optical Channel Waveguides: An Inverse Scattering Approach, International Radio Science Union Meeting, Boulder, CO, January 5–7, 1993.

22. L. S. Tamil, "Synthesis of Integrated Optical Devices: An Inverse Scattering Approach, Progress in Electromagnetics Research Symposium, July 12–16, 1993, Pasadena, CA. .

23. L. S. Tamil and G. H. Aicklen, "Soliton Interaction in Saturable Nonlinear Medium," Conf. on Emerging Optoelectronic Technologies, July 23–38, 1994, Indian Institute of Science, Bangalore, India. *Invited paper* (with G. Aicklen).

24. D. B. Ge, A. K. Jordan, Y. Lin and L. S. Tamil, "A Numerical Inverse Scattering Technique to Synthesize Optical Waveguides of Prescribed Transmission Characteristics" Conf. on Numerical Electromagnetics, Nov. 6–11, 1994, Bejing, China.

25. Y. Yu, C. D. Cantrell and L. S. Tamil, "Finite Difference Analysis of Nonlinear Multilayered Optical Waveguides: Applicaiton to Switching" Conf. on Numerical Electromagnetics, Nov. 6–11, 1994, Bejing, China.

26. G. Aicklen and L. S. Tamil, "Soliton Interaction in Optical Fibers with Saturable Nonlinearity," OSA Annual Meeting, Dallas, TX Oct. 2–7, 1994.

27. A. K. Jordan and L. S. Tamil, "Electromagnetic Inverse Scattering theory: Applications to Optical Devices," OSA Annual Meeting, Dallas, TX Oct. 2–7, 1994.

Appendix A

L. S. Tamil and Y. Lin, " Synthesis and Analysis of Planar Optical Waveguides With Prescribed TM Modes"

Journal of the Optical Society of America A, Vol. 10. No. 9, pp. 1953–1962, 1993.

Synthesis and analysis of planar optical waveguides with prescribed TM modes

Lakshman S. Tamil and Yun Lin

Erik Jonsson School of Engineering and Computer Science and Center for Applied Optics,
University of Texas at Dallas, Box 830688, Richardson, Texas 75083-0688

An inverse-scattering approach to designing optical waveguides with prescribed propagation characteristics of TM modes is presented. The refractive-index profile of the waveguide is formulated as a solution to a nonlinear differential equation whose forcing function is the potential obtained from the application of inverse-scattering theory. This method can reconstruct smooth refractive-index profiles for planar waveguides that support single modes or multimodes. The cases of both zero and nonzero reflection coefficients characterizing the transmission properties of waveguides are discussed. A direct analysis technique based on a finite-difference scheme has been formulated to verify the results obtained by the inverse-scattering method, and the two approaches are in excellent agreement.

1. INTRODUCTION

The conventional method of designing optical waveguiding structures is to assume a refractive-index profile and solve the governing differential equation to find the various propagating modes and their propagation characteristics. If the propagation characteristics do not exhibit the expected behavior, the refractive index is changed and the propagation characteristics are again evaluated; this is repeated until the expected propagation behavior of the modes is obtained. Since the procedure is iterative, it is time consuming. Also, to obtain certain arbitrary transmission characteristics, one may not be able to guess the correct initial refractive-index profile. One normally thinks of initial profiles that have a mathematically closed form, such as parabolic and secant hyperbolic.

The procedure discussed in this paper, as opposed to the direct method, starts with the required propagation characteristics of the waveguide and obtains the refractive-index profile as the end result. We achieve this by transforming the wave equation for both the TE and the TM modes in the planar waveguide to a Schrödinger-type equation and then applying the inverse-scattering theory as formulated by Gel'fand and Levitan[1] and by Marchenko.[2] The inverse-scattering problem encountered here has a direct analogy to the inverse-scattering problem of quantum mechanics. The refractive-index profile of the planar waveguide is contained in the potential of the Schrödinger-type equation, and the propagating modes are the bound states of quantum mechanics.[3]

An inverse-scattering theory with a zero reflection coefficient characterizing the propagation property was applied by Yukon and Bendow to the design of planar waveguides.[4] In that investigation the refractive-index profiles were constructed only for the prescribed TE modes. The inverse problem of designing optical waveguides whose transmission property is characterized by a nonzero reflection coefficient was solved for TE modes by Jordan and Lakshmanasamy.[5] In this paper we have applied the inverse-scattering theory with both the zero and the non-zero reflection coefficients to design planar waveguides with prescribed TM modes.

In Section 2 we review the problem of electromagnetic wave propagation in a planar waveguide for both TE and TM cases,[6] then we present a way to transform wave equations into Schrödinger-type equations. In Section 3 we review Kay's inverse-scattering theory[7] and the Gel'fand–Levitan–Marchenko equation.[1,2] Inverse-scattering theory is then applied to planar waveguides for the case of TM modes in the zero and the nonzero reflection-coefficient conditions separately. We obtain the single-mode and the multimode refractive-index profiles with prescribed TM modes by solving a nonlinear differential equation, using the Runge–Kutta fourth-order approximation method, as discussed in Sections 4 and 5. In Section 5 we present the construction of the potentials for a single-mode planar waveguide for the nonzero reflection-coefficient case, using a rational function of wave number to obtain reflection coefficients.

To verify the results obtained by inverse-scattering theory, we have developed an efficient finite-difference method to find the propagation constants of guided TE and TM modes, and we present the method in Section 6. We start from the wave equations for TE and TM modes and transform them into a set of finite-difference equations. Then a matrix eigenvalue equation, from which the propagation constants can be found, is constructed. The numerical results are obtained for several graded-index waveguides, and we compare these results with previously published analytical solutions and results obtained by other numerical methods. The conclusions are given in Section 7.

2. PHYSICAL MODEL OF A PLANAR WAVEGUIDE

The wave equations for inhomogeneous planar optical waveguides can be derived from Maxwell's equations. If we take z as the propagation direction and let ω represent the frequency of laser radiation, we have the follow-
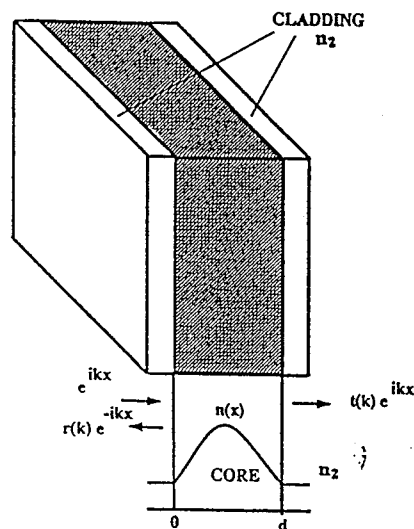
L. S. Tamil and Y. Lin

Fig. 1. Physical structure of the inhomogeneous symmetrical planar optical waveguide, showing reflection and transmission of an electromagnetic wave.

ing wave equations for one-dimensional inhomogeneous planar waveguides[6]:

$$\frac{d^2}{dx^2}E_y(x) + [k_0^2\epsilon(x) - \beta^2]E_y(x) = 0 \qquad (1)$$

for TE modes and

$$\frac{d^2}{dx^2}E_x(x) + \frac{d}{dx}\left[\frac{1}{\epsilon(x)}\frac{d\epsilon(x)}{dx}E_x(x)\right]$$
$$+ [k_0^2\epsilon(x) - \beta^2]E_x(x) = 0 \qquad (2)$$

for TM modes. The planar waveguide that we are considering here has a refractive index that varies continuously in the x direction. For the planar optical waveguide shown in Fig. 1, our problem is to find the refractive-index profile function in the core for a set of prescribed propagation constants.

We assume that this planar waveguide has a refractive-index profile guiding N modes. The propagation constants $\{\beta_n\}$ are $k_0 n_1 > \beta_1 > \beta_2 > \ldots \beta_N \geq k_0 n_\infty$, in which n_∞ is the value of $n(x)$ as $x \to \infty$ and $n_1 = \sup n(x)$. The design of an optical waveguide is analogous to the inverse problem encountered in quantum mechanics. We are, in effect, trying to obtain the potential function from the given bound states and scattering data. The wave equation for the TE modes can be easily transformed into an equivalent Schrödinger equation,

$$\frac{d^2}{dx^2}E_y(x) + [k^2 - V(x)]E_y(x) = 0, \qquad (3)$$

by letting

$$V(x) = -k_0^2[n^2(x) - n_\infty^2], \qquad (4)$$
$$k^2 = -\kappa_n^2 = -(\beta_n^2 - k_0^2 n_\infty^2). \qquad (5)$$

We can see that in our case the potential function $V(x)$ is continuous and $V(x) \to 0$ as $|x| \to \infty$. The TE mode cases have been solved by Yukon and Bendow[4] and Jordan and Lakshmanasamy,[5] and so our discussion will be restricted to TM modes.

We now need to transfer the wave equation for the TM modes into a Schrödinger-type equation to apply the inverse-scattering method. In Eq. (2) the first derivative of E_x can be eliminated if we let $E_x(x) = \epsilon^{-1/2}(x)\Phi(x)$. The wave equation then becomes

$$\frac{d\Phi^2}{dx^2} + \left\{\frac{1}{2\epsilon(x)}\frac{d^2\epsilon(x)}{dx^2} - \frac{3}{4\epsilon^2(x)}\left[\frac{d\epsilon(x)}{dx}\right]^2\right\}\Phi$$
$$+ [k_0^2\epsilon(x) - \beta^2]\Phi = 0. \qquad (6)$$

We are now able to obtain the equivalent Schrödinger equation,

$$\frac{d^2\Phi(x)}{dx^2} + [k^2 - V(x)]\Phi(x) = 0, \qquad (7)$$

by setting the potential function as

$$V(x) = \frac{3}{4\epsilon^2(x)}\left[\frac{d\epsilon(x)}{dx}\right]^2 - \frac{1}{2\epsilon(x)}\frac{d^2\epsilon(x)}{dx^2} - k_0^2[\epsilon(x) - n_\infty^2] \qquad (8)$$

and letting

$$k^2 = -\kappa_n^2 = k_0^2 n_\infty^2 - \beta_n^2. \qquad (9)$$

3. INVERSE-SCATTERING THEORY

The inverse-scattering theory of Kay and Moses[8] provides a way to obtain the potential from the reflection coefficient that characterizes the propagation properties of the planar waveguide. As the potential that we defined vanishes at infinity, we can apply the Gel'fand–Levitan–Marchenko equation to solve our problem. Let us consider a time-dependent formulation of the scattering. We take the Fourier transform of Eq. (7) [the transform pairs are $\Phi(x, k) \Leftrightarrow \Psi(x, t)$ and $k \Leftrightarrow t$] to obtain

$$\frac{\partial^2}{\partial x^2}\Psi(x, t) - \frac{\partial^2}{\partial t^2}\Psi(x, t) - V(x)\Psi(x, t) = 0, \qquad (10)$$

in which t is the time variable, with the velocity of light $c \equiv 1$. The incident plane wave is represented by the unit impulse

$$\Psi(x, t) = \delta(x - t), \quad x < 0, t < 0, \qquad (11)$$

which produces the reflected transient wave function

$$R(x + t) = \frac{1}{2\pi}\int_{-\infty}^{\infty} r(k)\exp[-ik(x + t)]dk$$
$$+ \sum_{n=1}^{N} A_n \exp[-i\kappa_n(x + t)], \qquad (12)$$

where $k^2 = -\kappa_n^2$ are the discrete eigenvalues of the Schrödinger-type equation [Eq. (7)], $r(k)$ is the complex reflection coefficient, and A_n are arbitrary constants normalizing the wave equation such that

$$\int_{-\infty}^{+\infty} \Phi(x)\Phi^*(x)dx = 1. \qquad (13)$$

The reflected transient is produced only after the incident unit impulse has interacted with the inhomogeneous

core of the optical waveguide, and therefore

$$R(x + t) = 0 \quad \text{for} \quad x + t \leq 0. \quad (14)$$

A linear transform independent of k can now relate the wave amplitude $\Psi(x, t)$ in the core region with the wave amplitude $\Psi_0(x, t)$ in the exterior region:

$$\Psi(x, t) = \begin{cases} \Psi_0(x, t) + \int_{-x}^{x} K(x, \xi')\Psi_0(\xi', t)d\xi' & x > 0 \\ \Psi_0(x, t) & x \leq 0 \end{cases} \quad (15)$$

Here the exterior field is

$$\Psi_0(x, t) = \delta(x - t) + R(x + t). \quad (16)$$

From physical consideration, since $\Psi(x, t)$ is a rightward-moving transient,

$$\Psi(x, t) = 0 \quad \text{for} \quad t < x. \quad (17)$$

Thus the kernel $K(x, t) = 0$ for $t > x$ and $K(x, t) = 0$ for $t \leq -x$. We substitute Eq. (16) into Eqs. (15) and use Eqs. (14) and (17) to obtain the integral equation

$$K(x, t) + R(x + t) + \int_{-x}^{x} K(x, \xi')R(\xi' + t)d\xi' = 0,$$
$$t < x. \quad (18)$$

By substituting Eqs. (15) into Eq. (10), we can show that the kernel $K(x, t)$ satisfies a differential equation of the same form as Eq. (10), provided that the following conditions are imposed:

$$K(x, -x) = 0, \quad (19)$$

$$2\frac{d}{dx}K(x, x) = V(x). \quad (20)$$

We can now see how the solution of the integral Eq. (18) for the function $K(x, t)$ can lead to the synthesis of optical waveguides.

4. DESIGN EXAMPLE 1: ZERO REFLECTION COEFFICIENT

The reflection coefficient characterizes the propagation properties of optical waveguides. A zero reflection coefficient characterizes a system with propagating modes only, whereas a nonzero reflection coefficient characterizes a system with both guided and unguided modes. Let us first consider the special case of a zero reflection coefficient.[8] We substitute Eq. (12) for $r(k) = 0$ in the Gel'fand–Levitan–Marchenko equation [Eq. (18)] to obtain

$$K(x, t) + \sum_{n=1}^{N} A_n \exp[\kappa_n(x + t)]$$
$$+ \sum_{n=1}^{N} A_n \int_{-x}^{x} K(x, \xi)\exp[\kappa_n(t + \xi)]d\xi = 0. \quad (21)$$

It is clear from Eq. (21) that the solution for $K(x, t)$ should have the form[8]

$$K(x, t) = \sum_{n=1}^{N} f_n(x)\exp(\kappa_n t). \quad (22)$$

We substitute Eq. (22) into Eq. (21) to produce a system of equations for $f_n(x)$:

$$A_n \sum_{\nu=1}^{N} \left\{ \frac{\exp[(\kappa_\nu + \kappa_n)x]}{\kappa_n + \kappa_\nu} \right\} f_\nu(x) + f_n(x) + A_n \exp(\kappa_n x) = 0, \quad (23)$$

where $n = 1, 2, \ldots N$. This system can be conveniently written as

$$\mathbf{Af} + \mathbf{B} = 0, \quad (24)$$

where $\mathbf{f}$ and $\mathbf{B}$ are column vectors with f_n and $B_n = A_n \exp(\kappa_n x)$, respectively, and $\mathbf{A}$ is a square matrix with elements

$$A_{\nu n} = \delta_{\nu n} + A_\nu \left\{ \frac{\exp[(\kappa_\nu + \kappa_n)x]}{\kappa_\nu + \kappa_n} \right\}, \quad (25)$$

in which $\delta_{\nu n}$ is a Kronecker delta. The solution for $\mathbf{f}$ is $\mathbf{f} = -\mathbf{A}^{-1}\mathbf{B}$, and from Eq. (22) $K(x, x) = \mathbf{E}^T\mathbf{f}$, where $\mathbf{E}$ is a column vector with element $E_n = \exp(\kappa_n x)$ and T denotes transpose. Now

$$\frac{d}{dx}A_{\nu n} = A_\nu \exp[(\kappa_\nu + \kappa_n)x] = B_n E_n, \quad (26)$$

and so

$$K(x, x) = E_n f_n = -E_n A_{\nu n}^{-1}B_\nu = A_{\nu n}^{-1}\frac{d}{dx}A_{n\nu} \quad (27)$$

when written with subscript notation and the summation convention. The $K(x, x)$ given by Eq. (22) can be recognized in the form

$$K(x, x) = \text{tr}\left(\mathbf{A}^{-1}\frac{d\mathbf{A}}{dx} \right) = \frac{d}{dx}\ln(\det \mathbf{A}), \quad (28)$$

and therefore the potential $V(x)$, according to Eq. (20), is

$$V(x) = -2\frac{d^2}{dx^2}\ln(\det \mathbf{A}). \quad (29)$$

Given N modes with desired propagation constants, we can obtain a potential function as given by Eq. (29). Here we have N degrees of freedom that are due to N arbitrary constants $\{A_n \mid n = 1, 2, \ldots N\}$.

For TE modes the refractive-index profile is simply given by

$$n^2(x) = n_\infty^2 - \frac{V(x)}{k_0^2}, \quad (30)$$

in which k_0 is the free-space wave number. For TM modes obtaining the refractive-index profile is more complicated because it is a solution to a nonlinear differential equation [Eq. (8)]. The nonlinear differential equation can be solved only numerically. First we transform Eq. (8) into a convenient form by setting $\epsilon(x) = \exp[y(x)]$. We then obtain

$$\frac{1}{2}\frac{d^2y(x)}{dx^2} - \frac{1}{4}\left[\frac{dy(x)}{dx} \right]^2 + k_0 \exp[y(x)]$$
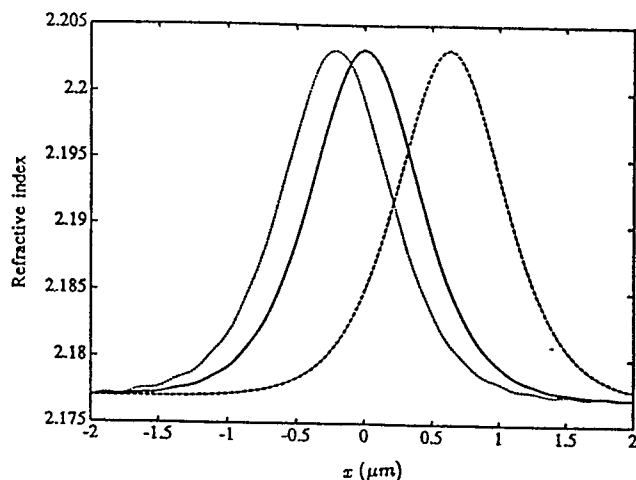$$+ [V(x) - k_0^2 n_\infty^2] = 0. \quad (31)$$

L. S. Tamil and Y. Lin

Fig. 2. Reconstructed refractive-index profiles for a single prescribed TM mode with $\beta_1 = 17.2$ and $A_1 = 2\kappa_1 = 3.7386$, 0.4, and 7, corresponding to the solid, dashed, and dotted curves, respectively.

This is a constant-coefficient equation that yields the refractive-index profile $\sqrt{\epsilon(x)}$, provided that the potential $V(x)$ is given.

To demonstrate some practical examples, let us compute the refractive-index profiles for two cases: the single-mode case and the N-mode case.

For the single-mode case, Eq. (23) becomes

$$A_1 \exp(\kappa_1 x) + f_1(x) + \left[\frac{A_1 \exp(2\kappa_1 x)}{2\kappa_1}\right] f_1(x) = 0. \quad (32)$$

Then the potential has the form

$$V(x) = \frac{-4\kappa_1 A_1 \exp(2\kappa_1 x)}{[1 + A_1 \exp(2\kappa_1 x)/2\kappa_1]^2}, \quad (33)$$

where A_1 is an arbitrary constant. Note that κ_1 can be obtained from

$$\kappa_1^2 = \beta_1^2 - k_0^2 n_\infty^2. \quad (34)$$

For a desired propagation constant β_1, we can get a set of refractive-index profiles corresponding to different arbitrary choices of A_1; see Fig. 2. We use the following data relating to the waveguide: $n(\infty) = n_s = 2.177$, wavelength $\lambda = 0.8$ μm, and $\beta_1 = 17.20$ $(\mu\text{m})^{-1}$. We obtain the refractive-index profiles by solving Eq. (31), using the potential $V(x)$ obtained from Eq. (33). Runge–Kutta's fourth-order approximation is applied in solving Eq. (31).[9] We can see from Fig. 2 that the maximum value of the refractive index lies on the positive side of $x = 0$ when $A_1 < 2\kappa_1$, on the negative side of $x = 0$ when $A_1 > 2\kappa_1$, and at $x = 0$ when $A_1 = 2\kappa_1$.

We substitute $A_1 = 2\kappa_1$ into Eq. (33) to obtain

$$V(x) = -2\kappa_1^2 \operatorname{sech}^2 \kappa_1 x. \quad (35)$$

This potential is everywhere negative and goes to zero as x goes to infinity. Also, the potential is symmetric about its minimum point. We can truncate the potential at the point where the potential is 1% of its maximum value to find the width of the core d. The refractive-index profile corresponding to this potential is shown by the solid curve in Fig. 2.

Similarly, for the N-mode case we need to construct the potential from Eq. (25) first and then solve Eq. (31) for the refractive-index profiles. For a set of prescribed propagation constants, every arbitrary choice of normalization constants will produce a different potential and a corresponding refractive-index profile. To construct a symmetric refractive-index profile with a single peak, we found that the normalization constants $\{A_n \mid n = 1, 2, \ldots N\}$ must satisfy the following equation[10]:

$$A_n = \sqrt{2\kappa_n P_n}, \quad (36)$$

where

$$P_n = (-1)^{n-1} \prod_{\nu=1(\nu \neq n)}^{N} \frac{\kappa_\nu + \kappa_n}{\kappa_\nu - \kappa_n}, \quad n = 1, 2, \ldots N, \quad (37)$$

for the reflectionless case. Here N is the number of guided modes in the planar waveguide. For the case $N = 5$ we use the sets of arbitrary normalization constants $\{A_n \mid n = 1, 2, \ldots N\}$ to compute the refractive-index profiles, and these are shown in Fig. 3. The symmetric
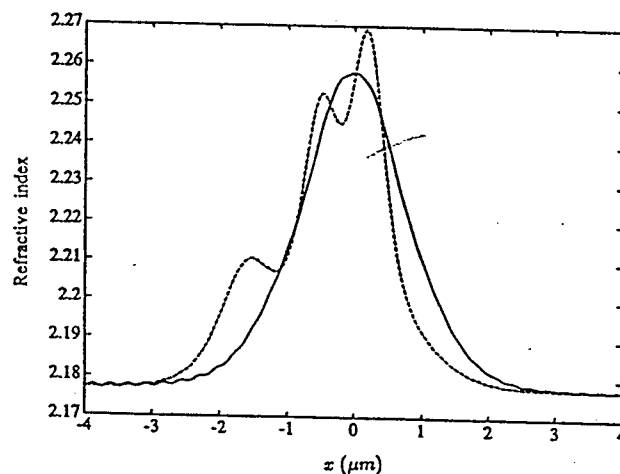

Fig. 3. Reconstructed refractive-index profiles for five prescribed TM modes with $A_n = \{1, 2, 3, 3, 1\}$ (dashed curve) and for A_n satisfying Eq. (36) (solid curve).
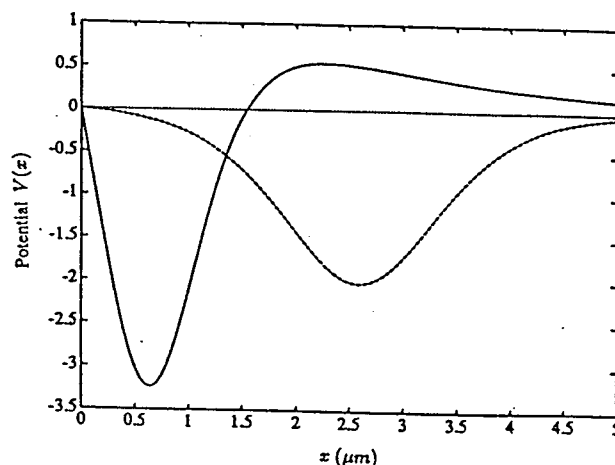

Fig. 4. Potentials of a waveguide characterized by a three-pole reflection coefficient. The solid curve corresponds to $a = 1.0$, $c_1 = 0.8$, and $c_2 = 0.499$. The dashed curve corresponds to $a = 1.0$, $c_1 = 0.05$, $c_2 = 0.1$.

profile obtained from Eq. (36) is shown by the solid curve in the figure.

5. DESIGN EXAMPLE 2: NONZERO REFLECTION COEFFICIENT

In Section 4 we took advantage of the fact that the reflection coefficient was zero, which simplified the problem considerably. Now we are going to solve the problem with a nonzero reflection coefficient. We follow the work of Jordan and Lakshmanasamy.[5]

We take the rational-function approximation for our scattering data. We represent our reflection coefficient by using a three-pole rational function of transverse wave number k[5]. One pole lies on the upper imaginary axis of the complex k plane, which represents a discrete spectrum of the function $R(x + t)$ [Eq. (12)] characterizing the propagating mode. Two symmetric poles lie in the lower half of the k plane, which represent the continuous spectrum of $R(x + t)$ characterizing the unguided modes. The three-pole reflection coefficient can be written as

$$r(k) = \frac{r_0}{(k - k_1)(k - k_2)(k - k_3)}, \qquad (38)$$

where r_0 can be determined by the normalization condition $r(0) = -1$, which ensures total reflection at $k = 0$. k_1 and k_2 have the following forms: $k_1 = -c_1 - ic_2$ and $k_2 = c_1 - ic_2$. The third pole on the positive imaginary axis is $k_3 = ia$.

The pole positions are confined to certain allowed regions that are determined by the law of conservation of energy, which can be represented by $|r(k)|^2 \leq 1$ for all real k; see Fig. 3 of Ref. 5 for details.

It has been shown that the reconstructed potential function $V(x)$ has the following form:

$$V(x) = 2\left[\frac{d[\mathbf{a}^T(x)]}{dx} - \mathbf{a}^T(x)\mathbf{A}^{-1}(x)\frac{d[A(x)]}{dx}\right]\mathbf{A}^{-1}(x)\mathbf{b}, \quad (39)$$

in which $\mathbf{a}$ and $\mathbf{b}$ are column vectors and are given by

$$\mathbf{a}^T(x)$$
$$= [1 \quad x \quad \exp(\eta_1 x) \quad \exp(-\eta_1 x) \quad \exp(\eta_2 x) \quad \exp(-\eta_2 x)], \qquad (40)$$

$$\mathbf{b}^T = [0 \quad 0 \quad 0 \quad 0 \quad 0 \quad -a(c_1^2 + c_2^2)], \qquad (41)$$

where

$$\eta_1 = [\tfrac{1}{2}a^2 + c_2^2 - c_1^2 + \tfrac{1}{2}(a^2 - 4c_2^2)^{1/2}(a^2 + 4c_1^2)^{1/2}]^{1/2}; \qquad (42)$$

$$\eta_2 = [\tfrac{1}{2}a^2 + c_2^2 - c_1^2 - \tfrac{1}{2}(a^2 - 4c_2^2)^{1/2}(a^2 + 4c_1^2)^{1/2}]^{1/2}. \qquad (43)$$

Matrix $\mathbf{A}(x)$ is given by

$$\begin{bmatrix} 0 & 1 & 0 & 0 & 0 & 0 \\ 0 & 0 & f(\eta_1) & a(c_1^2 + c_2^2) & 0 & 0 \\ 0 & 0 & 0 & 0 & f(\eta_2) & a(c_1^2 + c_2^2) \\ 1 & -x & \exp(-\eta_1 x) & \exp(\eta_1 x) & \exp(-\eta_2 x) & \exp(\eta_2 x) \\ 0 & -1 & -\eta_1 \exp(-\eta_1 x) & \eta_1 \exp(\eta_1 x) & \eta_2 \exp(-\eta_2 x) & \eta_2 \exp(\eta_2 x) \\ 0 & 0 & \eta_1^2 \exp(-\eta_1 x) & \eta_1^2 \exp(\eta_1 x) & \eta_2^2 \exp(-\eta_2 x) & \eta_2^2 \exp(\eta_2 x) \end{bmatrix}, \quad (44)$$
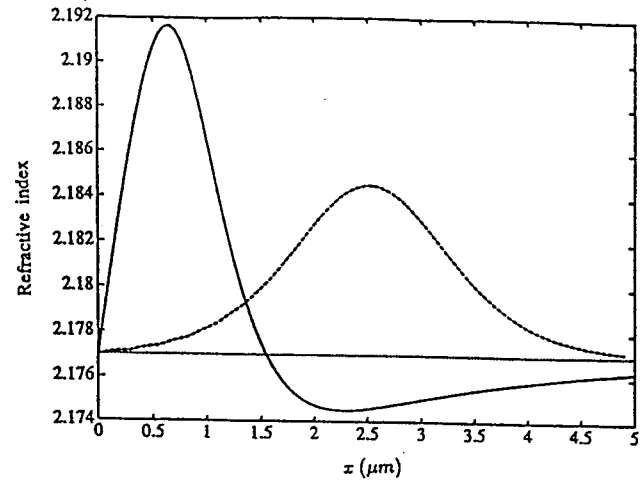

Fig. 5. Reconstructed refractive-index profiles corresponding to the potentials shown in Fig. 4.

where

$$f(x) = x^3 + (2c_2 - a)x^2$$
$$+ (c_1^2 + c_2^2 - 2ac_2)x - a(c_1^2 + c_2^2). \qquad (45)$$

So it is possible to construct the potential from the three poles of the reflection coefficient by means of the above equations. We choose two examples. In example 1, the poles are determined by the parameters $a = 1.0$, $c_1 = 0.8$, and $c_2 = 0.499$; example 2 has different unguided modes characterized by $c_1 = 0.05$, $c_2 = 0.1$, and the same propagating mode characterized by $a = 1.0$. Figure 4 shows the plots of the potential functions for examples 1 and 2. In example 2 we see that the potential is negative everywhere.

Figure 5 shows the refractive index profiles for the TM mode in both of the examples discussed above obtained when one substitutes the potentials into Eq. (31) and solves for $\sqrt{\epsilon(x)}$. We note that a depressed cladding is obtained in example 1, and we also see that the profiles that we find resemble the profiles that we normally find in practical optical waveguides.[11]

6. VERIFICATION BY ANALYSIS

To verify the results obtained by inverse-scattering theory, a finite-difference based analysis scheme is developed here. We use this method to find the propagation constants of the guided TM modes of an optical waveguide with an arbitrary refractive-index profile. Owing to its simplicity and flexibility, this method is proved to be effective.

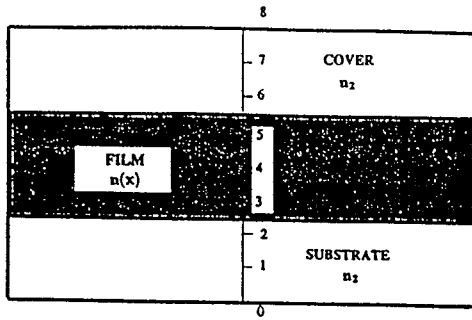We consider a symmetric planar waveguide. For the TM modes we have[5]

Fig. 6. Planar optical waveguide showing grid points in the substrate, the film, and the cover.

$$E_y = H_x = H_z = 0, \tag{46}$$

$$E_x = \left(\frac{\beta}{\omega\epsilon}\right)H_y, \tag{47}$$

$$E_z = -\left(\frac{j}{\omega\epsilon}\right)\frac{\partial H_y}{\partial x}, \tag{48}$$

with the H_y component obeying the wave equation

$$n^2\frac{\partial}{\partial x}\left(\frac{1}{n^2}\frac{\partial H_y}{\partial x}\right) = [\beta^2 - n^2(x)k_0^2]H_y(x). \tag{49}$$

For the one-dimensional graded-index planar waveguide, the refractive index is a function of x, and the wave equation can be transformed into

$$\frac{d^2H_y(x)}{dx^2} - \frac{2}{n(x)}\frac{d[n(x)]}{dx}\frac{dH_y(x)}{dx}$$
$$+ [n^2(x)k_0^2 - \beta^2]H_y(x) = 0. \tag{50}$$

If H_y and its derivative are single-valued, finite, and continuous functions of x, we have the following finite-difference approximations to the differentials:

$$\frac{dH}{dx} \simeq \frac{H_{i+1} - H_{i-1}}{2h}, \tag{51}$$

$$\frac{d^2H}{dx^2} \simeq \frac{H_{i+1} - 2H_i + H_{i-1}}{h^2}, \tag{52}$$

in which we have used H instead of H_y for simplicity. We have $H_{i-1} = H(x - h)$, $H_i = H(x)$, and $H_{i+1} = H(x + h)$, in which h is the distance between the grid points and i is the index of the grid point. We obtain Eq. (53) by substituting the finite-difference approximation of the first and the second derivatives of H into Eq. (50):

$$\left(\frac{1}{h^2} + \frac{1}{n_i h}\frac{dn_i}{dx}\right)H_{i-1} + \left(n_i^2 k_0^2 - \beta^2 - \frac{2}{h^2}\right)H_i$$
$$+ \left(\frac{1}{h^2} - \frac{1}{n_i h}\frac{dn_i}{dx}\right)H_{i+1} = 0, \tag{53}$$

in which $n_i = n(ih)$ and the value of dn_i/dx is the derivative of the refractive index n at $x = ih$.

We have chosen three grid points in each region: the substrate, the film, and the cover, for the purpose of illus-

tration (see Fig. 6). For the case considered here the boundary conditions are

$$H_0 = 0, \tag{54}$$

$$H_8 = 0; \tag{55}$$

that is, the field vanishes at the ends of the cladding. An absorbing boundary condition would have been more appropriate; however, it is not used here.

We can write a finite-difference equation at every grid point from $i = 1$ to $i = 7$. We use the function $f(i)$ to represent the derivative of $n(i)$ that is obtained again by a finite-difference approximation and is denoted by

$$f(i) = \frac{dn(i)}{dx}. \tag{56}$$

Note that f goes to zero in the substrate and in the cover region. The refractive indices in the substrate and the cover are represented by n_s and n_c, respectively. At $i = 1$ $H_0 = 0$, and so

$$\left(n_s^2 k_0^2 - \beta^2 - \frac{2}{h^2}\right)H_1 + \frac{1}{h^2}H_2 = 0. \tag{57}$$

At $i = 2$,

$$\frac{1}{h^2}H_1 + \left(n_s^2 k_0^2 - \beta^2 - \frac{2}{h^2}\right)H_2 + \frac{1}{h^2}H_3 = 0. \tag{58}$$

In the film, at $i = 3$,

$$\left[\frac{1}{h^2} + \frac{1}{n(1)h}f(1)\right]H_2 + \left[n^2(1)k_0^2 - \beta^2 - \frac{2}{h^2}\right]H_3$$
$$+ \left[\frac{1}{h^2} - \frac{1}{n(1)h}f(1)\right]H_4 = 0. \tag{59}$$

At $i = 4$,

$$\left[\frac{1}{h^2} + \frac{1}{n(2)h}f(2)\right]H_3 + \left[n^2(2)k_0^2 - \beta^2 - \frac{2}{h^2}\right]H_4$$
$$+ \left[\frac{1}{h^2} - \frac{1}{n(2)h}f(2)\right]H_5 = 0. \tag{60}$$

At $i = 5$,

$$\left[\frac{1}{h^2} + \frac{1}{n(3)h}f(3)\right]H_4 + \left[n^2(3)k_0^2 - \beta^2 - \frac{2}{h^2}\right]H_5$$
$$+ \left[\frac{1}{h^2} - \frac{1}{n(3)h}f(3)\right]H_6 = 0. \tag{61}$$

At $i = 6$,

$$\frac{1}{h^2}H_6 + \left[n_c^2 k_0^2 - \beta^2 - \frac{2}{h^2}\right]H_6 + \frac{1}{h^2}H_7 = 0, \tag{62}$$

At $i = 7$, since $H_8 = 0$, we have

$$\frac{1}{h^2}H_6 + \left(n_c^2 k_0^2 - \beta^2 - \frac{2}{h^2}\right)H_7 = 0. \tag{63}$$

For convenience, we can rewrite these finite-difference equations as a matrix equation:

$$\mathbf{AH} = \begin{bmatrix} a_{11} - \beta^2 & a_{12} & 0 & 0 & 0 & 0 & 0 \\ a_{21} & a_{22} - \beta^2 & a_{23} & 0 & 0 & 0 & 0 \\ 0 & a_{32} & a_{33} - \beta^2 & a_{34} & 0 & 0 & 0 \\ 0 & 0 & a_{43} & a_{44} - \beta^2 & a_{45} & 0 & 0 \\ 0 & 0 & 0 & a_{54} & a_{55} - \beta^2 & a_{56} & 0 \\ 0 & 0 & 0 & 0 & a_{65} & a_{66} - \beta^2 & a_{67} \\ 0 & 0 & 0 & 0 & 0 & a_{76} & a_{77} - \beta^2 \end{bmatrix} \begin{bmatrix} H_1 \\ H_2 \\ H_3 \\ H_4 \\ H_5 \\ H_6 \\ H_7 \end{bmatrix} = 0, \quad (64)$$

in which the elements of matrix **A** are defined by

$$a_{12} = -\frac{2}{h^2} + n_2^2 k_0^2 = a_{N,N}, \quad (65)$$

$$a_{12} = \frac{1}{h^2} = a_{N,N-1}, \quad (66)$$

and, for $2 \leq i < N$,

$$a_{i,i-1} = \begin{cases} \dfrac{1}{h^2} & 2 \leq i \leq N_1, \quad N_1 + N_2 < i < N \\ \dfrac{1}{h^2} + \dfrac{f(i)}{n(i)h} & N_1 < i \leq N_1 + N_2 \end{cases}, \quad (67)$$

$$a_{i,i+1} = \begin{cases} \dfrac{1}{h^2} & 2 \leq i \leq N_1, \quad N_1 + N_2 < i < N \\ \dfrac{1}{h^2} - \dfrac{f(i)}{n(i)h} & N_1 < i \leq N_1 + N_2 \end{cases}, \quad (68)$$

$$a_{i,i} = \begin{cases} n_2^2 k_0^2 - \dfrac{2}{h^2} & 2 \leq i \leq N_1, \quad N_1 + N_2 < i < N \\ n^2(i) k_0^2 - \dfrac{2}{h^2} & N_1 < i \leq N_1 + N_2 \end{cases} \quad (69)$$

$f(i)$ is the derivative of the refractive index at $x = ih$; N_1, N_2, and N_3 are the number of grid points in the substrate, the film, and the cover, respectively; and $N = N_1 + N_2 + N_3$ is the total number of grid points. The other elements of the matrix that are not defined above are zeros.

The matrix **A** can now be split into

$$\mathbf{A} = \mathbf{B} - \beta^2 \mathbf{I}, \quad (70)$$

where **I** is the identity matrix and the matrix **B** has the following simple form:

$$\mathbf{B} = \begin{bmatrix} a_{11} & a_{12} & 0 & 0 & 0 & 0 & 0 \\ a_{21} & a_{22} & a_{23} & 0 & 0 & 0 & 0 \\ 0 & a_{32} & a_{33} & a_{34} & 0 & 0 & 0 \\ 0 & 0 & a_{43} & a_{44} & a_{45} & 0 & 0 \\ 0 & 0 & 0 & a_{54} & a_{55} & a_{56} & 0 \\ 0 & 0 & 0 & 0 & a_{65} & a_{66} & a_{67} \\ 0 & 0 & 0 & 0 & 0 & a_{76} & a_{77} \end{bmatrix}. \quad (71)$$

Equation (64) can now be rewritten in the form

$$\mathbf{B} - \beta^2 \mathbf{IH} = 0. \quad (72)$$

To find the propagation constants of the guided TM modes, we must solve the eigenvalue problem of Eq. (72),

which has a nontrivial solution if and only if β^2 are eigenvalues of **B**. So, finally, we have

$$\{\beta\} = \sqrt{\text{eig}[\mathbf{B}]} \quad (73)$$

for both odd and even modes. For the TE modes the situation is much easier, since the wave equation has a simpler form than that for the TM modes. The field component E_y obeys the wave equation[6]

$$\frac{\partial^2 E_y(x)}{\partial x^2} = [\beta^2 - n^2(x) k_0^2] E_y(x). \quad (74)$$

We can find a matrix expression similar to the one we found for the TM modes. In the TE case we need not calculate the derivative of the refractive-index profile.

For the given refractive-index profile distribution $n = n(x)$ the matrix **B** can be constructed and the propagation constants $\{\beta\}$ can be obtained by solving for the eigenvalues of this matrix.

Before we attempt to analyze the refractive-index profiles obtained by the application of inverse-scattering theory, we would like to see whether the finite-difference technique developed here provides the right result. To do that, we have applied the technique to various refractive-index profiles, such as parabolic and Gaussian, for which results are already available in the literature.[12] The results corresponding to TM modes are given in Tables 1 and 2 and show that our analysis technique is accurate and powerful.

Having established the accuracy of the finite-difference technique, now we can use this technique on the arbitrary refractive-index profiles that we have obtained. Figure 7 shows the dispersion characteristics for the refractive-index profile with the single symmetric peak shown in Fig. 3. The normalized frequency V has been determined from the waveguide thickness and the free-space wavelength of the propagating modes. Here we have $V = k_0 d \sqrt{n_1^2 - n_2^2} = 37.6883$. The normalized propagation constant that we used here is defined by

$$b = \frac{(\beta/k_0)^2 - n_2^2}{n_1^2 - n_2^2}. \quad (75)$$

Here n_2 is the refractive index of the cladding and n_1 is the maximum refractive index of the core. The number of TM modes present is the same number that we started with in reconstructing the profile. When analyzed, the refractive-index profiles corresponding to the nonzero reflection coefficient, as shown in Fig. 5, yield the dispersion characteristics shown in Fig. 8. Again we see the consistency in the number of modes obtained by analysis and the number of modes used in the synthesis of the profile.

Table 1. Mode Spectra β_γ/k_0 (TM) of Symmetric Truncated Parabolic Index Profile of A_g^+-Diffused Waveguide with $n_2 = 1.5125$, $n_1 = 1.5991$, $\lambda = 0.6328$ μm, and Thickness $d = 9.1400$ μm

Mode Number (γ)	β_γ/k_0 from Ref. 12	β_γ/k_0 from Finite-Difference Method	
		$N_2 = 84^a$	$N_2 = 168^a$
0	1.5966	1.5966	1.5966
1	1.5915	1.5915	1.5915
2	1.5864	1.5864	1.5864
3	1.5813	1.5813	1.5813
4	1.5762	1.5762	1.5762
5	1.5711	1.5711	1.5711
6	1.5659	1.5658	1.5659
7	1.5607	1.5604	1.5605
8	1.5556	1.5546	1.5548
9	1.5503	1.5498	1.5499
10	1.5451	1.5439	1.5443
11	1.5399	1.5387	1.5390
12	1.5346	1.5326	1.5336
13	1.5294	1.5288	1.5290
14	1.5241	1.5228	1.5231
15	1.5188	1.5139	1.5143

$^a N_2$ is the number grid points in the core.

Table 2. Mode Spectra β_γ/k_0 (TM) of Symmetric Truncated Gaussian Index Profile of A_g^+-Diffused Waveguide with $n_2 = 1.5125$, $n_1 = 1.6014$, $\lambda = 0.6328$ μm, and Thickness $d = 9.1700$ μm

Mode Number (γ)	β_γ/k_0 from Ref. 12	β_γ/k_0 from Finite-Difference Method	
		$N_2 = 84^a$	$N_2 = 168^a$
0	1.5984	1.5984	1.5984
1	1.5925	1.5925	1.5925
2	1.5867	1.5868	1.5867
3	1.5811	1.5812	1.5811
4	1.5756	1.5757	1.5757
5	1.5702	1.5704	1.5703
6	1.5649	1.5651	1.5650
7	1.5596	1.5598	1.5596
8	1.5545	1.5542	1.5544
9	1.5494	1.5487	1.5490
10	1.5444	1.5424	1.5431
11	1.5395	1.5387	1.5390
12	1.5347	1.5341	1.5341
13	1.5297	1.5283	1.5284
14	1.5251	1.5220	1.5222
15	1.5204	1.5192	1.5195

$^a N_2$ is the number grid points in the core.

Though we have shown that the number of modes is correct, this is not sufficient proof that the reconstructed refractive-index profiles have the same propagation constants for each of the specified modes. To check this, we have compared the propagation constants of various modes that we used in reconstructing the refractive-index profile of the waveguide with the propagation constants obtained by analysis for the normalized frequency at which the propagation constants are prescribed. The results are shown in Table 3, and the last two columns of the table agree well. This shows that the inverse technique outlined here can be used to synthesize waveguides with prescribed TM modes.

7. DISCUSSION AND CONCLUSIONS

We have developed a method based on inverse-scattering theory that can be used to design planar optical waveguides that transmit a prescribed number of TM modes with prescribed propagation constants. The results have been verified by means of finite-difference analysis. This procedure, in conjunction with the technique for designing planar optical waveguides for prescribed TE modes developed in Refs. 4 and 5, provides the complete inverse-scattering procedure for designing planar optical waveguides with prescribed propagation characteristics. However, it should be mentioned that only the characteristics of one kind of mode (TE or TM) can be prescribed in a waveguide, as the two kinds of mode are governed by two different differential equations.

One important question that should be answered when we fabricate actual waveguides with refractive-index profiles obtained with the technique described here is with what precision the $n(x)$ should be fabricated to provide the desired mode configuration. To answer this question we have changed $V(x)$ [$V(x)$ is related to $n(x)$ through Eq. (30)] uniformly over the spatial distance x by 1%, 5%, and 10%
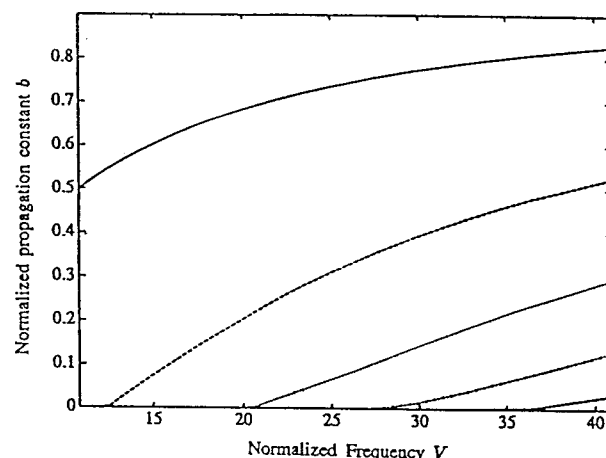

Fig. 7. Dispersion characteristics of the reconstructed refractive-index profile shown as the solid curve in Fig. 3.
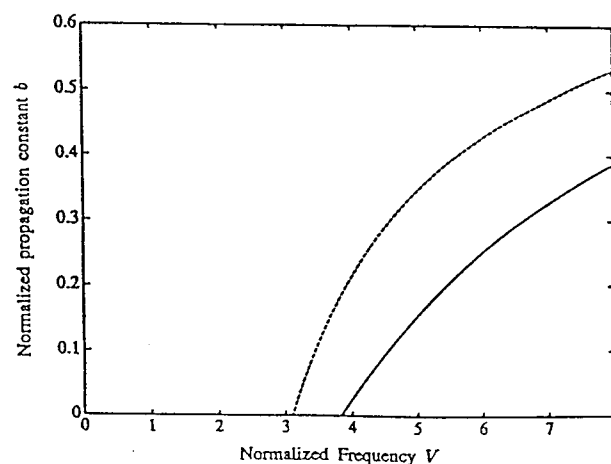

Fig. 8. Dispersion characteristics of the reconstructed refractive-index profiles shown in Fig. 5.

Table 3. Prescribed TM Mode Spectra Used in Reconstructing Refractive Index of Planar Waveguide and Spectra Obtained by Authors

Number of Modes (N)	Mode Number (γ)	Prescribed Mode Spectra β_γ/k_0	β_γ/k_0 Obtained by Our Analysis
1	0	2.18997	2.18995
2	0	2.20556	2.20553
	1	2.18417	2.18398
3	0	2.20926	2.20916
	1	2.19140	2.19100
	2	2.18061	2.18036
5	0	2.21288	2.21266
	1	2.20003	2.19968
	2	2.18998	2.18968
	3	2.18278	2.18254
	4	2.17845	2.17797
7	0	2.21466	2.21452
	1	2.20473	2.20449
	2	2.19630	2.19606
	3	2.18927	2.18915
	4	2.18397	2.18379
	5	2.18010	2.17997
	6	2.17778	2.17753

Table 4. Change in Propagation Constant from Uniform Change in $V(x)$ Along x

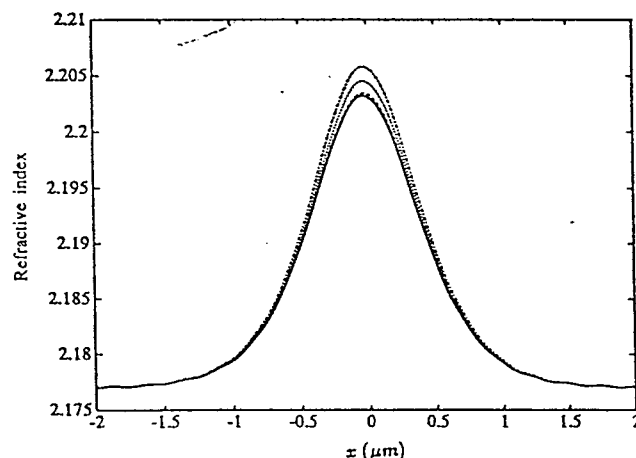|	Effective Index (β/k_0) Obtained by Our Analysis			
Prescribed Effective Index (β/k_0)	$\dfrac{\Delta V(x)}{V(x)} = 0\%$	$\dfrac{\Delta V(x)}{V(x)} = 1\%$	$\dfrac{\Delta V(x)}{V(x)} = 5\%$	$\dfrac{\Delta V(x)}{V(x)} = 10\%$
2.18997	2.18995	2.18998	2.19016	2.19024

Fig. 9. Refractive-index profile corresponding to a uniform change in $V(x)$ along x. The original profile corresponds to the solid curve. Uniform changes of 1%, 5%, and 10% correspond to the dashed, dotted, and dashed–dotted curves, respectively.

and have computed the corresponding change in the propagation constants for a typical single-mode profile. Figure 9 is a plot of a refractive-index profile corresponding to a uniform change in $V(x)$ along x, and Table 4 provides the computed results of changes in the propagation constant β due to the uniform change in $V(x)$ along x. We see that a change in $\Delta V/V$ in the range of 1–5% does not significantly affect the mode characteristics of the waveguide.

It is also important to analyze the effect of the arbitrary constants A_n on the shape of the resultant refractive-index

profiles. Figure 10 shows the variation in the shape of the refractive index as a function of changes in the choice of the constants $\{A_n \mid n = 1, 2, \ldots N\}$. Our inference is that the shape is not highly sensitive to the changes in the constants A_n.

The technique developed here may find application in the design of waveguiding structures for the spatial transmission of images and for optical interconnections.
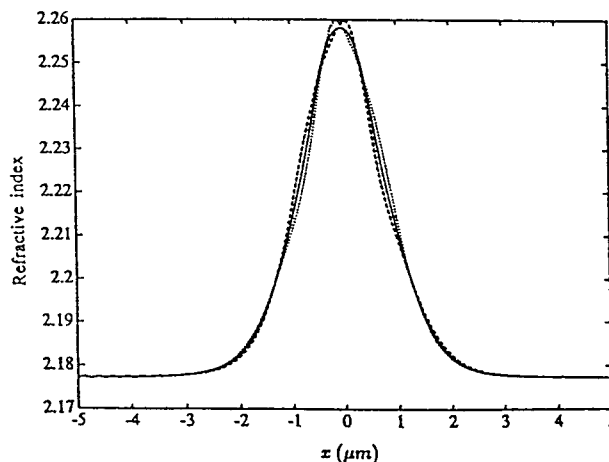

Fig. 10. Refractive-index profile (five modes) with change of values for the constants A_n. A_n satisfying Eq. (36) is shown by the solid curve. An increase of A_1, A_2, and A_3 by 10% and a decrease of A_4 and A_5 by 10% is shown by the dashed curve. A decrease of A_1, A_2, and A_3 by 10% and an increase of A_4 and A_5 by 10% is shown by the dotted curve.

L. S. Tamil and Y. Lin

ACKNOWLEDGMENTS

REFERENCES

1. I. M. Gel'fand and B. M. Levitan, "On the determination of a differential equation by its spectral function," Transl. Am. Math. Soc. Ser. 21, 253–304 (1955).
2. V. A. Marchenko, "Concerning the theory of a differential operator of second order," Dokl. Vses. Akad. Skh. Nauk. T2, 457–463 (1950).
3. D. Marcuse, *Light Transmission Optics* (Van Nostrand, Princeton, N.J., 1972), pp. 100–105.
4. S. P. Yukon and B. Bendow, "Design of waveguides with prescribed propagation constants," J. Opt. Soc. Am. 70, 172–179 (1980).
5. A. K. Jordan and S. Lakshmanasamy, "Inverse scattering theory applied to the design of single-mode planar optical waveguides," J. Opt. Soc. Am. A 6, 1206–1212 (1989).
6. T. Tamir, *Guided-Wave Optoelectronics* (Springer-Verlag, New York, 1990), Chap. 2.
7. I. Kay, "The inverse scattering problem," Rep. EM-74 (New York University, New York, 1955).
8. I. Kay and H. Moses, "Reflectionless transmission through dielectrics and scattering potentials," J. Appl. Phys. 27, 1503–1508 (1956).
9. H. Levy and E. A. Baggott, *Numerical Solution of Differential Equations* (Springer-Verlag, New York, 1976).
10. P. Deift and E. Trubowitz, "Inverse scattering on the line," Comm. Pure Appl. Math. 32, 121–251 (1979).
11. T. Okoshi, *Optical Fibers* (Academic, New York, 1976), Chap. 7.
12. I. Savatinova and E. Nadjakov, "Modes in diffused optical waveguides (parabolic and Gaussian models)," Appl. Phys. 8, 245–250 (1975).

Appendix B

D. W. Mills and L. S. Tamil, "Analysis of Planar Optical Waveguides Using Scattering Data"

Journal of the Optical Society of America A, Vol. 9, No. 10, pp. 1769-1778, Oct. 1992

Analysis of planar optical waveguides using scattering data

Duncan W. Mills and Lakshman S. Tamil*

*Erik Jonsson School of Engineering and Computer Science and Center for Applied Optics,
University of Texas at Dallas, BE28, Richardson, Texas 75083–0688*

Gradient-index planar optical waveguides with exponential and sech² x refractive-index profiles are analyzed. By using a scattering framework, reflection and transmission coefficients for the infinite exponential profile are derived, and these scattering data are analyzed to obtain mode propagation constants and describe the effects of varying the height of the refractive-index profile. The theory is then developed to account for truncations of refractive-index profiles, the effects of a finite core width on the propagation constants for sech² x potentials are illustrated, the behavior of the bound modes in response to variations in the width of the waveguide core is described, and the appearance of leaky modes for the truncated structure is discussed.

1. INTRODUCTION

Planar dielectric waveguides are the basic structures in guided-wave photonic components and photonic integrated circuitry. Most of the processes used for fabricating dielectric waveguides, the diffusion and ion implantation techniques in particular, lead to dielectric-waveguide layers whose refractive indices vary gradually over the cross section. In many applications such graded-index profiles have advantages over their step-index counterparts. The index may be graded to reduce multimode dispersion[1] or designed to provide a larger core width, allowing for stronger confinement of the fundamental guided mode.[2] In turn, the refractive-index profile and the core width significantly affect the spectrum of propagation constants.[3,4]

The analysis of planar optical devices with gradient refractive-index profiles can be carried out by using a number of standard methods. When analytic or semianalytic techniques are used, the method employed will depend on whether the effects being studied are merely perturbations of a waveguide with known solutions or are stronger variations that require new solutions. A limited number of refractive-index profiles, such as the parabolic, exponential, and hyperbolic-secant types, allow for exact analytic solutions when they are considered infinite in extent, but analyzing the effect of a finite core width, which is a necessary part of any practical design, requires more elaborate techniques.

In this paper, efficient, exact analysis of the effects of altering parameters related to the waveguide geometry is carried out by analyzing the transmission coefficient of two waveguide structures. First, we consider the effects of varying the depth of an infinitely wide exponential profile, and, after formulating the transmission coefficient of a truncated structure, we apply a similar analysis to examine the effects of a finite core width on the mode structure of a truncated sech² x profile. In both cases we study the phase of the transmission coefficient to determine the number of bound modes, and it is shown that the imaginary part of the transmission coefficient provides useful information regarding critical parameters of the waveguide (depth of the refractive index, core width) at the mode cutoff points.

2. PLANAR-WAVEGUIDE THEORY

Consider the planar graded-index waveguide consisting of an inhomogeneous core with a varying refractive index $n(x)$ surrounded by two cladding layers of constant refractive index n_2 as shown in Fig. 1. This structure supports electromagnetic fields governed by the vector wave equations

$$\nabla^2 \mathbf{E} + \nabla\left[\mathbf{E} \cdot \frac{\nabla n^2(x)}{n^2(x)}\right] - \frac{n^2(x)}{c^2}\frac{\partial^2 \mathbf{E}}{\partial t^2} = 0, \quad (1)$$

$$\nabla^2 \mathbf{H} + \frac{1}{n^2(x)}\nabla n^2(x) \times (\nabla \times \mathbf{H}) - \frac{n^2(x)}{c^2}\frac{\partial^2 \mathbf{H}}{\partial t^2} = 0, \quad (2)$$

in which $\mathbf{E}$ and $\mathbf{H}$ are the electric and magnetic fields, respectively, the refractive-index profile $n(x)$ is a function of only the x coordinate, and c is the velocity of light in free space. The waveguide supports TE and TM modes that are assumed to have the form

$$E_y(x, z, t) \equiv E_y(x)\exp(i\beta z)\exp(-i\omega t) \quad \text{(TE)}, \quad (3)$$

$$E_x(x, z, t) \equiv E_x(x)\exp(i\beta z)\exp(-i\omega t) \quad \text{(TM)}, \quad (4)$$

where z is the direction of propagation, ω is the frequency, and β is the longitudinal propagation constant. It has been assumed that the waveguide is infinite in extent along the y axis, reducing the vector wave equations to[5]

$$\frac{d^2 E_x}{dx^2} + \frac{d}{dx}\left[\frac{1}{n^2(x)}\frac{dn^2(x)}{dx}E_x(x)\right]$$
$$+ [k_0^2 n^2(x) - \beta^2]E_x(x) = 0 \quad \text{(TM)}, \quad (5)$$

$$\frac{d^2 E_y}{dx^2} + [k_0^2 n^2(x) - \beta^2]E_y = 0 \quad \text{(TE)}. \quad (6)$$

Here k_0 is the free-space wave number. The equation for the TE field takes the form of a Schrödinger equation, which is particularly well suited to analysis using scatter-
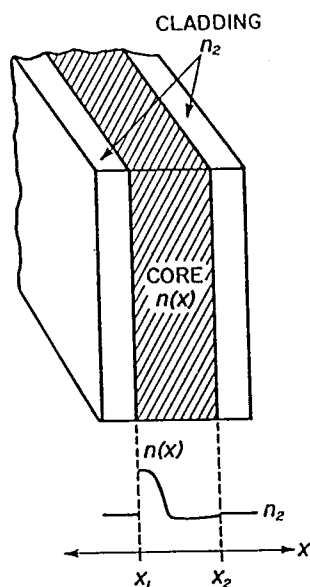
D. W. Mills and L. S. Tamil

Fig. 1. Planar dielectric waveguide consisting of a core with graded refractive index surrounded by a cladding with constant refractive index.

ing data; for the purposes of this paper attention will be confined to the TE modal fields described by Eq. (6).

Defining the complex transverse propagation constant $k (\equiv k_r + ik_i)$ as

$$k^2 = k_0^2 n_2^2 - \beta^2 \qquad (7)$$

brings Eq. (6) into the form

$$\frac{d^2 E_y}{dx^2} + [k^2 - v(x)]E_y = 0, \qquad (8)$$

whose potential

$$v(x) \equiv k_0^2[n_2^2 - n^2(x)] \qquad (9)$$

varies across the waveguide core and vanishes in the cladding. Equation (9) clearly illustrates how the depth of the potential may be varied by changing the wavelength, altering the refractive-index profile, or both. In this scheme the mode cutoff condition, $\beta = k_0 n_2$, is obtained when

$$k = 0. \qquad (10)$$

The discrete set of guided modes characterized by $k_0 n_2 < \beta < k_0 n_1$, or, equivalently, by $0 < \text{Im } k < \text{Im}[k_0(n_1^2 - n_2^2)^{1/2}]$, is represented by points along the positive imaginary axis of the complex k plane. In scattering theory the guided modes are termed bound states and are distinguished by their discrete eigenvalues k.

3. MODELING BY SCATTERING COEFFICIENTS

A. Scattering Coefficients and Jost Solutions
The potentials considered here satisfy the Faddeev condition[6]

$$\int_{-\infty}^{+\infty} (1 + |x|)|v(x)|dx < \infty, \qquad (11)$$

which is valid for well-behaved nonsingular potentials, which are suitable for use as refractive-index profiles, including truncated potentials. In effect, this condition dictates that $v(x)$ should fall off at infinity at least as fast as $1/x^{2+\epsilon}$ for any positive definite ϵ. This implies, as a weaker condition,

$$\lim v(x) \rightarrow 0, \qquad x \rightarrow \pm\infty. \qquad (12)$$

A plane wave $\exp(+ikx)$ incident upon the potential from $x = -\infty$ will give rise to a reflected portion taking the form

$$r_-(k)\exp(-ikx) \qquad (13)$$

as $x \rightarrow -\infty$ as well as to a transmitted wave

$$t_-(k)\exp(+ikx) \qquad (14)$$

as $x \rightarrow \infty$ (see Fig. 2).[7] An alternative (but equivalent) viewpoint is provided by the coefficients $r_+(k)$ and $t_+(k)$ shown in the same figure.

The Schrödinger equation admits a pair of Jost solutions, denoted $f_+(k, x)$ and $f_-(k, x)$, defined according to their asymptotic behavior:

$$\lim_{x \rightarrow +\infty} f_+(k, x)\exp(-ikx) = \lim_{x \rightarrow -\infty} f_-(k, x)\exp(+ikx) = 1. \qquad (15)$$

The pairs $\{f_+(k, x), f_+(-k, x)\}$ and $\{f_-(k, x), f_-(-k, x)\}$ comprise sets of linearly independent solutions to the Schrödinger equation, permitting construction of the linear combinations

$$f_+(k, x) = a(k)f_-(-k, x) + b(k)f_-(k, x),$$
$$f_-(k, x) = c(k)f_+(-k, x) + d(k)f_+(k, x). \qquad (16)$$

Matching the solutions at arbitrary x provides

$$t_\pm(k)f_\mp(k, x) = f_\pm(-k, x) + r_\pm(k)f_\pm(k, x). \qquad (17)$$

Comparing Eqs. (16) and (17) gives

$$a(k) \equiv \frac{1}{t_-(k)}, \qquad b(k) \equiv \frac{r_-(k)}{t_-(k)},$$

$$c(k) \equiv \frac{1}{t_+(k)}, \qquad d(k) \equiv \frac{r_+(k)}{t_+(k)}. \qquad (18)$$

Equations (16) generate a set of four consistency relations among the coefficients. The first two,

$$a(k)c(-k) + b(k)d(k) = 1,$$
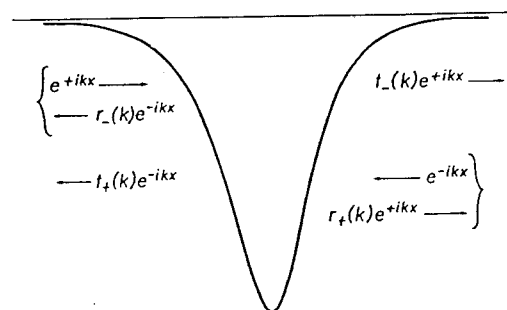$$a(k)d(-k) + b(k)c(k) = 0, \qquad (19)$$

Fig. 2. Scattering by an arbitrary potential $v(x)$: plane waves from $x = \pm\infty$ produce the scattering data $r_\pm(k), t_\pm(k)$.

44

arise when the second of Eqs. (16) is substituted into the first. The reverse substitution gives

$$c(k)a(-k) + d(k)b(k) = 1,$$

$$c(k)b(-k) + d(k)a(k) = 0. \qquad (20)$$

The Wronskian, defined as $W[f, g] \equiv fg' - gf'$ (the prime denoting differentiation with respect to the coordinate), provides a set of relations

$$\frac{2ik}{t_-(k)} = \frac{2ik}{t_+(k)} = W[f_-(k, x), f_+(k, x)] \qquad (21)$$

so that $t_-(k) = t_+(k) \equiv t(k)$, a result that is a direct consequence of the asymptotic behavior stipulated in relation (12). In addition,

$$2ik \frac{r_\pm(k)}{t(k)} = \mp W[f_\mp(k, x), f_\pm(-k, x)] \qquad (22)$$

follows from Eqs. (16) and (21).

B. Guided Modes

For guided modes the Jost solutions reduce to the bound-state wave functions. For bound states one seeks the asymptotic behavior

$$E_y^{bound}(x) \sim \exp(\mp\kappa x), \qquad x \to \pm\infty \qquad (\kappa > 0), \qquad (23)$$

a condition satisfied by the Jost solutions when they are proportional, i.e., where the Wronskian [Eq. (21)] vanishes. This occurs [see Eqs. (16)] at values of $k(\equiv i\kappa)$ such that

$$\frac{1}{t(k)} = 0 ; \qquad (24)$$

that is, the bound-state eigenvalues correspond to the poles of $t(k)$ that lie upon the positive Im k axis. The Jost solutions are related by

$$f_+(i\kappa, x) = b(i\kappa)f_-(i\kappa, x),$$

$$f_-(i\kappa, x) = d(i\kappa)f_+(i\kappa, x). \qquad (25)$$

The consistency relation, Eqs. (19), takes the form

$$b(i\kappa)d(i\kappa) = 1. \qquad (26)$$

The corresponding normalized fields are then

$$E_y^{bound}(x) = c_+ f_+(i\kappa, x) \equiv c_- f_-(i\kappa, x), \qquad (27)$$

where

$$c_- = c_+ b(i\kappa), \qquad c_+ = c_- d(i\kappa). \qquad (28)$$

C. Leaky Modes

A discrete set of poles representing leaky modes is in general present in the lower half of the complex k plane. In the ray picture the guided modes of Subsection 3.B correspond to rays that are trapped in the guide by total internal reflection. The refracting leaky modes, on the other hand, correspond to quasi-trapped rays that proceed along the waveguide, outside the critical angle for total internal reflection but nonetheless persisting for some distance along the guide, since only a fraction of their power leaks away each time the ray is refracted at the core–cladding

interface.[8] Close to the source the leaky modes represent a significant fraction of the launched field. At large distances along the waveguide their contribution is significantly reduced, decaying exponentially at a rate that is dependent on the refractive-index profile.[9] In scattering terminology these are referred to as resonant states.

Consider a pole in the lower half of the complex plane,

$$k \equiv \rho_r + i\rho_i \qquad (\rho_i < 0). \qquad (29)$$

Inverting Eq. (7) for the propagation constant β, one obtains

$$\beta = [k_0^2 n_2^2 + \rho_i^2 - \rho_r^2 - i(2\rho_r\rho_i)]^{1/2} \equiv \beta_r + i\beta_i, \qquad (30)$$

so that the leaky-mode field [Eq. (3)] takes the form

$$E_y(x, z) = E_y(x)\exp(-\beta_i z)\exp(i\beta_r z). \qquad (31)$$

According to Eq. (30), the rate of decay is a function of both ρ_r and ρ_i. In general, $\beta_i > 0$, and so the field in Eq. (31) represents a decaying wave propagating in the positive z direction.

The leaky modes, as they apply here, are a direct consequence of truncating the refractive-index profile by introducing core–cladding interfaces that act as refracting boundaries. They will be reconsidered in Subsection 4.C, following the discussion of truncation.

Figure 3 summarizes the pole positions for a typical waveguide potential. Included are the bound states along the positive Im k axis, the complex lower-k-plane poles representing leaky modes, and poles along the negative Im k axis.

D. Waveguide Properties from Reflection and Transmission Coefficients

For the cases considered in this paper $t(k)$ is devoid of zeros on the upper half-plane and exhibits only simple poles (see Ref. 10). Levinson[11] observed (for the half-line) that the number of bound states N can be ascertained by analyzing the phase of the transmission coefficient. This can be extended to the full line, as considered here (see Ref. 10). Consider the contour integral

$$-\frac{1}{2\pi i} \int_C d \ln t(k) \equiv \frac{1}{2\pi i} \int_C \frac{-dt(k)/dk}{t(k)} dk = \sum_{p=1}^{N} \rho_p = N, \qquad (32)$$

where C is a closed counterclockwise contour enclosing all the N simple poles of $t(k)$ in the upper half-plane. Equa-
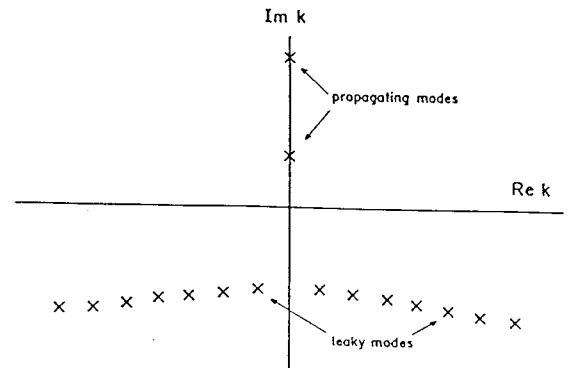

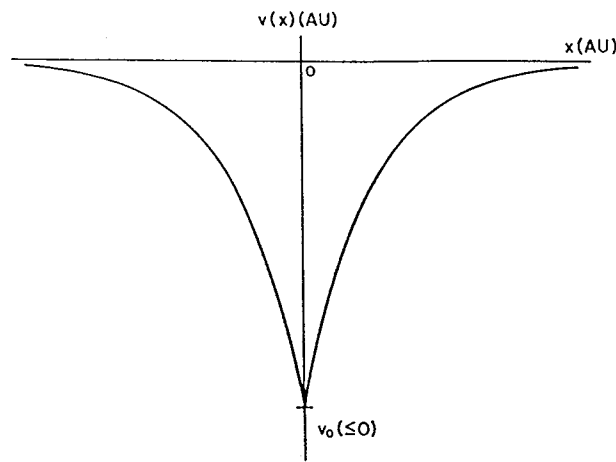Fig. 3. General arrangement of poles in the complex k plane.

Fig. 4.   Exponential potential.

tion (32) is a direct application of the argument principle,[12] where we have denoted the order of the pth pole by ρ_p ($\rho_p = 1$ for simple poles). Let us consider the integral along the various segments of the contour consisting of a line from $-R$ to $-\epsilon$, a semicircle, denoted C_1, of radius ϵ enclosing the origin [to allow for cases, such as truncated potentials, in which $t(k)$ has a zero at the origin], another line from $+\epsilon$ to $+R$, and a semicircular arc of radius R, denoted C_2. Taking the limits $R \to \infty$ and $\epsilon \to 0$ gives

$$I = \lim_{R \to \infty, \epsilon \to 0} -\frac{1}{2\pi i}\left\{ \int_{-R}^{-\epsilon} d\ln[t(k)] + \int_{C_1} d\ln[t(k)] \right.$$
$$\left. + \int_{+\epsilon}^{R} d\ln[t(k)] + \int_{C_2} d\ln[t(k)] \right\}. \quad (33)$$

After the integration and the substitution of the polar form for the transmission coefficient $t(k) = |t(k)| \exp[i\phi(k)]$, Eq. (33) reduces to the desired relation between the phase change and the number of bound states:

$$N = \frac{1}{2\pi}[\phi(-\infty) - \phi(+\infty)]. \quad (34)$$

This result follows directly from the fact that, if the potential is a member of the Faddeev class (the case under consideration), then $1/t(k) - 1 \sim 1/k$ and $[dt(k)/dk]/t(k) \sim 1/k^2$ as $k \to \infty$, and therefore the integral over the infinite semicircle vanishes. The application of Levinson's theorem will be taken up in Subsection 3.F following a derivation of the scattering data for the infinite-exponential potential.

E.   Reflection and Transmission
Coefficients: Infinite-Exponential Profile
The exponential profile is generated by a potential of the form[13]

$$v(x) = v_0 \exp(-|x|), \quad (35)$$

as shown in Fig. 4. We assume $v_0 < 0$.

Solutions to the Schrödinger equation will provide the exact form of $r_\pm(k)$ and $t_\pm(k)$ as well as the Jost solutions for the infinite-exponential profile. If the constant $a \equiv 2(-v_0)^{1/2}$, the substitution

$$u \equiv a \exp(-x/2) \quad (x > 0),$$
$$u \equiv a \exp(x/2) \quad (x < 0) \quad (36)$$

brings the Schrödinger equation into the form of Bessel's equation:

$$\frac{d^2 E_y}{du^2} + \frac{1}{u}\frac{dE_y}{du} + \left[1 - \frac{(2ik)^2}{u^2}\right]E_y = 0. \quad (37)$$

To identify the reflection and transmission coefficients we seek solutions with the asymptotic forms

$$t_+(k)\exp(-ikx), \quad x \to -\infty,$$
$$\exp(-ikx) + r_+(k)\exp(-ikx), \quad x \to +\infty. \quad (38)$$

By defining the constant $\nu = 2ik$, one can write well-behaved solutions of Eq. (37) as linear combinations of Bessel functions $J_{\pm\nu}(u)$, whose behavior as $x \to \pm\infty$ is represented by the small-argument approximation

$$J_{\pm\nu}(u) \approx \frac{(u)^{\pm\nu}}{2^{\pm\nu}\Gamma(\pm\nu + 1)}. \quad (39)$$

Consider solutions of the form

$$C_2 J_{-\nu}(u) + C_3 J_\nu(u), \quad x > 0,$$
$$C_1 J_{-\nu}(u), \quad x < 0, \quad (40)$$

with the appropriate form of u selected for each region. The requirement that these solutions and their first derivatives be continuous at $x = 0$ provides a set of two equations:

$$C_1 J_{-\nu}(a) - C_2 J_{-\nu}(a) = C_3 J_\nu(a),$$
$$C_1 \dot{J}_{-\nu}(a) + C_2 \dot{J}_{-\nu}(a) = C_3 \dot{J}_\nu(a), \quad (41)$$

where a dot indicates a derivative with respect to the argument. The constant C_3 can be evaluated if we define the k-dependent coefficients

$$\lambda_\pm \equiv \frac{a^{\pm 2ik}}{2^{\pm 2ik}\Gamma(\pm 2ik + 1)} \quad (42)$$

and reduce expressions (40) to the form

$$C_2\lambda_- \exp(ikx) + C_3\lambda_+ \exp(-ikx), \quad x \to \infty,$$
$$C_1\lambda_- \exp(-ikx), \quad x \to -\infty, \quad (43)$$

and comparison with expressions (38) indicates

$$C_3\lambda_+ \equiv 1,$$
$$t_+(k) \equiv C_1\lambda_-,$$
$$r_+(k) \equiv C_2\lambda_-. \quad (44)$$

Equations (41) may be solved for the remaining two constants, so that

$$t_+(k) = \frac{2^{(2\nu-1)}}{a^{2\nu}}\frac{\Gamma(\nu + 1)}{\Gamma(-\nu + 1)}\frac{J_\nu(a)\dot{J}_{-\nu}(a) - \dot{J}_\nu(a)J_{-\nu}(a)}{J_{-\nu}(a)\dot{J}_{-\nu}(a)}, \quad (45)$$

$$r_+(k) = \frac{-2^{(2\nu-1)}}{a^{2\nu}}\frac{\Gamma(\nu + 1)}{\Gamma(-\nu + 1)}\frac{J_\nu(a)\dot{J}_{-\nu}(a) + \dot{J}_\nu(a)J_{-\nu}(a)}{2J_{-\nu}(a)\dot{J}_{-\nu}(a)}, \quad (46)$$

where it is emphasized that the k dependence of the coefficients enters through the constant ν. The numerator of
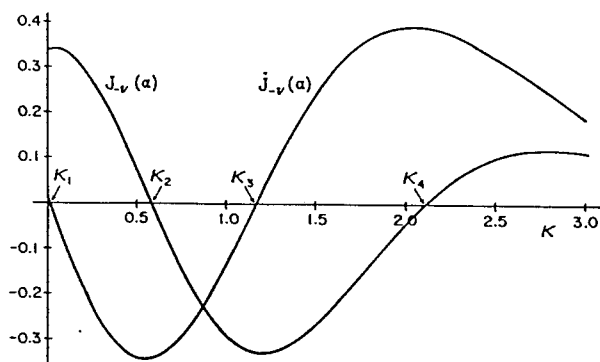
Fig. 5. Eigenvalues $\kappa_1, \ldots, \kappa_4$ for the exponential potential; $v_0 = -7.7$. The highest state (κ_1) is barely supported at this depth.
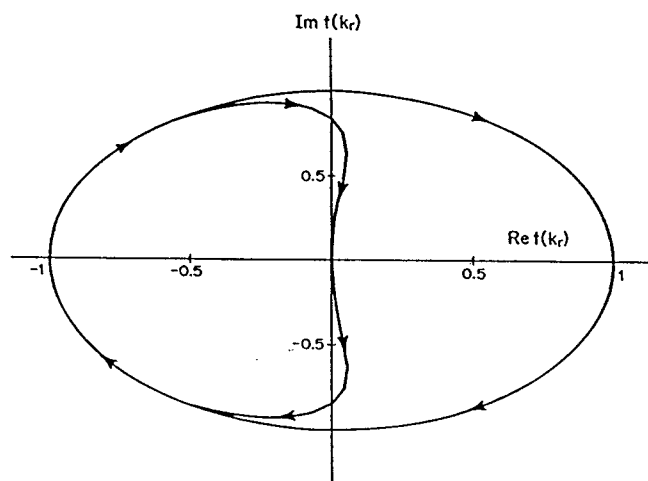

Fig. 6. Count of the bound states provided by the parametric plot of the phase of the $t(k)$, shown here as k_r proceeds from $-\infty$ to $+\infty$, indicating two bound states for $v_0 = -3$ (exponential profile).

the transmission coefficient remains finite for positive Im k, leaving the propagation constants for the even and odd modes to be determined by the zeros of the Bessel function and of its derivative.[14] Figure 5 illustrates these functions for $v_0 = -7.7$, showing four bound states.

F. Analysis of the Exponential Profile

For the case of the infinite untruncated exponential potential, it is clear that the amplitude v_0 controls the number of bound states. Consider the parametric plot in Fig. 6, which shows Im $t(k_r)$ (vertical axis) versus Re $t(k_r)$ for $k_r \in (-\infty, +\infty)$. The value of v_0 is -3. At the lower limit of k_r we have Im $t(k_r) \to 0$, Re $t(k_r) \to 1$, and the plot proceeds into the fourth quadrant as k_r increases. As $k_r \to 0$ the phase $\phi(k)$ has swept out one cycle of 2π. Subsequently, another cycle is traversed, indicating the presence of two bound states according the discussion in Subsection 3.D. In Fig. 7 a similar plot is shown for $v_0 = -0.75$, indicating a single bound state.

Comparison of Figs. 6 and 7 indicates that Im $t(k_r)$ contains important information regarding the number of bound states. Along the Re k axis, Im $t(k; v_0)$ is an odd function (for emphasis, the v_0 dependence is shown explicitly) whose typical form is shown in Fig. 8. The number of zero crossings depends on the number of modes; as v_0 is reduced, the zero crossings move toward the origin. As a mode is squeezed out, a pair of these zero crossings con-

verges, causing a rapid variation of Im $t(k_r)$ in the vicinity of the origin. According to Fig. 8, the exponential profile becomes single mode for values of $|v_0| < 1.446$. The transition from four modes to three occurs at $v_0 = -7.62$, which is consistent with Fig. 5.

It is also evident that the slope of Im$[t(k_r; v_0)|_{k_r=0}$ undergoes a change in sign as a mode is lost; however, calculating the derivative results in longer run times than does the approximation illustrated in Fig. 9, which shows the variation of Im $t(k_r, v_0)|_{k_r=-10^{-5}}$ as a function of v_0. Critical values of v_0, where modes are created or destroyed, are indicated by the zero crossings of this function.

Strictly speaking, this tool is an approximation, but it is extremely reliable for small values of $|k_r|$. Little variation in the critical values is found for $k_r < 10^{-5}$; however, the inflection points proximal to the zero crossings become more pronounced as k_r is reduced. In general, one can be confident that a good approximation is being obtained if the plot is nearly vertical in the region between the two inflection points. The illusion of a singularity in the vicinity of the critical values is an artifact of the plotting process; the inset in Fig. 9 is representative of the true behavior near these points.

Depth of the potential is just one parameter controlling the number of bound states. If the potential has compact support, i.e., if $v(x)$ is nonzero only in a finite interval, the
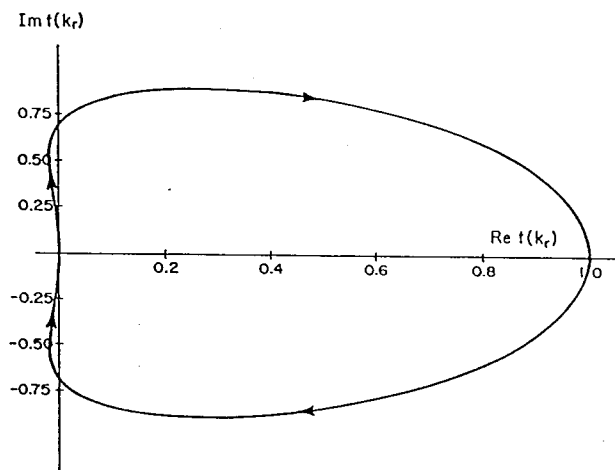

Fig. 7. Parametric plot for $k_r \in [-\infty, +\infty]$, indicating single-mode operation at $v_0 = -0.75$ (exponential profile).
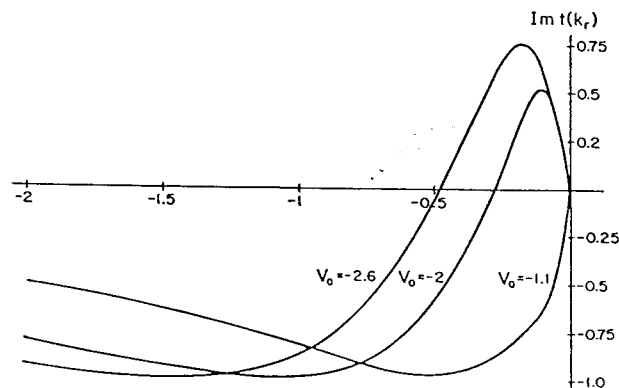

Fig. 8. Imaginary part of the transmission coefficient for three values of v_0, indicating the effects of reducing the depth of the potential (exponential profile).
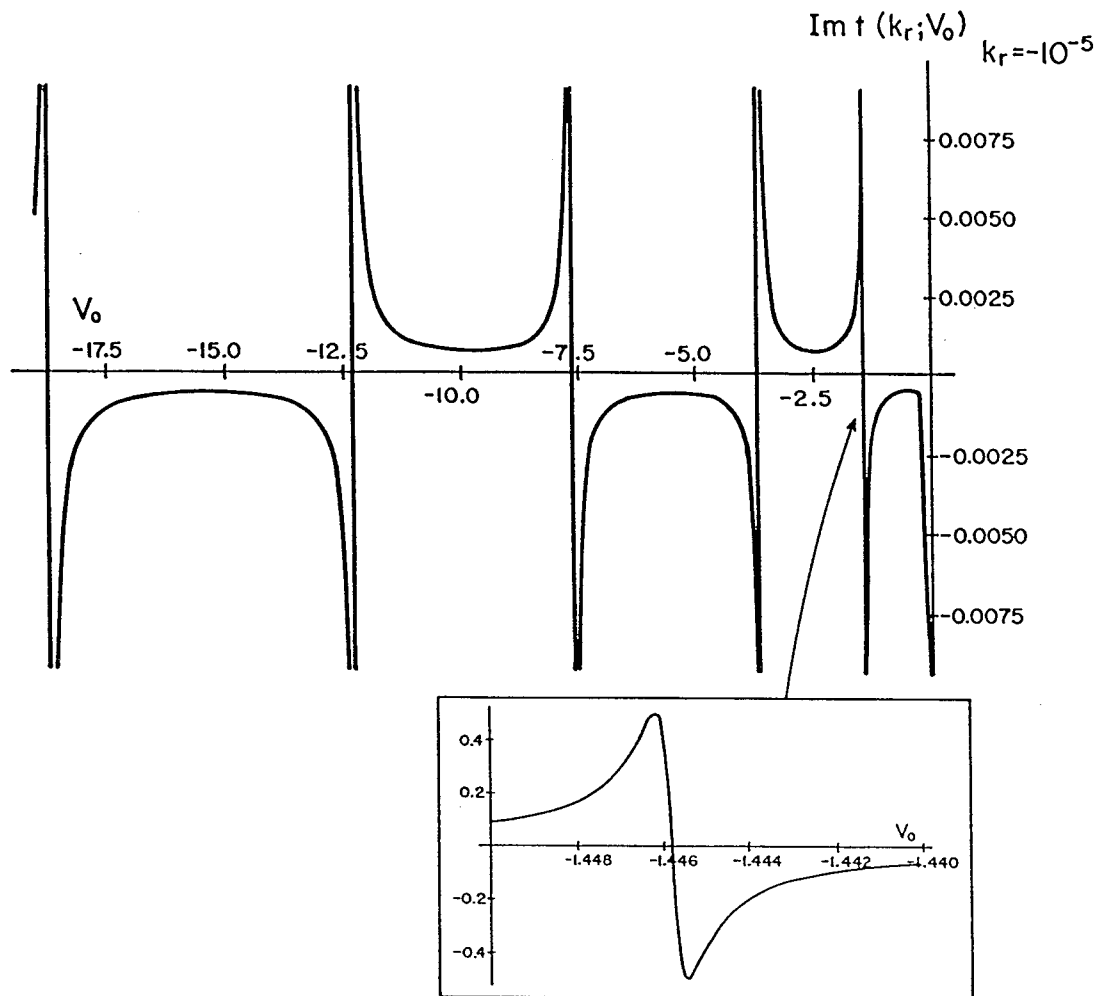
Fig. 9.   Critical values of v_0 represented by zero crossings.   Inset shows detail at $v_0 \approx -1.445$ (exponential profile).

number of bound states will be dictated by the width of the potential as well as its depth.   In Section 4, we discuss truncated potentials and examine the effects of a finite width on the mode structure.

4.   TRUNCATION OF REFRACTIVE-INDEX PROFILES

A. General Theory
For the purposes of this paper truncation consists of slicing a potential, such as the one illustrated in Fig. 10 (where the truncations are indicated by dashed lines), thereby creating an accurate model of a guided-wave structure.   The region $x_1 < x < x_2$ constitutes the core. Truncating the potential to zero in the regions $x \leq x_1$ and $x \geq x_2$ creates two cladding regions, each with refractive index n_2.   Note that the only restriction on x_1, x_2 is that $x_2 > x_1$; each may take on positive or negative values, permitting a large degree of flexibility in the resulting core-refractive-index profiles.

In this section a general formulation of the truncation problem[10] is derived, providing an expression for the transmission coefficient of a doubly truncated potential.   In the procedure considered here this transmission coefficient will be written in terms of the Jost solutions corresponding to the original untruncated (baseline) structure.

A notable restriction is that the Jost solutions for the baseline structure must be known *a priori.*

Note that the process of truncation creates three distinct regions separated by two discontinuities, one each at the points x_1 and x_2.   The requirements of continuity of the Jost solutions and their derivatives at these points can
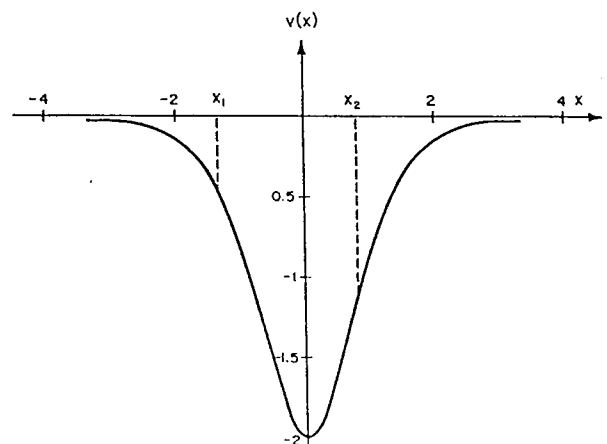
Fig. 10.   Truncated potential $v(x)$ corresponding to waveguide structure with core–cladding interfaces. $v(x) = -2 \, \mathrm{sech}^2 x$; x_1 and x_2 are the truncation points.

be imposed to formulate the transmission coefficient of the doubly truncated structure, which can subsequently be analyzed for the presence of propagating and leaky modes. The integral form of the Jost solutions,[15]

$$f_{\pm}(k,x) = \exp(\pm ikx) \mp \int \frac{\sin k(x-z')}{k} v(z') f_{\pm}(k,z') dz' \tag{47}$$

{where the limits on the integral are $[-\infty, x]$ and $[x, \infty]$ for $f_-(k,x)$ and $f_+(k,x)$, respectively}, combined with the requirements of continuity, provide the necessary equations. It is sufficient to consider continuity of either $f_+(k,x)$ or $f_-(k,x)$; if the latter is selected, note that in each region the Jost solution for the doubly truncated potential can be written as follows:

For the cladding ($x < x_1$),

$$f_-^{TT}(k,x) = \exp(-ikx), \tag{48}$$

and for the cladding ($x > x_2$),

$$f_-^{TT}(k,x) = c^{TT}(k)\exp(-ikx) + d^{TT}(k)\exp(ikx), \tag{49}$$

which is a form of Eq. (17).

For the core ($x_1 < x < x_2$),

$$f_-^{TT}(k,x) \equiv f_-^T(k,x) = c^T(k) f_+^0(-k,x) + d^T(k) f_+^0(k,x). \tag{50}$$

The notation $f_{\pm}^0(k,x)$ has been used to denote the Jost solutions for the untruncated (baseline) potential. The origin of Eq. (50) is as follows. Implicit in the integral form of the Jost solutions is the observation that the form of the Jost solution $f_-^{TT}(k,x)$ in the core is unaffected by the truncation at point x_2; hence the first equality in Eq. (50). (The single superscript T indicates quantities associated with a potential that is truncated *only* at point x_1.) The linear combination in Eq. (50) follows from Eqs. (16) and the equivalence $f_+^T(k,x) \equiv f_+^0(k,x)$ in the region $x > x_1$.

Imposing the requirements of continuity of $f_-^{TT}(k,x)$ and its derivative at point x_2, one obtains an equation for $c^{TT}(k)$:

$$c^{TT}(k) \equiv \frac{1}{t^{TT}(k)} = \frac{\exp(ikx_2)}{2ik}[-f_-^{T\prime}(k,x_2) + ik f_-^T(k,x_2)]. \tag{51}$$

Likewise, the coefficients $c^T(k)$, $d^T(k)$ follow from the boundary conditions at $x = x_1$:

$$c^T(k) = \frac{\exp(-ikx_1)}{2ik}[f_+^{0\prime}(k,x_1) + ik f_+^0(k,x_1)], \tag{52}$$

$$d^T(k) = \frac{-\exp(-ikx_1)}{2ik}[f_+^{0\prime}(-k,x_1) + ik f_+^0(-k,x_1)]. \tag{53}$$

When substituted into Eq. (50), these coefficients yield an expression for the transmission coefficient of the double truncated structure,

$$t^{TT}(k) = -4k^2 \exp[-ik(x_2-x_1)](f_a f_b - f_c f_d)^{-1}, \tag{54}$$

where

$$f_a \equiv f_+^{0\prime}(k,x_1) + ik f_+^0(k,x_1),$$

$$f_b \equiv -f_+^{0\prime}(-k,x_2) + ik f_+^0(-k,x_2),$$

$$f_c \equiv f_+^{0\prime}(-k,x_1) + ik f_+^0(-k,x_1),$$

$$f_d \equiv -f_+^{0\prime}(k,x_2) + ik f_+^0(k,x_2). \tag{55}$$

The transmission coefficient is now written in terms of the Jost solutions for the original potential and known constants related to the width of the potential. It is particularly interesting that the requirements of continuity provide relations [Eqs. (52) and (53)] that are nothing more than the Wronskians given by Eqs. (21) and (22). In Ref. 10, where *singly* truncated structures are treated, the Wronskians are used at the starting point of the analysis; that approach is completely consistent with the (physically more intuitive) continuity requirement imposed here.

B. Truncation of $v(x) = -2 \operatorname{sech}^2 x$ (Single Mode)

In general, the width of the waveguide is controlled by the parameters x_1 and x_2. As these are varied, causing a change in the core width, the poles of $t^{TT}(k)$ move in the complex k plane. As an example, consider truncation of the baseline potential $v(x) = -2 \operatorname{sech}^2 x$ according to the procedure indicated in Subsection 4.A. The baseline Jost solutions take the form[16]

$$f_+^0(k,x) = \exp(\pm ikx)\left(\frac{ik \mp \tanh x}{ik - 1}\right). \tag{56}$$

Therefore

$$t^{TT}(k) = \frac{(2k)^2(k-i)(k+i)}{p(k,x_1,x_2)}, \tag{57}$$

where the denominator is a function of k:

$$p(k,x_1,x_2) \equiv (2k^2 + 2ik \tanh x_1 + \operatorname{sech}^2 x_1)$$
$$\times (2k^2 - 2ik \tanh x_2 + \operatorname{sech}^2 x_2)$$
$$- \exp[2ik(x_2 - x_1)]\operatorname{sech}^2 x_1 \operatorname{sech}^2 x_2, \tag{58}$$

whose zeros identify the poles of $t^{TT}(k)$. In this form it is clear that $p(k,x_1,x_2)$ is not a polynomial in k unless $|x_1|$ or $|x_2|$ approaches infinity. Two examples are considered below.

1. Case i: x_1 Variable; $x_2 \to \infty$

The example of case i provides analytic solutions for the pole positions, given by the roots of the equation

$$2k^2 + 2ik \tanh x_1 + \operatorname{sech}^2 x_1 = 0, \tag{59}$$

resulting in two poles $k_{\pm} \equiv i\kappa_{\pm}$, one each on the upper and lower Im k axes:

$$\kappa_{\pm} = \tfrac{1}{2}[-\tanh x_1 \pm (1 + \operatorname{sech}^2 x_1)^{1/2}], \tag{60}$$

which are shown in Fig. 11. Note that $\kappa_1 \to 0$ only in the limit of a vanishing waveguide, indicating that the fundamental mode has zero cutoff in a planar waveguide with symmetric cladding indices and always propagates.
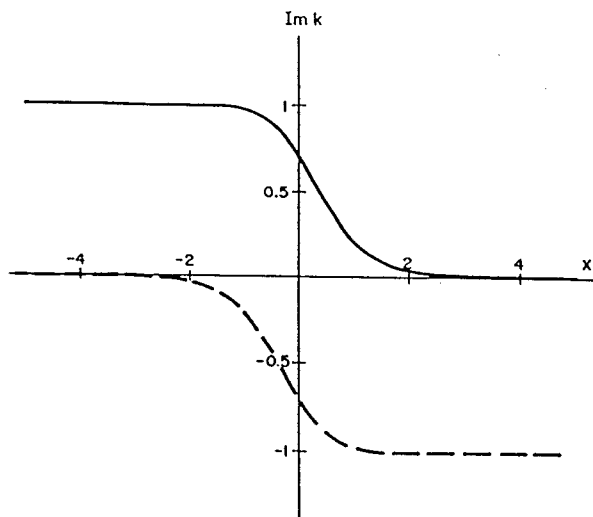
Fig. 11. Variation of the pole corresponding to the propagating mode (solid curve) as a function of truncation point x_1. The emergence of a pole corresponding to a leaky mode (dashed curve) is also shown here as a function of truncation point. $v(x) = -2 \operatorname{sech}^2 x$.
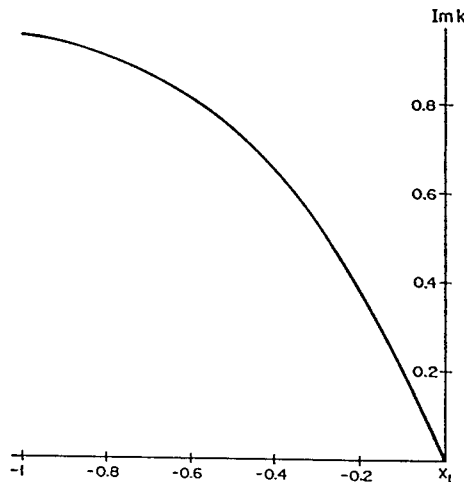
2. Case ii: $x_1 = -x_2$ (both variable)
In the example of case ii the core is progressively narrowed in a symmetric fashion about $x = 0$. Figures 12 and 13 illustrate the motion of the poles as x_1 varies. Figure 12 illustrates that, as in the previous example, the bound state is always present. The pole on the lower Im k axis, shown in Fig. 13, moves down the axis as the waveguide is narrowed.

C. Truncation of $v(x) = -N(N + 1)\operatorname{sech}^2 x$ (Multimode)
The two-mode ($\kappa_1 = 1, \kappa_2 = 2$) member of the family of $\operatorname{sech}^2 x$ potentials,

$$v(x) = -6 \operatorname{sech}^2 x, \qquad (61)$$

can be analyzed in a similar manner. When the Jost solutions for the above potential,[16]

$$f_\pm^0(k, x) = \exp(\pm ikx)\frac{1 + k^2 \pm 3ik \tanh x - 3 \tanh^2 x}{(k + i)(k + 2i)}, \qquad (62)$$

are substituted into Eq. (54), the resulting transmission coefficient yields two poles that appear on the upper Im k axis. For the case of a symmetric truncation ($x_2 = -x_1$) they exhibit the behavior illustrated in Fig. 14. A fundamental mode, which propagates for all waveguide widths, is characterized by values of κ_2 that range from 2 (for an infinitely wide waveguide) to 0; the latter is obtained when the waveguide disappears (at $x_2 = -x_1 = 0$). A higher-order mode characterized by κ_1 begins at unity and becomes progressively less tightly bound as the waveguide is narrowed, until $x_1 = -0.73$ (i.e., a waveguide width of 1.46), when the mode reaches cutoff and κ_1 proceeds onto the lower Im k axis, as shown.

In this example the core width is the geometrical variable controlling the number of propagating modes. Parametric plots given in Figs. 15 and 16 (analogous to those for the exponential profile) illustrate two-mode ($x_2 = 2.0$) and single-mode ($x_2 = 0.65$) behavior. The transition to single-mode behavior at $x_2 = 0.73$ (see

Fig. 12. Variation of pole position representing the propagating mode as the core width is narrowed for $x_2 = -x_1$ and $v(x) = -2 \operatorname{sech}^2 x$.
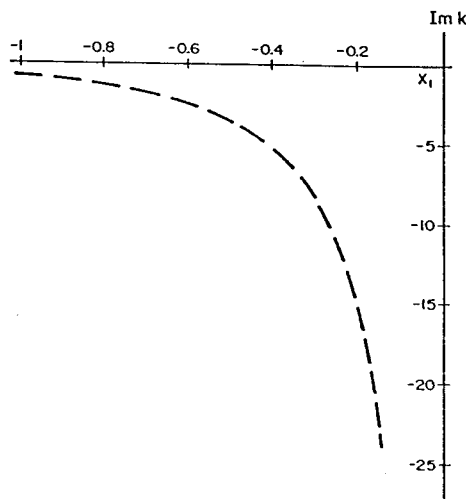

Fig. 13. Emergence of a pole on the lower Im k axis as a function of truncation point x_1. $v(x) = -2 \operatorname{sech}^2 x$.
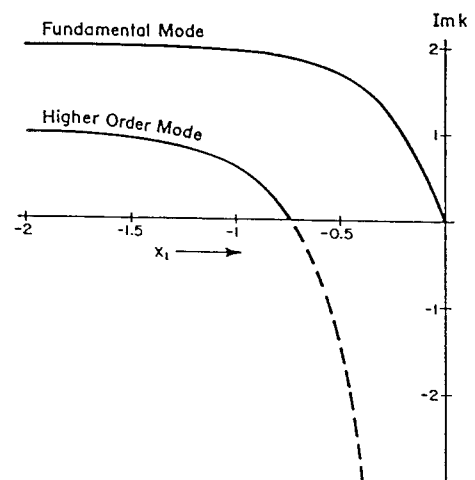

Fig. 14. Variation of poles corresponding to propagating modes (solid curve) for a two-mode case ($N = 2$) as a function of truncation point. The disappearance of the higher-order mode (at $x_1 = -0.73$) and the appearance of a pole on the lower imaginary axis (dashed curve) are also shown. $v(x) = -6 \operatorname{sech}^2 x$.
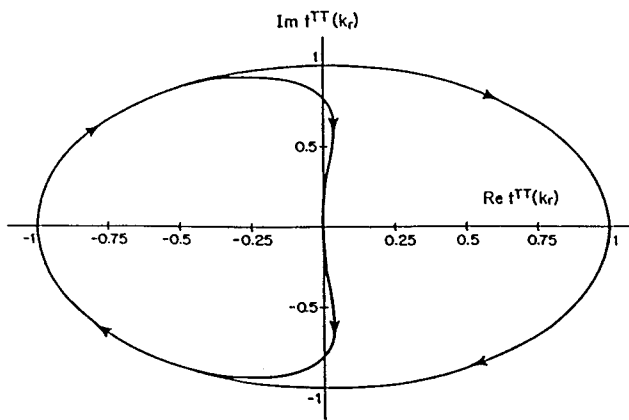
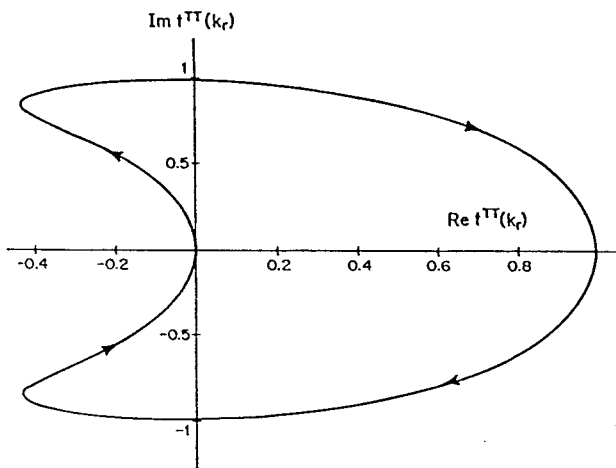Fig. 15.   Parametric plot for $k_r \in [-\infty, +\infty]$, indicating the presence of two propagating modes for $x_2 = 2.0$. $v(x) = -6 \operatorname{sech}^2 x$.

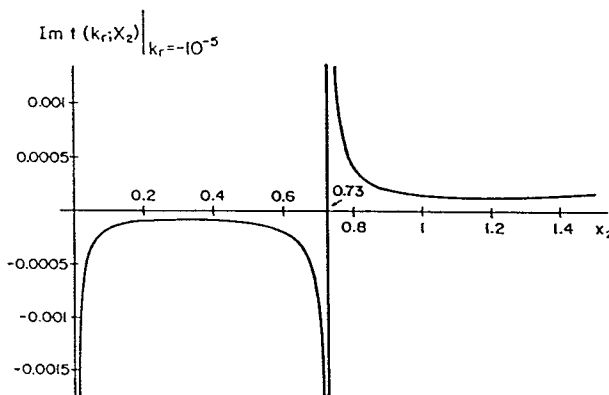Fig. 16.   Parametric plot for $k_r \in [-\infty, +\infty]$, indicating single-mode operation for $x_2 = 0.65$. $v(x) = -6 \operatorname{sech}^2 x$.

Fig. 17.   Critical value of $x_2 = 0.73$, indicating transition to single-mode operation. $v(x) = -6 \operatorname{sech}^2 x$.

Fig. 14) is verified in Fig. 17, where $\operatorname{Im} t^{TT}(k_r; x_2)|_{k_r=-10^{-5}}$ is plotted as a function of x_2.

A potential truncated in the manner that we have described supports an infinite number of leaky modes. They represent the discrete set of complex eigenvalues of Eq. (8), which are identified by poles in the lower complex k plane.[17]   The poles with larger values of ρ_r [see Eq. (31)] contribute the largest loss.

A general study of the behavior of the leaky modes is beyond the scope of this paper.   It is clear from our results

that as guided modes proceed through cutoff, their eigenvalues may proceed onto the lower $\operatorname{Im} k$ axis rather than directly becoming leaky modes.   Marcuse[18] considered this question for a step-index planar waveguide, and he found similar behavior for the first odd mode.[19]   To cite a further example in our own data, the simple two-mode potential considered in Subsection 4.C indicated that two poles on the lower imaginary axis, initially located in the vicinity of $k_i = -1.2$ and $k_i = -1.03$, converged and disappeared from the axis at $k_i \simeq -1.113$ as x_2 varied from 1.63 to 1.626.   A systematic study of these and related questions merits serious consideration.

5.   CONCLUSIONS

A theory has been developed for modeling and analyzing planar optical waveguides with $\operatorname{sech}^2 x$ and exponential profiles as representative examples.   The waveguide properties, such as the number of propagating modes and the value of their propagation constants, can be obtained from the analysis of scattering coefficients.   The technique has been further extended to analysis of waveguides formed by truncated refractive-index profiles.   Critical parameters, such as the core widths at which modes attain cutoff, can be obtained by using this method.   The influence of variable core width on the behavior of propagating and leaky modes is demonstrated in this paper.

Calculations indicate that the truncated profiles that model typical refractive-index profiles in waveguides do not always have scattering coefficients in the form of a rational function of the complex transverse wave number k.   This is an important result, because earlier synthesis procedures using inverse scattering theory have assumed only rational functions of k for scattering data (see Ref. 2). In principle, the method is applicable to a class of refractive-index profiles for which the Jost solutions can be obtained.

REFERENCES

1. A. W. Snyder and J. D. Love, *Optical Waveguide Theory* (Chapman & Hall, New York, 1983), pp. 23–24.
2. A. K. Jordan and S. Lakshmanasamy, "An inverse scattering theory applied to the design of single-mode planar optical waveguides," J. Opt. Soc. Am. A **6**, 1206–1212 (1989).
3. S. P. Yukon and B. Bendow, "Design of waveguides with prescribed propagation constants," J. Opt. Soc. Am. **70**, 172–179 (1980).
4. D. W. Mills and L. S. Tamil, "A new approach to the design of graded-index guided wave devices," IEEE Microwave Guided Wave Lett. **1**, 87–89 (1991).
5. D. Marcuse, *Light Transmission Optics*, 2nd ed. (Prentice-Hall, Englewood Cliffs, N.J., 1983).
6. K. Chadan and P. C. Sabatier, *Inverse Problems in Quantum Scattering Theory*, 2nd ed. (Springer-Verlag, New York, 1989).

7. P. G. Drazin and R. S. Johnson, *Solitons: An Introduction* (Cambridge U. Press, Cambridge, 1989), pp. 46–48.
8. J. A. Kong, *Electromagnetic Wave Theory*, 2nd ed. (Wiley, New York, 1990), p. 324; R. E. Collin, *Field Theory of Guided Waves* (Institute of Electrical and Electronics Engineers, New York, 1991), p. 718.
9. A. W. Snyder and J. D. Love, *Optical Waveguide Theory* (Chapman & Hall, New York, 1983), p. 166.
10. G. L. Lamb, *Elements of Soliton Theory* (Wiley, New York, 1977), pp. 60–62. The truncation concept is attributed to J. R. Cox.
11. N. Levinson, "On the uniqueness of the potential in a Schrödinger equation for a given asymptotic phase," K. Dan. Vidensk. Selsk. Mat. Fys. Medd. 25(9), 1–29 (1949).
12. S. Geltman, *Topics in Atomic Collision Theory* (Academic, New York, 1969), p. 21.
13. M. L. Goldberger and K. M. Watson, *Collision Theory* (Wiley, New York, 1964), p. 254.
14. H. Kogelnik, "Theory of optical waveguides," in *Guided-Wave Optoelectronics*, T. Tamir, ed. (Springer-Verlag, New York, 1988).
15. F. Constantinescu and E. Magyari, *Problems in Quantum Mechanics* (Pergamon, New York, 1971), p. 298.
16. G. L. Lamb, *Elements of Soliton Theory* (Wiley, New York, 1977), p. 54.
17. A. W. Snyder and J. D. Love, *Optical Waveguide Theory* (Chapman & Hall, New York, 1983), p. 536.
18. D. Marcuse, *Theory of Dielectric Waveguides*, 2nd ed. (Academic, Boston, Mass., 1991), pp. 31–34.
19. D. Marcuse, *Theory of Dielectric Waveguides*, 2nd ed. (Academic, Boston, Mass., 1991), p. 39.

Appendix C

D. W. Mills and L. S. Tamil, "Synthesis of Guided Wave Optical Interconnects"

IEEE Journal of Quantum Electronics, Vol.29, No. 11, pp. 2825–2834, 1993

Synthesis of Guided Wave Optical Interconnects

Duncan W. Mills and Lakshman S. Tamil, *Member, IEEE*

Abstract—We have designed a guided wave optical intercon-
nect which reduces or eliminates clock skew by ensuring si-
multaneous delivery of clock pulses to chips mounted on a
wafer. The interconnect consists of a multimode trunk wave-
guide and a set of branch waveguides, one per chip, each of
which couples one mode out of the trunk waveguide. The elim-
ination of clock skew is accomplished by taking advantage of
the different group velocities of the modes inherent in multi-
mode waveguides and suitably tailoring the propagation con-
stants of the trunk waveguide according to the location of the
respective chip on the wafer. Inverse scattering theory, specif-
ically the method of Darboux transformations, is employed to
design the refractive index profiles of the trunk waveguides,
using the set of propagation constants selected during the first
stage of the design, as input data. It is shown that by using
transverse coupling and suitable design of the trunk and branch
waveguides, efficient coupling from the trunk to the branch
waveguides can be ensured. Techniques for ensuring a sym-
metric trunk refractive index profile are investigated.

I. INTRODUCTION

HIGH-speed computer circuitry requires the distribu-
tion of information and/or clock pulses between var-
ious hardware elements within the system, including
boards, chips, and logical elements within a chip. Ideally,
the clock signals reach their intended destinations simul-
taneously, but in practice, the exact arrival times are
skewed since the clock signal emanates from a single
source to various locations distributed at different lengths
from the clock source. In the past, a number of techniques
for reducing clock skew in standard VLSI systems con-
sisting of metal or polysilicon interconnects have been
suggested. These include layouts composed of equal-
length lines [1], or breaking the chip into blocks, each
with an internally generated high-frequency clock con-
trolled by a low-frequency chipwide clock [2]. Aside from
the fact that it is not always practical to arrange circuit
elements to meet these physical requirements, a large
amount of metal wiring is required to implement these
schemes. The trend towards higher data rates, resulting
in a skew which is a larger percentage of the clock pulse
duration, has produced further clock distribution schemes
[3]–[5]. This paper presents a method for designing
guided-wave optical interconnects with reduced clock
skew, applicable in a chip-to-chip or intrachip situation.

The potential advantages offered by optical intercon-
nections over standard wire or polysilicon lines are dis-
cussed in a good review article [6], which suggests that
optics can alleviate problems stemming from resistive and
capacitive loading in wire/poly lines, which is delete-
rious to the signal amplitude and shape, particularly at
higher frequencies.

In this paper, it is proposed that graded-index guided
wave interconnects can effectively reduce clock skew by
suitable design of the refractive index profile [7]. This
design is accomplished by properly tailoring the propa-
gation constants of the guided modes to provide equal
propagation times to a set of detectors. The scheme pre-
sented in this paper employs several optical channels, each
having a different refractive index profile. This includes
a main multimode channel and several single-mode wave-
guides coupled to the main line. Total system design takes
into account the problem of clock skew as well as efficient
coupling between the trunk and branch waveguides.

Section II of this paper describes the relation between
clock skew and the guided-mode spectrum, followed by
a description of the proposed optical interconnection lay-
out. Section III provides the physical model of the optical
waveguide used as the building block of the optical inter-
connect circuitry. The refractive index profile of the mul-
timode guide is then carried out using an efficient recon-
struction algorithm which generates a refractive index
profile based on the guided mode spectrum and desired
coupling characteristics between the main waveguide and
the single-mode guides. These are discussed in Sections
IV and V, respectively. Design examples are provided in
Section VI, leading to conclusions in Section VII.

II. OPTICAL INTERCONNECT CIRCUIT

The interconnect network is to be mounted on a GaAs
wafer (10.16 cm in diameter), as shown in Fig. 1. The
goal of the interconnect circuit is to deliver a pulse from
the source to each of the detector points on the wafer si-
multaneously. The circuit consists of N detectors or chips
at points $P_{(1)} \cdots P_{(N)}$ connected by a network of inte-
grated optical waveguides consisting of a N-mode trunk
line feeding N branches, which are generally of a different
design from the trunk.

Denoting the refractive index of the waveguide clad-
ding (assumed, for simplicity, to be the same on both sides
of the guiding layer) by n_2, a pulse impressed upon a given
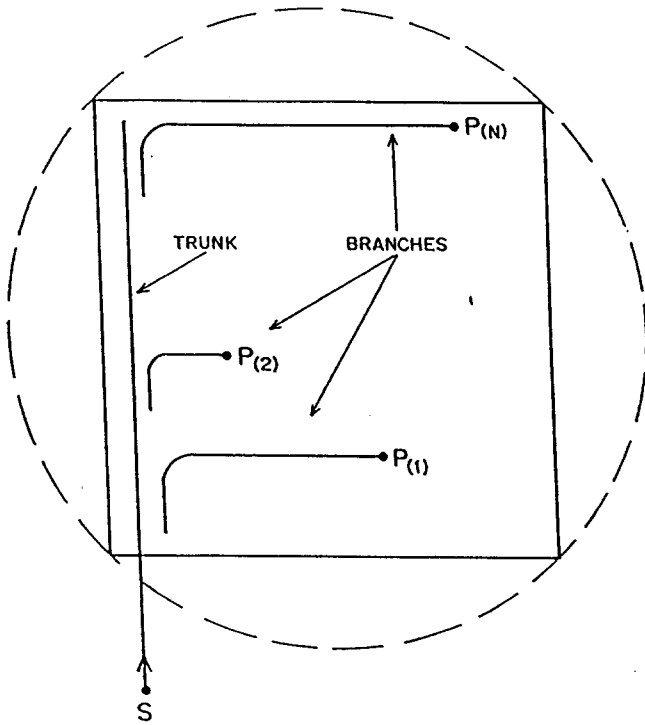mode with propagation constant β travels at the group ve-

Fig. 1. The optical interconnect. Refractive index profiles are designed so that a pulse launched from point S reaches each of the points $P_{(1)} \cdots P_{(N)}$ simultaneously.

locity v_g, where

$$\frac{1}{v_g} = \frac{d\beta}{d\omega} = \frac{\omega}{\beta} \frac{n_2^2}{c^2} \qquad (1)$$

so that a pulse traverses a given length L in time

$$\tau = \frac{\omega}{\beta} \frac{n_2^2}{c^2} L. \qquad (2)$$

Here, ω denotes the angular frequency of the radiation, and c is the vacuum velocity of light. Consider a clock pulse launched into the interconnect at point S. The time for a given mode to propagate from S to a designated $P_{(m)}$ is

$$\tau_m = \frac{\omega}{\beta_m} \frac{n_2^2}{c^2} L^{(m)}, \qquad m = 1, \cdots, N \qquad (3)$$

where $L^{(m)}$ is the distance from the source to $P_{(m)}$, and β_m is the propagation constant of the mode delivering the signal to $P_{(m)}$.

For the purpose of this analysis, the important quantities are the total distances from the source to the points $P_{(m)}$. Arranging these in order of increasing length

$$L_N > L_{N-1} > \cdots > L_1 \qquad (4)$$

so that $L_N = \max \{L^{(m)}\}$, $L_1 = \min \{L^{(m)}\}$, the points $P_{(1)} \cdots P_{(N)}$ will be synchronized if the propagation constants satisfy

$$\frac{\beta_2}{\beta_1} = \frac{L_2}{L_1}; \quad \frac{\beta_3}{\beta_2} = \frac{L_3}{L_2}; \quad \cdots; \quad \frac{\beta_N}{\beta_{N-1}} = \frac{L_N}{L_{N-1}}. \qquad (5)$$

This provides us with a set of N propagation constants

$$\beta_1 < \beta_2 < \cdots < \beta_N \qquad (6)$$

which must be supported as propagating modes within the interconnect. The propagation constants themselves are restricted to the range

$$k_0 n_2 < \beta_m < k_0 n_{max} \qquad (7)$$

where n_{max} is the maximum core refractive index, and n_2 the refractive index of the cladding.

The design of the interconnect circuit consists of two interrelated parts. The first concerns the design of the refractive index profile for the multimode trunk waveguide, based upon the spectrum generated in (5). The second involves the design of the branch waveguides, each of which must efficiently couple off the appropriate mode from the trunk and deliver it to the designated point. This raises the issue of waveguide coupling. In Sections III–VI, we illustrate the application of inverse scattering theory to the related problems of refractive index profile design and coupling.

III. WAVEGUIDE MODEL FOR OPTICAL INTERCONNECT

The waveguide model consists of a one-dimensional planar structure with graded-index core $n(x)$ and cladding layers of constant refractive index n_2, as shown in Fig. 2 [8].

With propagation taken along the z axis, the TE modes take the form

$$E_y(x) e^{i(\omega t - \beta z)} \qquad (8)$$

where the electric field $E_y(x)$ is given by

$$\frac{d^2 E_y}{dx^2} + [k_0^2 n^2(x) - \beta^2] E_y = 0. \qquad (9)$$

Rearrangement of the parameters by defining the transverse wavenumber k^2 and the potential $v(x)$,

$$k^2 \equiv k_0^2 n_2^2 - \beta^2$$

$$v(x) \equiv k_0^2 [n_2^2 - n^2(x)] \qquad (10)$$

brings (9) into the Schrodinger equation form

$$\frac{d^2 E_y}{dx^2} + (k^2 - v(x)) E_y = 0. \qquad (11)$$

Here, $k_0 = \omega/c$ is the free space wavenumber, β is the propagation constant, and c is the velocity of light in vacuum. From these considerations it is clear that n_2 represents the asymptotic refractive index of the corresponding waveguide, provided

$$v(x) \rightarrow 0 \text{ as } x \rightarrow \pm\infty. \qquad (12)$$

The exact model for the waveguide is a channel geometry However, for the sake of mathematical simplicity, we consider the planar geometry with one transverse coordinate. For certain separable refractive index profiles, th
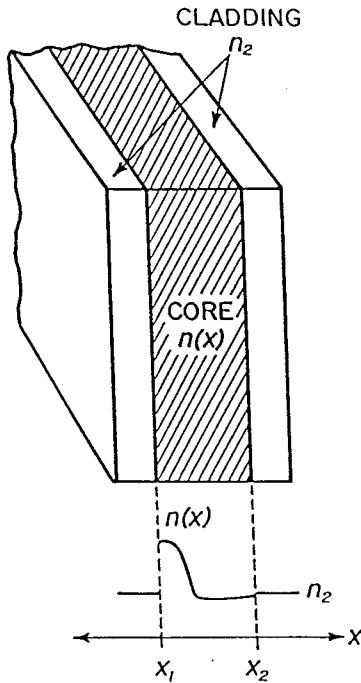
Fig. 2. One dimensional planar waveguide with variable core refractive index $n(x)$ surrounded by cladding layers of constant refractive index n_2.

two-dimensional refractive index surface can be written in the additive form [9],

$$n^2(x, y) = n_2^2 + n_x^2(x) + n_y^2(y) \qquad (13)$$

in which case the y-dependent portion of the refractive index can be designed using the results of planar geometry, resulting in a complete design of $n(x, y)$.

IV. RECONSTRUCTION BY TRANSFORMS

Inverse scattering theory provides a framework whereby the potential of the Schrodinger equation can be reconstructed from a set of eigenvalues selected *a priori*. Inverse reconstruction, based on the solution of the Gelfand–Levitan integral equation, has recently been applied to the design of monomode waveguides [8], [10]. In general, this technique is cumbersome when several bound states are present. As an alternative, we will employ the method of transformations (known variously as Darboux or Crum–Krein transformations [11], [12]) to obtain multimode potentials suitable for refractive index design in optical interconnects.

For these purposes, it is useful to have a basic understanding of scattering parameters related to the potentials of the Schrodinger equation, which we assume to behave asymptotically as

$$v(x) \to 0, x \to \pm\infty. \qquad (14)$$

A plane wave e^{+ikx} incident on the potential from $x = -\infty$, we give rise to a reflected portion taking the form,

$$r_-(k) e^{-ikx} \qquad (15)$$

as $x \to -\infty$, as well as a transmitted wave,

$$t_-(k) e^{+ikx} \qquad (16)$$

as $x \to \infty$ [13]. Similarly, the coefficients $r_+(k)$ and $t_+(k)$ can be defined, where it can be shown that $t_+(k) = t_-(k) \equiv t(k)$. The Schrodinger equation then admits a pair of Jost solutions, $f_+(k, x)$ and $f_-(k, x)$, defined according to their asymptotic behavior:

$$f_\pm(k, x) e^{\mp ikx} = 1 \qquad x \to \pm\infty. \qquad (17)$$

The pairs $\{f_+(k, x), f_+(-k, x)\}$ and $\{f_-(k, x), f_-(-k, x)\}$ comprise sets of linearly independent solutions to the Schrodinger equation, allowing construction of the linear combinations in terms of the transmission coefficient $t(k)$ and the pair of reflection coefficients $r_+(k)$ and $r_-(k)$:

$$f_+(k, x) = \frac{1}{t(k)} f_-(-k, x) + \frac{r_-(k)}{t(k)} f_-(k, x) \qquad (18)$$

and

$$f_-(k, x) = \frac{1}{t(k)} f_+(-k, x) + \frac{r_+(k)}{t(k)} f_+(k, x). \qquad (19)$$

The scattering data, consisting of these scattering coefficients and the bound state eigenvalues,

$$k_m = i\kappa_m \qquad (\kappa_m > 0) \qquad (20)$$

along with the normalization constants, completely characterize the form of the potential. The bound state wavefunctions are characterized by exponential decay for large $|x|$, and there is a direct one-to-one correspondence between these bound states and the guided waveguide modes characterized by a discrete spectrum of propagation constants

$$\beta_m = \sqrt{k_0^2 n_2^2 - k_m^2} \equiv \sqrt{k_0^2 n_2^2 + \kappa_m^2}. \qquad (21)$$

It is clear from (17)–(19) that the eigenvalues are poles of the transmission coefficient which lie on the upper imaginary axis of the complex k plane and that the bound state wavefunctions, which behave asymptotically as $e^{\mp \kappa_m x}$, are merely the Jost solutions evaluated at these poles:

$$f_\pm(i\kappa_m, x) = \frac{r_\mp(i\kappa_m)}{t(i\kappa_m)} f_\mp(i\kappa_m, x) \qquad (22)$$

from which follows the important relation,

$$\frac{r_+(i\kappa_m)}{t(i\kappa_m)} \frac{r_-(i\kappa_m)}{t(i\kappa_m)} = 1. \qquad (23)$$

A rather extensive derivation leads to alternative representations of the ratio of scattering coefficients implied by (22), useful for quantifying waveguide coupling [14]:

$$2ik \frac{r_\pm(k)}{t(k)} = \int_{-\infty}^{+\infty} f_\mp(k, x) v(x) e^{\mp ikx} dx. \qquad (24)$$

Equation (5) provides a prescription for constructing a spectrum beginning with the highest mode, β_1, whose value is arbitrary, subject only to the requirement $\beta_1 > k_0 n_2$, and building upon it until the fundamental mode, characterized by β_N, is added to the spectrum.

The transform procedure is a technique which allows for the construction of N − mode potentials by specifying

a priori a set of bound state eigenvalues, derived from the set $\{\beta_1, \beta_2, \cdots, \beta_N\}$ via (10):

$$k_m \in \{i\kappa_1, i\kappa_2, \cdots, i\kappa_N\} \qquad (25)$$

where

$$\kappa_N \geq \kappa_{N-1} \geq \cdots \geq \kappa_1 > 0. \qquad (26)$$

The following discussion does not constitute proof of the transformation method, for which interested readers are referred to reference [12]. Rather, it outlines the practical steps necessary to construct a particular class of potentials which suit the purposes of refractive index profile design.

In the method outlined here, we are adding the N bound states to some chosen initial potential designated $v_0(x)$ which is assumed to contain no bound states. As additional input data, we require the explicit from of the Jost solutions $f_{\pm}^b(k, x)$ associated with $v_0(x)$.

Defining the N linear combinations of the Jost solutions as

$$\gamma_m \equiv (-1)^{m+1} f_+^b(i\kappa_m, x) + \rho_m f_-^b(i\kappa_m, x)$$

$$m = 1, \cdots, N \qquad (27)$$

where ρ_m is an arbitrary positive definite parameter, the corresponding N-mode potential is simply:

$$v_N(x) = v_0(x) - 2\frac{d^2}{dx^2}\ln W(\gamma_1, \cdots, \gamma_N). \qquad (28)$$

In the above equation, the quantities $W(\;)$ denote Wronskians, i.e.,

$$W(\gamma_1, \gamma_2, \cdots, \gamma_N)$$

$$\equiv \begin{vmatrix} \gamma_1 & \gamma_2 & \cdots & \gamma_N \\ \gamma_1' & \gamma_2' & \cdots & \gamma_N' \\ \cdot & \cdot & \cdots & \cdot \\ \cdot & \cdot & \cdots & \cdot \\ \gamma_1^{(N-1)} & \gamma_2^{(N-1)} & \cdots & \gamma_M^{(N-1)} \end{vmatrix} \qquad (29)$$

whose rows consist of functions $\gamma_1 \cdots \gamma_N$ differentiated with respect to x from zero to $N - 1$ times. Equation (29) clearly illustrates the manner in which the N bound states are progressively added in stages represented by rows and columns of the Wronskian.

The Jost solutions corresponding to the generated potential take the form

$$f_+(k, x; N) \equiv \frac{(-1)^N}{\prod\limits_{m=1}^{N}(\kappa_m - ik)}$$

$$\cdot \frac{W(\gamma_1, \cdots, \gamma_N, f_+^b(k, x))}{W(\gamma_1, \cdots, \gamma_N)}$$

$$f_-(k, x; N) \equiv \frac{1}{\prod\limits_{m=1}^{N}(\kappa_m - ik)}$$

$$\cdot \frac{W(\gamma_1, \cdots, \gamma_N, f_-^b(k, x))}{W(\gamma_1, \cdots, \gamma_N)}. \qquad (30)$$

Designating the scattering data for $v_0(x)$ as $T(k)$, $R_{\pm}(k)$, the data pertaining to the potential constructed in the preceding algorithm is simply:

$$t(k) = \frac{k + i\kappa_1}{k - i\kappa_1}\frac{k + i\kappa_2}{k - i\kappa_2} \cdots \frac{k + i\kappa_N}{k - i\kappa_N}T(k)$$

$$r_{\pm}(k) = (-1)^N\frac{k + i\kappa_1}{k - i\kappa_1}\frac{k + i\kappa_2}{k - i\kappa_2} \cdots \frac{k + i\kappa_N}{k - i\kappa_N}R_{\pm}(k) \qquad (31)$$

clearly illustrating the presence of N poles representing the N bound states.

The normalization constants,

$$c_m^2 \equiv \left[\int_{-\infty}^{+\infty} f_+^2(k_m, x)\, dx\right]^{-1} \equiv Im\{\text{Res } r_+(k_m)\}$$

$$d_m^2 \equiv \left[\int_{-\infty}^{+\infty} f_-^2(k_m, x)\, dx\right]^{-1} \equiv Im\{\text{Res } r_-(k_m)\} \qquad (32)$$

which play a critical role in waveguide coupling, are related through the transmission coefficient:

$$c_m d_m = -i \text{ Res } \{t(k_m)\}. \qquad (33)$$

The normalization constants c_m^2 also transform in a controlled way as the potential is constructed. It can be shown that (see [12])

$$c_m^2 = \frac{2\kappa_m}{\rho_m}P_m \qquad (34)$$

where

$$P_m \equiv \left((-1)^{m-1}\prod_{l=m}^{N}\frac{\kappa_l + \kappa_m}{\kappa_l - \kappa_m}\right)T(i\kappa_m)$$

$$m = 1, 2, \cdots, N. \qquad (35)$$

In effect, to every set of N 3-tuples

$$\{v_0(x), \kappa_m, \rho_m\} \qquad m = 1, \cdots, N \qquad (36)$$

there corresponds a unique N-mode potential $v_N(x)$. In this paper, we will assume

$$v_0(x) = 0,$$

$$f_{\pm}^b(k, x) = e^{\pm ikx} \qquad (37)$$

with pertinent scattering data

$$T(k) = 1,$$

$$R_{\pm}(k) = 0. \qquad (38)$$

To demonstrate the procedure used here, we have used three sets of data shown in Table I, and have reconstructed the refractive index profiles shown in Figs. 3-5. Unless otherwise indicated, we assume

$$n_2 = 3.0$$

$$\lambda = 0.9 \ \mu\text{m}, \qquad (39)$$

throughout this paper. In Fig. 3, the eigenvalues are equally spaced and all $\rho_m = 1$. The resulting refractive

TABLE I
DATA CHARACTERIZING THE REFRACTIVE INDEX PROFILES OF FIGS. 3-5

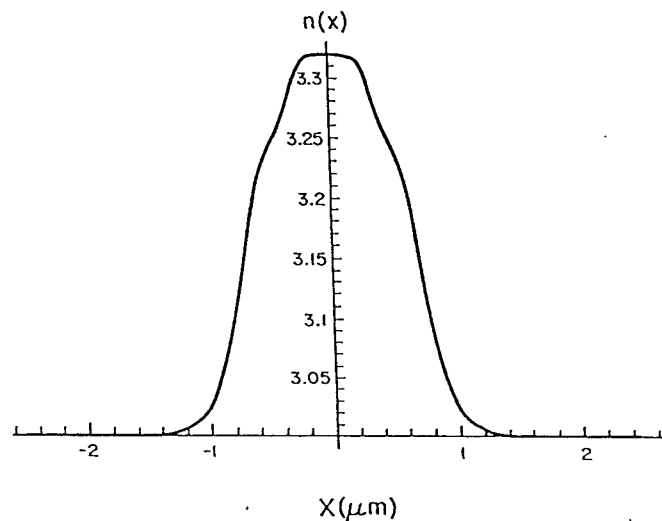| β_m ($\times k_0 n_2$), ρ_m	Fig. 3	Fig. 4	Fig. 5
β_5, ρ_5	1.09752, 1	1.05169, 1	1.09752, 547
β_4, ρ_4	1.07611, 1	1.05269, 1	1.07611, 0.003
β_3, ρ_3	1.05369, 1	1.05369, 1	1.05369, 0.01
β_2, ρ_2	1.03202, 1	1.05469, 1	1.03202, 96
β_1, ρ_1	1.01034, 1	1.05459, 1	1.01034, 235

Fig. 3. The smooth, symmetric trunk refractive index profile resulting from evenly spaced eigenvalues and $\rho_m = 1$ for all m.
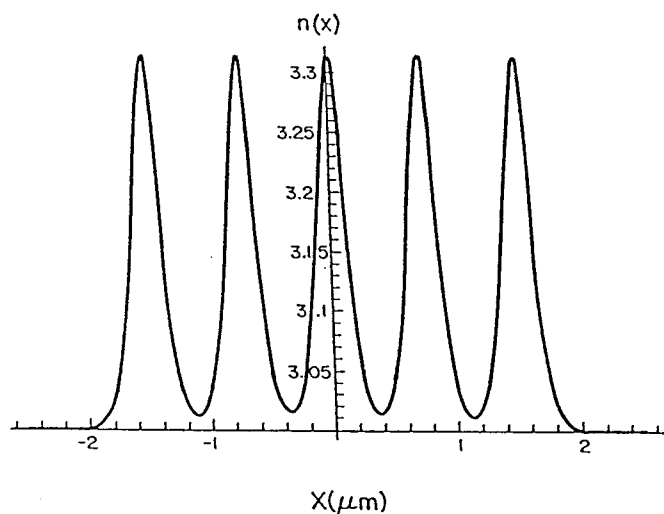

Fig. 4. Trunk refractive index profile resulting from five-fold near degeneracy. Symmetry is retained since $\rho_m = 1$ for all m.

index profile is symmetric about the origin and provides a smooth single channel. If near-degeneracies are introduced into the spectrum, splits will occur in the refractive index profile. The nature and extent of the splits will depend upon the number of modes involved. This is illustrated in Fig. 4, where we introduce a quasi-degeneracy across the entire spectrum, causing the expected split of the refractive index profile into five channels. The profile remains symmetric about the origin. When the original spectrum is restored, but one or more of the { $\rho_m | m = 1$,
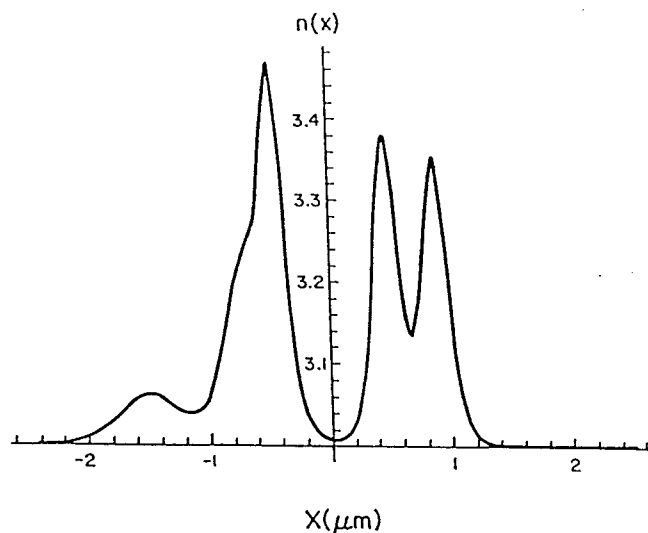

Fig. 5. Trunk refractive index profile with same spectrum as in Fig. 3. The ρ_m are varied as indicated in Table I.

TABLE II
PROPAGATION CONSTANTS FOR SMOOTH PROFILE
SECOND COLUMN GIVES RESULTS OF FINITE
DIFFERENCE METHOD APPLIED TO
POTENTIAL IN FIG. 3

SMOOTH PROFILE, (Fig. 3), Direct method comparison	
β_m ($\times k_0 n_2$)	β_m ($\times k_0 n_2$), direct method
1.09752	1.09752
1.07611	1.07614
1.05369	1.05377
1.03202	1.03218
1.01034	1.01054

2, $\cdots$, N} deviate from unity (Fig. 5), the result is a splitting despite the wide spacing of the eigenvalues.

This example illustrates the application of the reconstruction procedure to typical spectra compatible with GaAs technology, with resulting refractive index profiles which are symmetric and well behaved. It is clear from our analysis that a material such as AlGaAs [15], with a large variation in refractive index as a function of mole fraction, is well suited to the proposed interconnect since it allows for a relatively large spread of propagation constants, and consequently, greater flexibility in placement of chips on the wafer.

As a check of our algorithm, one hundred data points representing the value of the refractive index profile shown in Fig. 3 were used as input to a finite-difference algorithm, solving (9), whose output considered of the corresponding five propagation constants. Results of this direct solution are given in the second column of Table II, showing excellent agreement with the exact propagation constants.

Completion of the optical interconnect problem involves design of the branch waveguides. In the next section we discuss transverse coupling between the trunk and branches, and show how the parameter ρ_m can be adjusted to provide the desired coupling characteristics.

V. Coupling to Branches

Efficient power transfer from the trunk to each branch can be accomplished by transverse coupling which will occur over the interaction length represented in Fig. 1 by the short spans along which the branches are parallel to the trunk waveguide. The analytical approach used here is based upon the standard perturbation technique, under an assumption of weak coupling [16], [17]. The novelty of our analysis lies in relating the scattering analysis of the previous section to the calculation of transverse coupling coefficients derived from coupled mode theory.

Fig. 6 shows two neighboring (nonoverlapping) waveguides, each of which is assumed to have a graded-index core with refractive index profiles $n_L(x)$ and $n_R(x)$, respectively. We will assume that each waveguide separately supports y-polarized TE modal fields $E_L(x)$ and $E_R(x)$ with propagation constants β_L and β_R, respectively. The interaction between the two fields will be represented by a z-dependent linear combination of the individual waveguide modes:

$$\mathcal{E}(x, z, t) = A(z)E_R(x)e^{i(\omega t - \beta_R z)} + B(z)E_L(x)e^{i(\omega t - \beta_L z)} \tag{40}$$

where the exact form of the z-dependent weighting coefficients $A(z)$ and $B(z)$ are to be determined. We will assume that the coupling is weak, i.e.,

$$\left| \frac{d^2 A(z)}{dz^2} \right| \ll \left| \beta_R \frac{dA(z)}{dz} \right| \quad \left| \frac{d^2 B(z)}{dz^2} \right| \ll \left| \beta_L \frac{dB(z)}{dz} \right|. \tag{41}$$

The interaction between the waveguides is represented by first-order differential equations:

$$\frac{dA(z)}{dz} = i\kappa_{RL} B(z) e^{-i(\beta_L - \beta_R)z} \tag{42}$$

and

$$\frac{dB(z)}{dz} = i\kappa_{LR} A(z) e^{i(\beta_L - \beta_R)z}. \tag{43}$$

The coupling coefficients,

$$\kappa_{RL} \equiv \left\{ \frac{I_{RL}}{2\beta_R N_{RR}} \right\} \tag{44}$$

and

$$\kappa_{LR} \equiv \left\{ \frac{I_{LR}}{2\beta_L N_{LL}} \right\} \tag{45}$$

are defined in terms of the various integrals

$$N_{RR} \equiv \int_{-\infty}^{+\infty} E_R^2(x)\, dx,$$

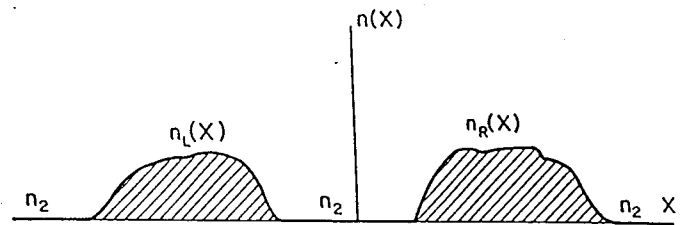$$I_{RL} \equiv \int_{-\infty}^{+\infty} E_R(x)\, v_R(x)\, E_L(x)\, dx \tag{46}$$

Fig. 6. Weakly-coupled waveguides used to model the coupling interaction.

and

$$N_{LL} \equiv \int_{-\infty}^{+\infty} E_L^2(x)\, dx$$

$$I_{LR} \equiv \int_{-\infty}^{+\infty} E_L(x)\, v_L(x)\, E_R(x)\, dx. \tag{47}$$

The coupling coefficients may be written in terms of the scattering data as follows. Let the model consist of two waveguides described by potentials $v_L(x)$ and $v_R(x)$. For the purposes of the analysis, let us shift $v_L(x)$ in the negative x direction by an amount s so that

$$E_R(x) \equiv f_-^R(i\kappa, x)$$

$$E_L(x) \equiv f_+^L(i\kappa, x + s)$$

$$v_R(x) = k_0^2[n_2^2 - n_R^2(x)]$$

$$v_L(x + s) = k_0^2[n_2^2 - n_L^2(x)]. \tag{48}$$

This form of the fields was chosen so that they have the simple asymptotic forms

$$E_R(x) \to e^{\kappa x} \text{ as } x \to -\infty,$$

$$E_L(x) \to e^{-\kappa s} e^{-\kappa x} \text{ as } x \to \infty. \tag{49}$$

The separation s is arbitrary, subject only to the condition that the potentials do not overlap to any large extent.

In the region comprising $v_R(x)$, $E_L(x)$, the field of the lefthand potential taken alone, takes the simple form,

$$E_L(x) = e^{ik(x + s)}|_{k = i\kappa} \tag{50}$$

enabling the interaction integral to be written as

$$
\begin{aligned}
I_{RL} &= e^{-\kappa s} \int_{-\infty}^{+\infty} f_-^R(k, x)\, v_R(x)\, e^{ikx}\, dx\Big|_{k = i\kappa} \\
&= e^{-\kappa s} \int_{-\infty}^{+\infty} \frac{r_+^R(k)}{t^R(k)} f_+^R(k, x)\, v_R(x)\, e^{ikx}\, dx\Big|_{k = i\kappa} \\
&= -2\kappa e^{-\kappa s} \frac{r_+^R(i\kappa)}{t^R(i\kappa)} \frac{r_-^R(i\kappa)}{t^R(i\kappa)} \\
&= -2\kappa e^{-\kappa s} \tag{51}
\end{aligned}
$$

where we have used (22)–(24). The coupling coefficients now take the explicit form

$$
\begin{aligned}
\kappa_{RL} &= \frac{I_{RL}}{2\beta_R N_{RR}} = \frac{-\kappa}{\beta_R} e^{-\kappa s} d_m^2 \\
&= \frac{-\kappa}{\beta_R} e^{-\kappa s} Im\{\text{Res } r_-^R(i\kappa)\}. \tag{52}
\end{aligned}
$$

Similarly,

$$\kappa_{LR} = \frac{I_{LR}}{2\beta_L N_{LL}} = \frac{-\kappa}{\beta_L} e^{-\kappa s} c_m^2$$

$$= \frac{-\kappa}{\beta_L} e^{-\kappa s} Im\{Res\ r_+^L (i\kappa)\}. \tag{53}$$

It is clear that the coupling coefficients consists of two parts: a factor depending only upon spectral information and waveguide separation, and a (more interesting) contribution from the normalization integral which is dependent upon the actual geometry of the potential. To highlight this, we will refer to the normalization constants as shape factors, denoted

$$F \equiv Im\{Res\ r_-(i\kappa)\}. \tag{54}$$

It is clear from simple integration of (42) and (43) that significant amounts of power can only be exchanged under conditions of phase matching.

$$\beta_L = \beta_R = \beta. \tag{55}$$

For the purposes of the optical interconnect circuit, assume that the right-hand waveguide, with amplitude $A(z)$, represents the single-mode branch. Assuming the branch to begin at some distance $z = z_0$ along the trunk, so that $A(z_0) = 0$, the coupled-mode equations have the solutions [17]

$$A(z) = \sqrt{\frac{\kappa_{RL}}{\kappa_{LR}}} B(z_0) \sin \Delta\beta_c z$$

$$B(z) = B(z_0) \cos \Delta\beta_c z, \tag{56}$$

where

$$\Delta\beta_c = \sqrt{\kappa_{RL} \kappa_{LR}}. \tag{57}$$

From (56) and (40) it is clear that the field of the composite trunk/branch waveguide closely approximates a two-mode system with propagation constants

$$\beta^{(+)} = \beta + \Delta\beta_c$$

$$\beta^{(-)} = \beta - \Delta\beta_c. \tag{58}$$

Under conditions of complete power transfer, i.e.,

$$\kappa_{RL} = \kappa_{LR} \tag{59}$$

complete power exchange occurs at intervals of

$$z_L = \frac{m\pi}{2\kappa_{RL}}; \quad m = 1, 3, 5, \cdots \tag{60}$$

measured from z_0 along the branch waveguide. Maximum power transfer is generally ensured by employing identical waveguides (not a viable option in our application), but it is clear from (53) and (52) that equal coupling coefficients can be ensured by suitable manipulation of the normalization constants of the various trunk waveguide modes and the corresponding branch modes. For branches placed to the right of the trunk, this amounts to

$$c_m^{2(trunk)} = d_m^{2(branch)}; \quad m = 1, \cdots, N. \tag{61}$$

Consequently, we will select a set of single mode branches, calculate $d_m^{2(branch)}$ and suitably tailor the trunk waveguide, using (28) and selecting approximate values of ρ_m based upon (61). In the next section, we consider various sets of branches and carry out the trunk design in accordance with these concepts.

VI. DESIGN EXAMPLES

The design process consists of selecting suitable single-mode branches, calculating their shape factors, and designing the trunk refractive index profile for maximum power transfer. Denoting the branch shape factors by $F_m^{(b)}$, this design process imposes a condition on the trunk through ρ_m:

$$\rho_m = \frac{2\kappa_m P_m}{F_m^{(b)}} \tag{62}$$

which follows directly from (34) and (61). It is clear that the ρ_m act as the critical parameter in matching waveguides for maximum power transfer. We emphasize that (62) is a condition freely imposed upon the ρ_m based on the mode spectrum and the form of the branch waveguides.

At this point, the goal of the analysis is to determine to what extent it is possible to provide maximum coupling between the branch and the trunk while adjusting the design parameters in such a way that the refractive index profiles are reasonably well behaved.

A smooth, symmetric trunk refractive index profile is clearly preferable to one with random variations and large gradients. Using the same mode spectrum employed to generate Figs. 3–5, we have determined that a step-index branch design is sufficiently flexible to achieve attractive profiles for the trunk waveguide, while maintaining conditions of maximum power coupling. This is an encouraging result, as step-index waveguides are easy to fabricate. In all cases considered, $n_2 = 3.0$, at a wavelength of 0.9 μm.

The step-index waveguide has been analyzed using standard methods (see [16]). The purpose of the following analysis is to put the step-index waveguide into the context of inverse scattering theory and to demonstrate its usefulness in the proposed interconnect. Consider a square well potential of width $D \equiv 2d$:

$$v(x) = \begin{cases} k_0^2(n_2^2 - n_1^2) & (-d < x < d) \\ 0 & \text{elsewhere} \end{cases} \tag{63}$$

whose corresponding refractive index profile is a step-index planar waveguide with constant core refractive index n_1. Defining the parameter

$$K \equiv \sqrt{k^2 - k_0^2\{n_2^2 - n_1^2\}} = \sqrt{k_0^2 n_1^2 - \beta^2} \tag{64}$$

we can write the Jost solutions and their derivatives for square well potential as

$$f_-(k, x) = a_s(k) \sin Kx + a_c(k) \cos Kx$$

$$f'_-(k, x) = Ka_s(k) \cos Kx - Ka_c(k) \sin Kx \tag{65}$$

and

$$f_+(k, x) = b_s(k) \sin Kx + b_c(k) \cos Kx$$

$$f'_+(k, x) = Kb_s(k) \cos Kx - Kb_c(k) \sin Kx. \quad (66)$$

In addition, for $x < -d$.

$$f_-(k, x) = e^{-ikx}$$

$$f'_-(k, x) = -ike^{-ikx} \quad (67)$$

and for $x > d$,

$$f_+(k, x) = e^{ikx}$$

$$f'_+(k, x) = ike^{ikx}. \quad (68)$$

Continuity of the Jost solutions and their derivatives at these boundaries gives the coefficients:

$$a_s(k) = \frac{-e^{ikd}\{K \sin Kd + ik \cos Kd\}}{K},$$

$$a_c(k) = \frac{e^{ikd}\{K \cos Kd - ik \cos Kd\}}{K},$$

$$b_s(k) = -a_s(k),$$

$$b_c(k) = a_c(k). \quad (69)$$

From the first of these, it is clear that the eigenvalue equation for the even modes is

$$\tan Kd = \frac{-ik}{K}. \quad (70)$$

The reflection coefficient [18],

$$r_-(k) = \frac{W[f_+(k, x), f_-(-k, x)]}{W[f_-(k, x), f_+(k, x)]} \quad (71)$$

follows in a straightforward way. Since,

$$W[f_-(k, x), f_+(k, x)]$$

$$= K(b_s(k)a_c(k) - a_s(k)b_c(k))$$

$$= 2Kb_s(k)a_c(k) \quad (72)$$

and

$$W[f_-(-k, x), f_+(k, x)] = 2K(b_s a_c(-k) - a_s(-k)b_c) \quad (73)$$

it follows that

$$r_-(k) = \frac{a_s(-k)b_c(k) - b_s(k)a_c(-k)}{2b_s(k)a_c(k)} \quad (74)$$

clearly illustrating how the pole locations are the respective even and odd mode eigenvalue equations. We are interested in the fundamental mode with eigenvalue $k_0 = i\kappa_1$, for which the residue is given by

$$F_1^{(b)} = \text{Res }\{r_-(i\kappa_1)\}$$

$$= -\frac{1}{2}e^{-2ikd}\frac{K \tan Kd - ik}{\frac{d}{dk}\{K \tan Kd + ik\}}\bigg|_{k=i\kappa_1}. \quad (75)$$

This expression can be simplified so that the coupling coefficient takes the form

$$|\kappa_{RL}| = \frac{K^2\kappa_1^2}{\beta(1 + \kappa_1 d)k_0^2(n_1^2 - n_2^2)}e^{-\kappa_{1}s}e^{2\kappa_1 d} \quad (76)$$

in exact agreement with the result obtained using the standard method [19].

Consider a set of branches consisting of five square wells of width $\{D_m \mid m = 1, 2, \cdots, 5\}$, and constant core refractive index $\{n_1^{(m)} \mid m = 1, 2, \cdots, m\}$. With the eigenvalue spectrum preselected, the design procedure amounts to a selection of branch core widths and core refractive indices which allow single-mode operation. Since $\beta_m^2 = k_0^2 n_2^2 + \kappa_m^2$, and $n_1^2 k_0^2 - \beta_m^2 > 0$, the minimum core refractive index is

$$\min\{n_1^{(m)}\} = \left(\frac{k_0^2 n_2^2 + \kappa_m^2}{k_0^2}\right). \quad (77)$$

Requiring the core width to be at least one wavelength nominally gives

$$\min\{D_m\} = 1 \ \mu\text{m}. \quad (78)$$

Table III lists the results of three sets of design data, beginning with a set of branches each 1 μm in width, their corresponding core refractive indexes, chosen so as to satisfy the eigenvalue equation for this width, and, in the last column, the corresponding values of ρ_m. Fig. 7 shows the resulting refractive index profile. In the second set, a similar pattern was followed, but for larger core widths, and the resulting trunk refractive index profile is plotted in Fig. 8. Comparison with the previous result shows a greater shift of the profile in the positive x direction, due mainly to the three ρ_m which are less than unity, in contrast to the first case, where all $\rho_m > 1$. Both trunks exhibit rather large index gradients, but are otherwise well behaved.

The third case is the most interesting. It is clear from earlier discussions that if we choose

$$\rho_m \simeq 1 \quad (79)$$

for all branch waveguides, a smooth, symmetric trunk refractive index profile will result. Since laser diodes emit even and odd field configurations, a symmetric trunk refractive index profile, allowing for even and odd guided modes, will result in more efficient coupling between the source and the trunk waveguide. In a somewhat tedious but effective analysis, whose objective was to satisfy (79) for all m, we began by plotting a given ρ_m (62) versus $n_1^{(m)}$ and D_m. Empirically it was found that the pair that satisfied the eigenvalue equation and the condition $\rho_m = 1$ lay in the vicinity of $\min\{n_1\}$, enabling one to narrow down the range of D_m values. A trial value of D_m was then selected, the corresponding $n_1^{(m)}$ found from the eigenvalue equation. Using this pair $(D_m, n_1^{(m)})$, ρ_m was then checked for its proximity to unity. We were satisfied to come within 3% of $\rho_m = 1$. If required, the procedure can be repeated until ρ_m is sufficiently close to any desired value.

61

TABLE III
DATA FOR STEP-INDEX BRANCHES CORRESPONDING TO TRUNKS IN FIGS. 7, 8, AND 3

STEP INDEX BRANCH DATA			
β_m ($\times k_0 n_2$)	d ($=D/2$), μm	n_1	ρ_m
Fig. 7			
1.09752	0.5	3.31	30.77
1.07611	0.5	3.25	99.81
1.05369	0.5	3.18	107.95
1.3202	0.5	3.11	7.83
1.01034	0.5	3.04	8.83
Fig. 8			
1.09752	1.0	3.30	5.89
1.07611	1.0	3.23	2.26
1.05369	1.0	3.17	0.54
1.3202	1.0	3.10	0.01
1.01034	1.0	3.03	0.003
Fig. 3, approx.			
1.09752	0.648	3.30613	1.00901
1.07611	0.664	3.24113	1.00456
1.05369	0.947	3.16782	0.984028
1.03202	1.1	3.10102	0.97903
1.01034	1.4	3.03384	1.00375

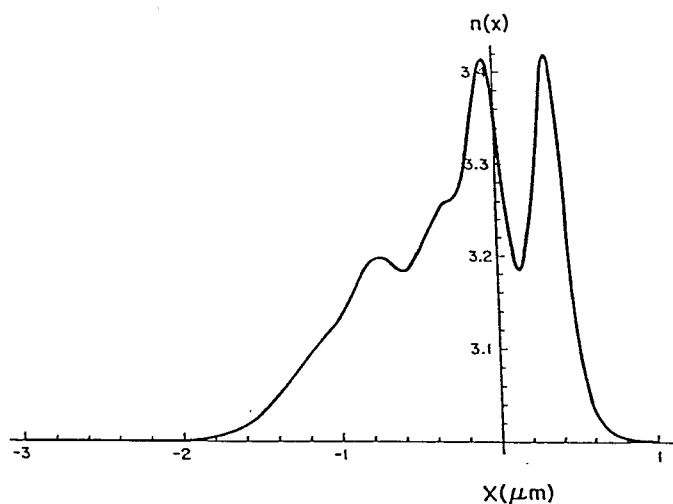Fig. 8. Trunk refractive index profile for step index branch waveguides of width 2 μm.

Fig. 7. Trunk refractive index profile for step index branch waveguides of width 1 μm.

It bears repeating that setting $\rho_m = 1$ for all modes merely guarantees a symmetric trunk refractive index profile. The smoothness of the profile will also depend upon the spectrum of propagation constants, as we have seen in Figs. 3–5. In fact, the smoothness of the refractive index profile shown in Fig. 3 is a direct consequence of the relatively equal spacing of the propagation constants. The more general question of creating a single, smooth guiding region for an arbitrary set of eigenvalues and normalization constants is considered in [10]. It is evident from our results, however, that the parameters governing th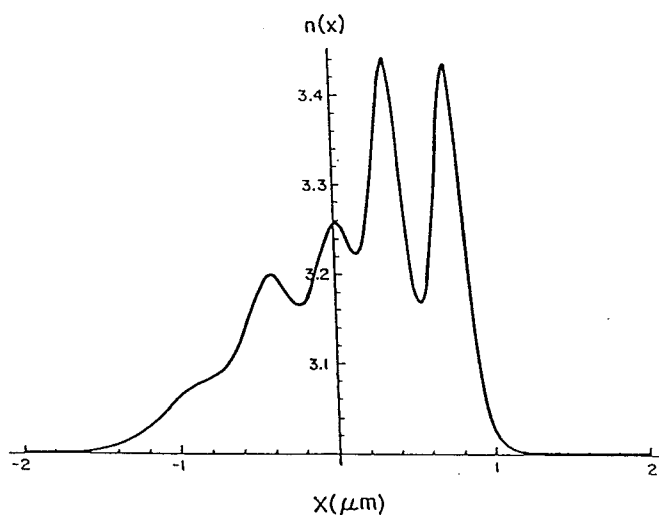e step-index branch waveguides are sufficiently flexible to couple to a large number of possible trunk waveguides designed using Darboux transformations.

VII. CONCLUSIONS

Guided wave optical interconnects consisting of graded-index optical waveguides were designed. It was possible to design an interconnect consisting of a multimode trunk waveguide coupled to several single mode branch waveguides, each of which delivers a selected mode to a detector. By exploiting the group velocity dispersion inherent in multimode waveguides, it was possible to select a set of propagation constants such that each of the modes can be delivered to its assigned detector simultaneously, thereby eliminating clock skew.

The synthesis of waveguides with prescribed propagation constants is the key to the design of this interconnect. Consequently, an inverse scattering algorithm was required to reconstruct the refractive index profile which would support guided modes with this preselected spectrum. It was determined that the method of transformations provided a flexible, efficient means of generating the multimode trunk refractive index profiles suited to our use. These profiles are continuous and decay rapidly in the transverse direction, making them well suited to practical systems. (An in-depth analysis of the effects of truncating such refractive index profiles to simulate core-cladding discontinuities is given in [20]).

By manipulating the normalized constants, it was possible to take full advantage of the possibilities of the transformation method. In particular, it was possible to efficiently couple the trunk waveguide and each of the branch waveguides, despite the fact that the trunk and branches consisted, in general, of different refractive index profiles. This analysis resulted in a formulation of waveguide coupling coefficients in terms of the scattering data pertaining to the corresponding potentials. It is emphasized that this formulation is completely general and

applicable to any waveguide systems in which the weak coupling approximation is valid.

In addition, it was found that proper manipulation of the normalization constants guaranteed trunk refractive index profiles which were symmetric and, under certain circumstances, free from large index gradients. However, it is clear that in general, the freedom of choosing unequal lengths for clock distribution is gained at the cost of the complexity of the waveguide profile.

Directions for future work include analyzing the sensitivity of the refractive index profiles to variations in the propagation constants, and an in-depth analysis of allowed variations in chip placement within the prescribed wafer area.

REFERENCES

[1] S. Dhar, M. A. Franklin, and D. F. Wann, "Reduction of clock delays in VLSI structures," in *Proc. IEEE Conf. on Computer Design: VLSI in Computers*, pp. 778–783, 1984.

[2] F. Anceau, "A synchronous approach for clocking VLSI systems," *IEEE J. Solid-State Circuits*, vol. SC-17, pp. 51–56, 1982.

[3] D. H. Hartman, P. J. Delfyette, and S. Z. Ahmad, "Optical distribution using mode locked semiconductor laser diode system," in *Proc. Optical Fiber Conf.* (OFC), 1991.

[4] B. D. Clymer and J. W. Goodman, "Optical clock distribution to silicon chips," *Opt. Engin.*, vol. 25, no. 10, pp. 1103–1108, 1986.

[5] R. L. Khalil, L. R. McAdams, and J. W. Goodman, "Optical clock distribution for high speed computers," *Proc. SPIE*, vol. 99, pp. 32–41, 1988.

[6] J. W. Goodman, F. J. Leonberger, S.-Y. Kung, and R. A. Athale, "Optical interconnections for VLSI systems," *IEEE Proc.*, vol. 72, July 1984.

[7] L. S. Tamil, "Optical interconnects: Design using an inverse scattering approach," Center for Applied Optics Res. Rep. UTD/CAO-24, June 1991.

[8] A. K. Jordan and S. Lakshmanasamy, "An inverse scattering approach to the design of planar optical waveguides," *J. Opt. Soc. Am. A*, vol. 6, no. 8, pp. 1206–1212, Aug. 1989.

[9] T. Tamir, Ed., *Guided Wave Optoelectronics*. New York: Springer, 1980.

[10] S. P. Yukon and B. Bendow, "Design of waveguides with prescribed propagation constants," *J. Opt. Soc. Am.*, vol. 70, no. 2, pp. 172–179, Feb. 1980.

[11] K. Chadan and P. C. Sabatier, *Inverse Problems in Quantum Scattering Theory*, 2nd ed. New York: Springer-Verlag, 1989.

[12] P. Deift and E. Trubowitz, "Inverse scattering on the line," *Comm. Pure and Appl. Math.*, vol. 32, pp. 121–251, 1979. (In particular, see Section III, Theorem 6.)

[13] P. G. Drazin and R. S. Johnson, *Solitons: An Introduction*. Cambridge, UK: Cambridge Univ. Press, 1989.

[14] Ref. [11], p. 329.

[15] S. Adachi, "GaAs, AlAs, and AlGaAs material parameters for use in research and device applications," *J. Appl. Phys.*, vol. 58, no. 3, Aug. 1985.

[16] D. Marcuse, *Light Transmission Optics*, 2nd ed. Englewood Cliffs, NJ: Prentice-Hall, 1983.

[17] A. Yariv and P. Yeh, *Optical Waves in Crystals*. New York: Wiley-Interscience, 1984.

[18] Ref. [11], p. 328.

[19] Ref. [16], p. 427.

[20] Duncan W. Mills and Lakshman S. Tamil, "Analysis of planar optical waveguides using scattering data," *J. Opt. Soc. Am. A*, vol. 9, no. 10, pp. 1769–1778, Oct. 1992.

Duncan W. Mills received the B.A. degree in physics from Wesleyan University and the M.S. degree in electrical engineering from George Washington University.

He is presently a Research Scientist at the University of Texas at Dallas, where he received his Ph.D. in electrical engineering in 1992. Prior to his present position, Dr. Mills worked at the U.S. Naval Research Laboratory engaged in projects involving ionospheric propagation and scatter in optical systems. His primary research interests are optical waveguides and electromagnetic theory.

He is a member of Eta Kappu Nu and the Optical Society of America.

Lakshman S. Tamil (S'83–M'88) was born on July 24, 1960, in Tamilnadu, India. He received the B.E. degree in electronics and communication engineering from the Madurai Kamaraj University, Madurai, India, in 1981, and the M.Tech. degree in microwave and optical communication engineering from the Indian Institute of Technology, Kharagpur, India, in 1983. He also received the M.S. degree in mathematics and the Ph.D. degree in electrical engineering from the University of Rhode Island, Kingston, in 1988.

Since 1988 he has been with the University of Texas at Dallas, Richardson, as an assistant professor of electrical engineering. He is also a member of the Center of Applied Optics in the same university. His research interests include fiber optics, photonic integrated devices and circuits, nonlinear guided wave optics, semiconductor lasers, inverse scattering theory, and numerical methods applied to electromagnetic problems.

Dr. Tamil is a member of Sigma Xi, Optical Society of America, Electromagnetics Academy, and is a elected member of Commission B and D of the International Union of Radio Science.

Appendix D

D. W. Mills and L. S. Tamil ,"Coupling in multilayer optical waveguides: an approach based on scattering data,"

Coupling in Multilayer Optical Waveguides: An Approach Based on Scattering Data

Duncan W. Mills[†] and Laksham S. Tamil, *Member, IEEE*

Abstract—Within the context of weak coupling theory, we derive representations of the coupling coefficients between neighboring waveguides by representing the field-dependent interaction integrals by algebraic expressions involving scattering data and we illustrate the contexts in which scattering theory can make a viable alternative to existing formulation of the waveguide coupling problem.

I. Introduction

COUPLING between waveguides in a multilayer optical structure is the cornerstone of optical spatial switching. This form of coupling, which arises when the evanescent fields of one waveguide perturb its neighbor, can be analyzed by several methods. Traditionally, the most popular approaches have been a weak-coupling perturbation analysis [1] or the analysis of local normal modes [2]. The problem continues to generate considerable interest, as evidenced by recent work formulating variational methods and finite-difference schemes [3]. The results presented in this paper were motivated by our recent interest in analysis of optical waveguides using scattering data (i.e., eigenvalues of the bound modes, reflection, and transmission coefficients).

Specifically, this paper shows that the traditional weak-coupling analysis of interacting waveguides can be reformulated in the language of scattering theory. We show that the coupling coefficients describing the interaction of two neighboring waveguides have straightforward representations in terms of their scattering data, eliminating the need to explicitly calculate the field-dependent interaction integrals by representing these integrals with straightforward algebraic expressions involving the guided-mode propagation constant and the residue of the reflection coefficient. In this paper no attempt is made to reformulate the mathematics of scattering theory, but rather to identify existing aspects of this theory which are useful when applying transverse coupling to waveguide design, and to illustrate the contexts in which scattering theory can make a viable alternative to existing methods.

II. Waveguide Model

Fig. 1 shows a multilayer planar waveguide consisting of two coupled graded-index (GRIN) guiding regions. For
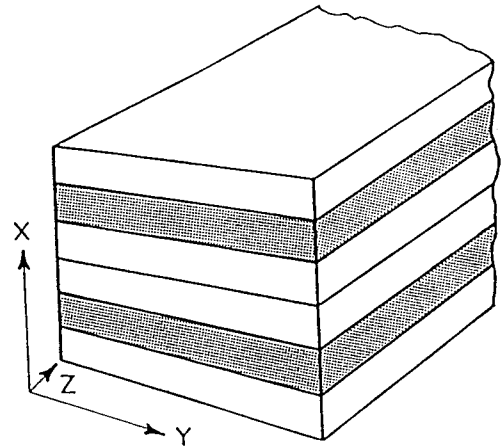
Fig. 1. Typical multilayer planar waveguide (two layers shown). Guideing regions are shown shaded.

the moment, consider a single planar graded-index waveguide consisting of an inhomogeneous core with a varying refractive index $n(x)$, surrounded by two cladding layers of constant refractive index n_2. To simplify the analysis we assume that each guiding region is infinite in the y direction and supports a single y-polarized TE mode of the form

$$E_y(x, z, t) \equiv E_y(x)e^{i\beta z}e^{-i\omega t}, \tag{1}$$

where z is the direction of propagation, ω is the frequency, and β is the longitudinal propagation constant. It has been assumed that the waveguide is infinite in extent along the y axis. Here, k_0 is the free space wavenumber. The field $E_y(x)r$ is defined by the scalar differential equation

$$\frac{d^2 E_y(x)}{dx^2} + \left[k_0^2 n^2(x) - \beta^2 \right] E_y(x) = 0. \tag{2}$$

This equation can take the form of a Schrödinger equation which is particularly well suited to analysis using scattering data. Defining the complex transverse propagation constant k ($\equiv k_r + ik_i$) as

$$k^2 = k_0^2 n_2^2 - \beta^2 \tag{3}$$

brings (2) into the Schrödinger form

$$\frac{d^2 E_y}{dx^2} + [k^2 - v(x)]E_y = 0, \tag{4}$$

whose potential

$$v(x) \equiv k_0^2 [n_2^2 - n^2(x)] \qquad (5)$$

varies across the waveguide core and vanishes in the cladding. Eq. (5) clearly illustrates how the depth of the potential may be varied either by changing the wavelength, altering the refractive index profile, or both. In this scheme the mode cutoff condition, $\beta = k_0 n_2$, is obtained when

$$k = 0. \qquad (6)$$

The discrete set of guided modes, characterized by $k_0 n_2 < \beta < k_0 n_1$, or equivalently by $0 < \mathrm{Im}\, k < \mathrm{Im}(k_0 \sqrt{n_2^2 - n_1^2})$, is represented by points along the positive imaginary axis of the complex k plane. In scattering theory, the guided modes are termed bound states, distinguished by their eigenvalues k. As the fundamental mode of a planar waveguide is TE, (4) is sufficient to describe the bound mode in a single-mode waveguide.

A. Scattering Coefficients and Jost Solutions

Scattering theory (direct and inverse) is concerned with the relationship between a Schrödinger potential $v(x)$ and its associated scattering data (i.e., reflection and transmission coefficients). A plane wave e^{+ikx} incident on the potential from $x = +\infty$ will give rise to a reflected portion taking the form

$$r_-(k) e^{-ikx} \qquad (7)$$

as $x \rightarrow -\infty$, as well as a transmitted wave,

$$t_-(k) e^{+ikx} \qquad (8)$$

as $x \rightarrow \infty$. An alternative viewpoint is provided by the coefficients $r_+(k)$ and $t_+(k)$, which define reflected and transmitted portions of a plane wave incident from $x = -\infty$.

The Schrödinger equation admits a pair of Jost solutions, denoted $f_+(k, x)$ and $f_-(k, x)$, defined according to their asymptotic behavior:

$$\lim_{x \rightarrow +\infty} f_+(k, x) e^{-ikx} = \lim_{x \rightarrow -\infty} f_-(k, x) e^{+ikx} = 1. \qquad (9)$$

The pairs $\{f_+(k, x), f_+(-k, x)\}$ and $\{f_-(k, x), f_-(-k, x)\}$ comprise sets of linearly independent solutions to the Schrödinger equation, allowing construction of the linear combinations [4]:

$$f_\pm(k, x) = \frac{1}{t(k)} f_\mp(-k, x) + \frac{r_\mp(k)}{t(k)} f_\mp(k, x). \qquad (10)$$

The Wronskian, defined as $W[f, g] \equiv fg' - gf'$ (the prime denoting differentiation with respect to the coordinate), provides a set of relations,

$$\frac{2ik}{t_-(k)} = \frac{2ik}{t_+(k)} = W[f_-(k, x), f_+(k, x)], \qquad (11)$$

so that $t_-(k) = t_+(k) \equiv t(k)$, a result which is a direct consequence of the asymptotic behavior stipulated in (9).

In addition,

$$2ik \frac{r_\pm(k)}{t(k)} = \mp W[f_\mp(k, x), f_\pm(-k, x)] \qquad (12)$$

follows from (10) and (11).

During the course of this analysis, it is useful to shift potentials along the axis. The scattering data changes in a controlled way under a shift. Consider a potential $v(x)$ with Jost solutions denoted $f_\pm(k, x)$ and corresponding scattering data $r_\pm(k), t(k)$. It is clear that the shifted potential $v(x - d)$ has a Jost solution of the form

$$\bar{f}_+(k, x) = e^{ikd} f_+(k, x - d). \qquad (13)$$

Using an overbar to denote the scattering coefficients of the shifted potential, it can be shown that the reflection coefficients associated with the translated potential are related to the original data by a simple phase shift:

$$\bar{r}_-(k) = e^{+2ikd} r_-(k),$$
$$\bar{r}_+(k) = e^{-2ikd} r_+(k), \qquad (14)$$

while the transmission coefficient is unaltered:

$$\bar{t}(k) = t(k). \qquad (15)$$

B. Guided Modes

Consider values of $k \,(\equiv ia)$ such that

$$\frac{1}{t(k)} = 0; \qquad (16)$$

that is, the bound state eigenvalues correspond to the poles of $t(k)$ which lie on the positive $\mathrm{Im}\, k$ axis. The Jost solutions exhibit the asymptotic behavior

$$E_y^{\mathrm{bound}}(x) \sim e^{\mp ax}, \qquad x \rightarrow \pm\infty \quad (a > 0). \qquad (17)$$

This implies

$$f_+(ia, x) = \frac{r_-(ia)}{t_-(ia)} f_-(ia, x),$$

$$f_-(ia, x) = \frac{r_+(ia)}{t_+(ia)} f_+(ia, x), \qquad (18)$$

resulting in the following useful relation:

$$\frac{r_-(ia)}{t_-(ia)} \frac{r_+(ia)}{t_+(ia)} = 1. \qquad (19)$$

The corresponding normalized guided-mode fields are then

$$E_y^{\mathrm{bound}}(x) = c_+ f_+(ia, x) \equiv c_- f_-(ia, x), \qquad (20)$$

where the $c_\pm$ are arbitrary constants. There is a one-to-one correspondence between the bound states of the quantum mechanics picture and these guided modes, and we will use these terms interchangeably.

66

III. TRANSVERSE COUPLING

In this section we review the salient features of wave interactions in a multilayer waveguide in the weak-coupling approximation and reformulate the problem in terms of scattering data.

Fig. 2 shows two neighboring (nonoverlapping) potentials corresponding to two waveguides separated by a distance s:

$$s = d_R - d_L \quad (d_L < 0). \tag{21}$$

Each waveguide is assumed to have a graded-index core with refractive index profiles $n_L(x)$ and $n_R(x)$:

$$n_L^2(x) = n_2^2 + \Delta n_L^2(x),$$
$$n_R^2(x) = n_2^2 + \Delta n_R^2(x). \tag{22}$$

We will assume that each waveguide separately supports y-polarized TE modal fields $E_L(x)$ and $E_R(x)$ with propagation constants β_L and β_R, respectively. The interaction between the two fields will be represented by a z-dependent linear combination of the individual waveguide modes:

$$\mathscr{E}(x, z, t) = A(z) E_R(x) e^{i(\omega t - \beta_R z)}$$
$$+ B(z) E_L(x) e^{i(\omega t - \beta_L z)}, \tag{23}$$

the exact form of the z-dependent weighting coefficients $A(z)$ and $B(z)$ being a function of the interaction strength induced by the transverse coupling. The governing equation for the field in (23),

$$\frac{\partial^2 \mathscr{E}}{\partial x^2} + \frac{\partial^2 \mathscr{E}}{\partial z^2} + \frac{\omega^2}{c^2} n^2(x) \mathscr{E} = 0, \tag{24}$$

where $n^2(x)$ is the refractive index of the composite structure,

$$n^2(x) = n_2^2 + \Delta n_L^2(x) + \Delta n_R^2(x), \tag{25}$$

dictates the coupling analysis which carries with it three explicit assumptions.

i) Each waveguide individually supports a single mode with propagation constants β_L and β_R.

ii) The coupling is weak, i.e.,

$$\left| \frac{d^2 A}{dz^2} \right| \ll \left| \beta_R \frac{dA}{dz} \right|, \quad \left| \frac{d^2 B}{dz^2} \right| \ll \left| \beta_L \frac{dB}{dz} \right|, \tag{26}$$

iii)

$$\int_{-\infty}^{+\infty} E_L(x) E_L(x) \, dx \ll \int_{-\infty}^{+\infty} E_{L,R}^2(x) \, dx. \tag{27}$$

Ignoring the second derivatives of $A(z)$ and $B(z)$, the wave equation reduces to a set of coupled first-order differential equation for the z-dependent coefficients:

$$\frac{dA}{dz} = i \kappa_{RL} B(z) e^{-i(\beta_L - \beta_R) z} + i \kappa_{RR} A(z),$$

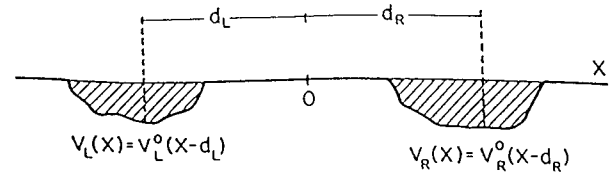$$\frac{dB}{dz} = i \kappa_{LR} A(z) e^{i(\beta_L - \beta_R) z} + i \kappa_{LL} B(z), \tag{28}$$

Fig. 2. Coupled potentials used to model the scattering picture of weakly coupled planar waveguides.

where the coupling coefficients

$$\kappa_{RL} = \frac{I_{RL}}{2 \beta_R N_{RR}},$$

$$\kappa_{RR} = \frac{I_{RR}}{2 \beta_R N_{RR}}, \tag{29}$$

are functions of the interaction and normalization integrals:

$$I_{RL} \equiv \int_{-\infty}^{+\infty} E_R(x) v_R(x) E_L(x) \, dx,$$

$$I_{RR} \equiv \int_{-\infty}^{+\infty} E_R(x) v_R(x) E_R(x) \, dx, \tag{30}$$

$$N_{RR} \equiv \int_{-\infty}^{+\infty} E_R^2(x) \, dx.$$

The coefficients κ_{LR} and κ_{LL} follow by interchanging L and R. The self-coupling coefficients κ_{LL} and κ_{RR} represent small corrections to the propagation constants and are usually ignored.

In the phase-matched case ($\beta_L = \beta_R \equiv \beta$), the solutions to (28) are

$$A(z) = \left\{ A(z_0) \cos \Delta \beta z + i \sqrt{\frac{\kappa_{RL}}{\kappa_{LR}}} B(z_0) \sin \Delta \beta z \right\},$$

$$B(z) = \left\{ B(z_0) \cos \Delta \beta z + i \sqrt{\frac{\kappa_{LR}}{\kappa_{RL}}} A(z_0) \sin \Delta \beta z \right\},$$

$$\tag{31}$$

where

$$\Delta \beta \equiv \sqrt{\kappa_{RL} \kappa_{LR}}, \tag{32}$$

and z_0 is the initial point of interaction. Given the initial condition $\mathscr{A}(z_0) = 0$, the solutions become

$$A(z) = i B(z_0) \sin \Delta \beta z,$$

$$B(z) = B(z_0) \cos \Delta \beta z, \tag{33}$$

provided

$$\kappa_{RL} = \kappa_{LR} \equiv \kappa, \tag{34}$$

so that complete power transfer occurs at intervals of $(\pi/2) \Delta \beta$ along the coupled length of the waveguides. Substituting these expressions for $A(z)$ and $B(z)$ into (23) indicates that the total electric fields consists of an ap-

proximate linear superposition of modes with propagation constants,

$$\beta^+ = \beta + \Delta\beta,$$
$$\beta^- = \beta - \Delta\beta. \tag{35}$$

The interaction and normalization integrals are the principal calculational hurdle associated with the weak-coupling model. The latter, as previously shown, have a convenient representation in terms of the scattering data. In the next paragraphs we outline established scattering relationships which are useful in representing the interaction integrals.

Consider two different potentials $v(x)$ and $\bar{v}(x)$. (These are not, in general, the potentials describing the two individual waveguides [4]). In the limit as $x \to -\infty$, it follows that

$$W\left[f_+(k, x), \bar{f}_+(k, x)\right] = \frac{2ik}{t(k)\bar{t}(k)}[r_-(k) - \bar{r}(k)], \tag{36}$$

while in the limit as $x \to \infty$, this Wronskian vanishes since $f_+(k, x) \equiv \bar{f}_+(k, x) \sim e^{ikx}$.

Now consider the derivative,

$$\frac{d}{dx} W\left[f_+(k, x), \bar{f}_+(k, x)\right]$$
$$= [\bar{v}(x) - v(x)]f_+(k, x)\bar{f}_+(k, x). \tag{37}$$

Integrating this expression yields

$$\int_{-\infty}^{+\infty} \frac{d}{dx} W\left[f_+(k, x), \bar{f}_+(k, x)\right] dx$$
$$= -W\left[f_+(k, x), \bar{f}_+(k, x)\right]\Big|_{x = -\infty}, \tag{38}$$

providing a convenient integral relation for the Wronskian:

$$\int_{-\infty}^{+\infty} [v(x) - \bar{v}(x)]f_+(k, x)\bar{f}_+(k, x)\, dx$$
$$= \frac{2ik}{t(k)\bar{t}(k)}[r_-(k) - \bar{r}_-(k)]. \tag{39}$$

Using similar steps, a companion expression can be derived:

$$\int_{-\infty}^{+\infty} [v(x) - \bar{v}(x)]f_-(k, x)\bar{f}_-(k, x)\, dx$$
$$= \frac{2ik}{t(k)\bar{t}(k)}[r_+(k) - \bar{r}_+(k)]. \tag{40}$$

If $\bar{v}(x) = 0$, (39) and (40) reduce to the useful form

$$\int_{-\infty}^{+\infty} f_\pm(k, x)v(x)e^{\pm ikx}\, dx = \frac{2ik}{t(k)}r_\mp(k). \tag{41}$$

Writing the guided-mode electric fields of the right-hand (or top) and left-hand (or bottom) waveguides in terms of the Jost solutions for the respective potentials $v_R^0(x)$ and $v_L^0(x)$ gives

$$E_R(x) \equiv f_-^{0R}(ia, x - d_R),$$
$$E_L(x) \equiv f_+^{0L}(ia, x - d_L), \tag{42}$$

where a bound state with eigenvalue $k = ia$ ($a > 0$) is assumed. With the help of (30) nd (42), we find

$$I_{LR} = e^{-ad_R}\int_{-\infty}^{+\infty} f_+^{0L}(k, x - d_L)v_l(x)e^{-ikx}dx\big|_{k = ia}$$
$$= -2ae^{-as}. \tag{43}$$

The normalization integral N_{LL} is simply [5]

$$N_{LL} = \int_{-\infty}^{+\infty} \left[f_+^{0L}(ia, x - d_L)\right]^2 dx = \frac{i}{\operatorname{Res} r_+^{0L}(ia)}. \tag{44}$$

Defining the shape factors

$$F_+^R \equiv \operatorname{Im}\{\operatorname{Res} r_-^{0R}(ia)\},$$
$$F_+^L \equiv \operatorname{Im}\{\operatorname{Res} r_+^{0L}(ia)\}, \tag{45}$$

gives

$$\kappa_{LR} = \frac{I_{LR}}{2\beta N_{LL}} = \frac{-a}{\beta}e^{-as}F_+^L, \tag{46}$$

and by the same token,

$$\kappa_{RL} = \frac{I_{RL}}{2\beta N_{RR}} = \frac{-a}{\beta}e^{-as}F_-^R. \tag{47}$$

Here, r_-^{0R} and r_+^{0L} are the reflection coefficients for a plane wave impinging from $x = -\infty$ and $x = +\infty$, respectively. These results indicate that when placed in the context of scattering theory, the directional coupling coefficients take on a particularly simple form consisting of a portion which is dependent solely upon the eigenvalue and the waveguide separation, multiplied by a factor whose value is dependent upon the inherent shape of the potential. The condition for complete power transfer takes the particularly simple form

$$F_+^L = F_-^R. \tag{48}$$

One form of this condition, which is likely to be encountered in practice, is simply

$$r_-^R(k) = r_+^L(k), \tag{49}$$

which implies

$$v_L(x) = v_R(-x), \tag{50}$$

and the intuitively appealing conclusion that a waveguide is coupled with 100% efficiency to its "mirror image."

IV. Design Examples

A. Step-Index Waveguides

Coupling in step-index waveguides has been analyzed using standard methods (see [5]); therefore, it can serve as a check for the coupled-mode formalism we have derived. Consider a square well potential of width $D \equiv 2d_0$:

$$v(x) = \begin{cases} k_0^2(n_0^2 - n_1^2), & -d_0 < x < d_0, \\ 0, & \text{elsewhere,} \end{cases} \tag{51}$$

whose corresponding refractive index profile is a step-index planar waveguide with constant core refractive index n_1. Defining the parameter

$$K \equiv \sqrt{k^2 - k_0^2(n_2^2 - n_1^2)} = \sqrt{k_0^2 n_1^2 - \beta^2}, \quad (52)$$

we can write the Jost solutions for square well potential as

$$f_-(k, x) = \begin{cases} a_s(k) \sin Kx \\ \quad + a_c(k) \cos Kx, & -d_0 \leq x \leq d_0, \quad (53) \\ e^{-ikx}, & x < -d_0, \end{cases}$$

and

$$f_+(k, x) = \begin{cases} b_s(k) \sin Kx \\ \quad + b_c(k) \cos Kx, & -d_0 \leq x \leq d_0, \quad (54) \\ e^{+ikx}, & x > d_0. \end{cases}$$

Continuity of the Jost solutions and their derivatives at these boundaries gives the coefficients:

$$a_s(k) = \frac{-e^{ikd_0}\{K \sin Kd_0 + ik \cos Kd_0\}}{K},$$

$$a_c(k) = \frac{e^{ikd_0}\{K \cos Kd_0 - ik \sin Kd_0\}}{K}, \quad (55)$$

$$b_s(k) = -a_s(k),$$

$$b_c(k) = a_c(k).$$

The reflection coefficient (from (11 and (12)), follows in a straightforward way:

$$r_-(k) = \frac{a_x(-k)b_c(k) - b_s(k)a_c(-k)}{2b_s(k)a_c(k)}, \quad (56)$$

whose pole locations lead to the familiar eigenvalue equations

$$\tan Kd_0 = \begin{cases} \dfrac{-ik}{K}, & \text{even,} \\ \dfrac{K}{ik}, & \text{odd.} \end{cases} \quad (57)$$

This result is applicable to both single- and multimode waveguides. We are interested in the fundamental mode with eigenvalue $k_1 = ia$, for which the residue is given by

$$\text{Res }\{r_-(ia)\} = -\frac{1}{2}e^{-2ikd_0} \left. \frac{K \tan Kd_0 - ik}{\dfrac{d}{dk}\{K \tan Kd_0 + ik\}} \right|_{k=ia}. \quad (58)$$

With the help of (47) and (57), the coupling coefficient takes the form

$$|\kappa_{RL}| = \frac{K^2 a^2}{\beta(1 + ad_0)k_0^2(n_1^2 - n_2^2)} e^{-as}e^{2ad_0}, \quad (59)$$

in exact agreement with the result obtained using the standard method [6].

B. Depressed-Cladding Waveguides

The foregoing result puts scattering theory in direct contact with established results, but provides little motivation to apply scattering theory as opposed to the conventional techniques, due largely to the fact that the guided-mode fields have straightforward representations and the interaction and normalization integrals can be readily calculated. As refractive index profiles become more complicated, the need for an alternative method becomes more compelling. Jordan and Lakshmanasamy [7] designed high-V-number single-mode planar waveguides using a rational reflection coefficient of the form

$$r_-(k) = \frac{-k_1 k_2 k_3}{(k - k_1)(k - k_2)(k - k_3)}, \quad (60)$$

which yields a single bound mode eigenvalue at $k_3 = ia$, and two poles $k_1 = -c_1 - ic_2$ and $k_1 = c_1 - ic_2$ in the lower half of the complex k plane which represent tunneling leaky waves. The authors showed that the Gelfand–Levitan reconstruction technique results in a corresponding potential

$$v(x) = 2\left[\frac{d\alpha}{dx} - \alpha(x)A^{-1}(x)A'(x)\right]A^{-1}(x)\gamma^T, \quad (61)$$

where α and γ are the row vectors

$$\alpha = \begin{bmatrix} 1 & x & e^{\eta_1 x} & e^{-\eta_1 x} & e^{-\eta_2 x} \end{bmatrix},$$

$$\gamma = \begin{bmatrix} 0 & 0 & 0 & 0 & 0 & -a(c_1^2 + c_2^2) \end{bmatrix}, \quad (62)$$

and $A(x)$ is a 6×6 matrix whose elements are listed in the Appendix. The parameters are defined,

$$\eta_1 = [(\sigma + p)/2]^{1/2},$$

$$\eta_2 = [(\sigma - \rho)/2]^{1/2},$$

$$\sigma = a^2 + 2c_2^2 - 2c_1^2, \quad (63)$$

$$\rho = [(a^2 - 4c_2^2)(a^2 + 4c_1^2)]^{1/2}.$$

Some restrictions apply to the relative location of the poles a, c_1, and c_2 brought about by requiring a real potential. Specifically,

$$0 < c_2 < \frac{-a}{2} \quad (64)$$

places a lower bound on c_2, and

$$\sigma > \rho \quad (65)$$

etches an upper limit on c_1 and c_2. This condition is identical to the one derived in [6] based upon the conservation of energy condition,

$$|r(k)|^2 \leq 1, \quad \text{all } \text{Re } k. \quad (66)$$

Each of the three refractive index profiles illustrated in Fig. 3 propagates a single mode with propagation constant

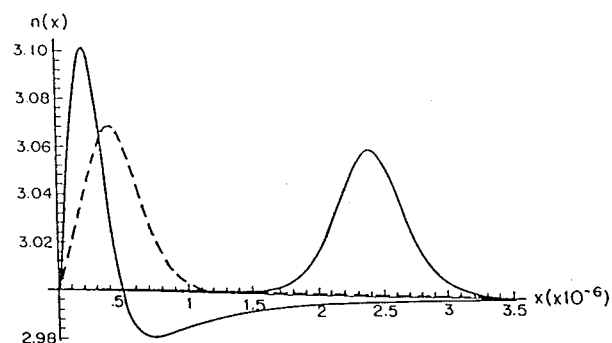$$\beta = 1.01034 k_0 n_2. \quad (67)$$

Fig. 3. Three depressed-cladding refractive index profiles for different (c_1, c_2): $(0, 0.001a)$ far right, $(0, 0.25a)$ dashed; $(0.499a, \sqrt{0.687}\,a)$ left.
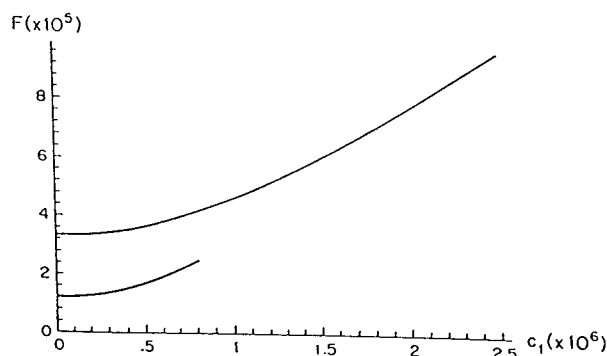

Fig. 4. Shape factors as a function of c_1 for $c_2 = 0.499a$ (top), and $c_2 = 0.25a$.

The depressed portion of the refractive index, characterized by a portion of the profile dipping below the nominal AlGaAs cladding value $n_2 = 3.0$, is most clearly evidenced as the poles for the tunneling leaky modes are moved farther from the lower Im k axis.

The residue at the pole representing the bound mode is easily found to be

$$\text{Res } r_-(ia) = ia \frac{(c_1^2 + c_2^2)}{\left(c_1^2 + (a + c_2)^2\right)} = ia \frac{\alpha^2 + \gamma^2}{\alpha^2 + (1 + \gamma)^2},$$
(68)

where $c_1 = \alpha a$ and $c_2 = \gamma a$. In Fig. 4, the shape factor, an indicator of coupling, is plotted as a function of c_1, showing a monotonic increase (for a given c_2) as the poles are moved out into the complex plane. Based on the form of the refractive index profiles themselves, this result is expected, as a decrease in c_1 is associated with translation of the optical channel along the positive x axis.

Fig. 3 suggests that for small values of c_1 and c_2, the refractive index profile approximates a sech$^2 x$ form, suitably scaled and translated a finite distance along the positive x axis. This is indeed the case, and such profiles (developed from a slightly different perspective) are taken up in the next section.

C. Truncated Refractive Index Profile Waveguides

We now consider the family of single-mode refractive index profiles based on truncated versions of the potential

$$v_s(x) = -4b^2 \text{ sech}^2 b\sqrt{2}\,x,$$
(69)

parameterized by the positive scaling constant b. Potentials of this form are single mode with a bound state eigenvalue $k = ib\sqrt{2}$. Eq. (69) is representative of a smooth function which decays relatively rapidly for large $|x|$, making it a suitable refractive index profile for waveguide design. For the purposes of this paper, a truncation is a discontinuity imposed upon a smooth potential, at a point $x = x_1$ such that

$$v(x) = 0, \quad (x < x_1).$$
(70)

Clearly, this creates a cladding region of constant refractive index

$$n(x) + N_2, \quad (x < x_1).$$
(71)

In previous work we completed an extensive analysis of these potentials from the standpoint of scattering theory, including the effects of truncations of the potentials to model core–cover interfaces, considering both single- and multimode waveguides [8]. In the present paper, we extend our analysis to include the effects of truncations upon the coupling coefficient. Although we restrict ourselves to single-mode waveguides arising from potentials of the form in (69), coupling between modes in multimode waveguides follows a similar analysis.

We have previously shown that the transmission coefficient may be written in terms of the Jost solution $f_+(k, x)$ of the corresponding untruncated potential. In the case of a single truncation at the point $x = x_1$, the transmission coefficient takes the particularly simple form

$$t^T(k) = 2ike^{ikx_1}[f'_+(k, x_1) + ikf_+(k, x_1)]^{-1}, \quad (72)$$

whose poles provide the eigenvalues (and corresponding propagation constants) as a function of x_1. Here the prime denotes differentiation with respect to the spatial coordinate. Up to this point the results are completely general.

The Jost solutions for potentials $v_s(x)$ (69) take the form

$$f_+(k, x) = e^{ikx}\left[\frac{ik - b\sqrt{2} \tanh b\sqrt{2}\,x}{ik - b\sqrt{2}}\right].$$
(73)

Used in conjunction with (72), the Jost solution provides an analytic expression for the bound state eigenvalue k,

$$k = \frac{i}{2}\left[-b\sqrt{2} \tanh b\sqrt{2}\,x_1 + b\sqrt{2} \sqrt{1 + \text{sech}^2 b\sqrt{2}\,x_1}\right].$$
(74)

The ratio

$$\frac{r_-^T(k)}{t^T(k)} = \frac{e^{ikx_1}}{2ik}[ikf_+(k, x_1) - f'_+(k, x_1)], \quad (75)$$

combined with (72) and (73), gives the reflection coefficient

$$r_-(k) = \frac{-be^{2ikx_1} \text{ sech}^2 b\sqrt{2}\,x_1}{(k - k_p)(k - k_n)},$$
(76)

where k_p and k_n lie on the positive and negative imaginary axes, respectively, taking the values

$$\frac{i}{2} b\sqrt{2} \left\{ -t_1 \pm \sqrt{\left(1 + \text{sech}^2 b\sqrt{2} x_1 \right)} \right\},$$

$$t_1 \equiv \tanh b\sqrt{2} x_1. \quad (77)$$

When (72) is reduced, the transmission coefficient has the simple form

$$t^T(k) = \frac{2k(k + ib\sqrt{2})}{(k - k_p)(k - k_n)}. \quad (78)$$

The shape factor of the multilayer planar waveguide coupler can be conveniently expressed as a function of the truncation point,

$$F^T = \frac{be^{2ik_p x_1} \text{sech}^2 b\sqrt{2} x_1}{\sqrt{2\left(1 + \text{sech}^2 b\sqrt{2} x_1\right)}}. \quad (79)$$

In Fig. 5 we plot the shape factor, along with $2k_p/i$, as a function of the truncation point x_1. For comparison, we have included the magnitude of the area under the potential

$$|A| = \frac{-4b}{\sqrt{2}} \left[1 - \tanh b\sqrt{2} x_1 \right], \quad (80)$$

which is also a monotonically decreasing function of x_1. It is interesting to note that the decrease in the shape factor more closely parallels the behavior of the area for a larger interval of x_1 than it does the eigenvalue itself.

In Section III we emphasized that the well-known coupled-mode electric field is effectively a two-mode solution for the composite double-well system representing the coupled waveguides. For two reasons, it is appropriate to follow up on the implications of (32). First, scattering theory provides a straightforward way to evaluate eigenvalues of a composite structure consisting of two nonoverlapping potentials, and second, it provides further verification that scattering analysis of the coupled-mode problem is consistent with known results.

Starting from first principles, it is straightforward to show that the transmission coefficient of the composite potential (see Fig. 2) takes the form [9]

$$t^c(k) = t^L(k) t^R(k) \sum_{m=0}^{\infty} \left(r_-^R(k) r_+^L(k) \right)^m$$

$$= t^L(k) t^R(k) \left(\frac{1}{1 - r_-^R(k) r_+^L(k)} \right). \quad (81)$$

The scattering data in this expression applies to the potentials $v_L(x)$ and $v_R(x)$. From this point we will reduce this general result to encompass the special case of two "mirror-image" single-mode truncated potentials separated by a distance $2d$ (i.e., $d_R = -d_L = d$) for which the scattering coefficients take the form of fractions made up of arbitrary k-dependent functions, the numerator and
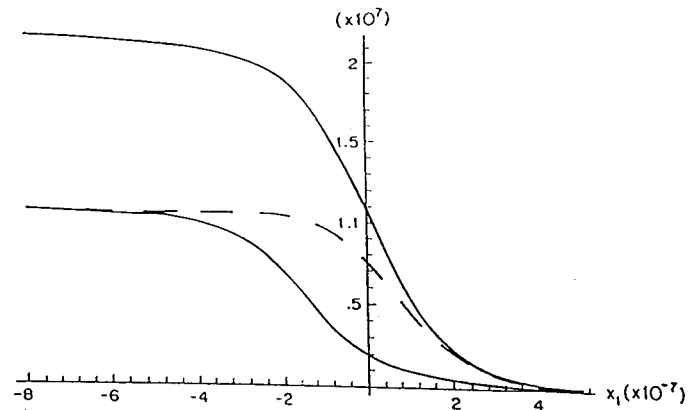
Fig. 5. From top to bottom: the area under the potential, the shape factor, and $2k_p/i$ as a function of the truncation point.

denominator denoted with the appropriate subscripts n and d:

$$r_-^R(k) = r_+^L(k) = e^{i2kd} \frac{r_n(k)}{r_d(k)}, \quad (82)$$

and

$$t^L(k) = t^R(k) = \frac{t_n(k)}{t_d(k)}, \quad (83)$$

so that the composite transmission coefficient can be written

$$t^c(k) = \frac{t_n^2(k)}{r_d^2(k) - e^{i4kd} r_n^2(k)}. \quad (84)$$

It is clear that for sufficiently large separations, the transmission coefficient will exhibit two closely spaced bound state eigenvalues lying close to the original single eigenvalue. As we mentioned, the corresponding propagation constants,

$$\beta^+ = \beta + \Delta\beta^+$$

$$\beta^- = \beta - \Delta\beta^-, \quad (85)$$

which are roots of the denominator of (84), provide an approximation to the coupling coefficient (see [1])

$$\kappa \simeq \Delta\beta^+ \simeq \Delta\beta^-, \quad (86)$$

provided that the waveguides are weakly coupled.

Consider the truncated single-mode potential of (69),

$$v_R(x) = \begin{cases} -4b^2 \text{sech}^2 b\sqrt{2} x, & x > 0, \\ 0, & x < 0, \end{cases} \quad (87)$$

whose reflection coefficient

$$r_-(k) = \frac{-b^2}{k^2 + b^2}, \quad (88)$$

71

follows directly from (76) with $x_1 = 0$. There is a single bound state eigenvalue at $k = ib$. The composite structure, consisting of this potential shifted a distance d along the $+x$ direction, and its mirror image, each with reflection coefficients (see (14))

$$r_+^L(k) = r_-^R(k) = e^{2ikd} \frac{-b^2}{k^2 + b^2}, \qquad (89)$$

has eigenvalues $k^\pm = \sqrt{\beta^{\pm 2} - k_0^2 n_0^2}$ given by the roots of the denominator of (84).

An approximation to the shape factor of the single-mode potential is found by inverting (47):

$$F \simeq \frac{-\beta}{b} e^{bs} \Delta\beta^+ \simeq \frac{-\beta}{b} e^{bs} \Delta\beta^-, \qquad (90)$$

where $s = 2d$. As the separation is increased, a convergence of β^+ and β^- towards β is expected, leading to better approximations to the shape factor.

In Table I we list the eigenvalues and corresponding approximate values of the shape factor (from (90)) against the exact value

$$\text{Im Res } r_-^R(ib) = \frac{b}{2} = 1.889 \times 10^6. \qquad (91)$$

(We have taken $b = 3.778 \times 10^6$). As d is increased, the expected rapid convergence to the correct shape factor is readily apparent. Physically, this is the result of the in-

TABLE I
EIGENVALUES AND CORRESPONDING SHAPE FACTORS (90) FOR THREE VALUES OF SEPARATION

s (μm)	eigenvalues (×10^6)		shape factors (×10^6)	
	k^+	k^-	Eq. (90), corresponding to $\Delta\beta^+$	Eq. (90), corresponding to $\Delta\beta^-$
1	3.733	3.819	1.977	1.812
2	3.777	3.779	1.893	1.885
3	3.778	3.778	1.889	1.889

TABLE II
REPRESENTATIVE VALUES OF THE SHAPE FACTOR FOR THE THREE TYPES OF REFRACTIVE INDEX PROFILE CONSIDERED IN THIS PAPER

Type of profile	Shape factor
Step Index	2.26×10^9
Truncated $Sech^2\ \alpha x$	$1.89 - 7.56 \times 10^6$
High -V Profile	$1.5 - 9.0 \times 10^5$

The step index profile has a width of 0.94 μm and a core refractive index $n_1 = 3.1$

replacing the explicit calculation of field-dependent interaction integrals with straightforward expressions involving the residues of the scattering data, the method provides further motivation to employ inverse scattering methods in the design of optical devices.

APPENDIX

The matrix $A(x)$:

$$\begin{bmatrix} 0 & 1 & 0 & 0 & 0 & 0 \\ 0 & 0 & f(\eta_1) & a(c_1^2 + c_2^2) & 0 & 0 \\ 0 & 0 & 0 & 0 & f(\eta_1) & a(c_1^2 + c_2^2) \\ 1 & -x & e^{-\eta_1 x} & e^{\eta_1 x} & e^{-\eta_2 x} & e^{\eta_2 x} \\ 0 & -1 & \frac{d}{dx}e^{-\eta_1 x} & \frac{d}{dx}e^{\eta_1 x} & \frac{d}{dx}e^{-\eta_2 x} & \frac{d}{dx}e^{\eta_2 x} \\ 0 & 0 & \frac{d^2}{dx^2}e^{-\eta_1 x} & \frac{d^2}{dx^2}e^{\eta_1 x} & \frac{d^2}{dx^2}e^{-\eta_2 x} & \frac{d^2}{dx^2}e^{\eta_2 x} \end{bmatrix}, \qquad (92)$$

creasing accuracy of the weak-coupling mode as the waveguides are separated. Representative values of shape factor for all the three types of profiles discussed here are shown in Table II for comparison.

Aside from the general analytic interest of this approximation, it may be advantageous to apply it in situations where the residue of the reflection coefficient is complicated or difficult to calculate. In our experience, this is often the case for refractive index profiles incorporating two truncations (to simulate two cladding regions), for which the residues undergo extremely rapid variations in the vicinity of the bound state eigenvalues. Certainly, further work is needed in this area.

V. CONCLUSION

Coupling in multilayer waveguide structures is studied here using scattering techniques. As inverse methods find wider applications in waveguide design, the scattering representation of transverse coupled modes developed here will be useful in the design of multilayer devices. By

where

$$f(\eta_m) = (\eta_m + ik_1)(\eta_m + ik_2)(\eta_m + ik_3), \quad m = 1, 2. \qquad (93)$$

REFERENCES

[1] D. Marcuse, *Theory of Dielectric Waveguides*, 2nd. ed. Boston: Academic Press, 1991.
[2] W. K. Burns and A. F. Milton, "Waveguide transitions and junctions," in *Guided Wave Optoelectronics*, T. Tamir, Ed. Berlin: Springer-Verlag, 1990.
[3] H. A. Haus and W. Huang, "Coupled-mode theory," *Proc. IEEE*, vol. 79, no. 10, pp. 1505–1518, Oct. 1991.
[4] K. Chadan and P. C. Sabatier, *Inverse Problems in Quantum Scattering Theory*, 2nd. ed. Berlin: Springer-Verlag, 1989.
[5] G. L. Lamb, *Elements of Soliton Theory*. New York: Wiley 1977, p. 52.
[6] D. Marcuse, *Light Transmission Optics*, 2nd. ed. Englewood Cliffs, NJ: Prentice-Hall, 1983.
[7] A. K. Jordan and S. Lakshmanasamy, "Inverse scattering theory applied to the design of single-mode planar optical waveguides," *J. Opt. Soc. Am. A*, vol. 6, no. 8, pp. 1206–1212, Aug. 1989.

[8] D. W. Mills and L. S. Tamil, "Analysis of planar optical waveguides using scattering data," *J. Opt. Soc. Am. A*, vol. 9, no. 10, pp. 1769–1778, Oct. 1992.

[9] J. A. Kong, *Electromagnetic Wave Theory*, 2nd. ed. New York: Wiley-Interscience, 1990.

Duncan W. Mills received the B.A. degree in physics from Wesleyan University, the M.S. degree in electrical engineering from George Washington University, and the Ph.D. degree in electrical engineering from the University of Texas at Dallas.

He is presently working at Verity Instruments, Carrollton, TX, where he is technical director of the ellipsometry and materials characterization project. Prior to his current position, Dr. Mills was a research scientist at the University of Texas at Dallas. He also worked at the Naval Research Laboratory engaged in projects involving ionospheric propagation and scatter in optical systems. His primary research interests are optical waveguides and electromagnetic theory.

He is a member of Eta Kappa Nu and the Optical Society of America.

Lakshman S. Tamil (S'83–M'88) received the B.E. degree in electronics and communication engineering from the Madurai Kamaraj University, Madurai, India, in 1981 and the M. Tech. degree in microwave and optical communication engineering from the Indian Institute of Technology, Kharagpur, India, in 1983. From the University of Rhode Island, Kingston, RI, he received the M.S. degree in mathematics and the Ph.D. degree in electrical engineering in 1988.

He joined the University of Texas at Dallas, Richardson, TX as an assistant professor in electrical engineering in 1988 and he is currently an Associate Professor in the same department. He is also a member of the Center for Applied Optics in the same university. His research interests include fiber optics, photonic integrated devices and circuits, nonlinear guided wave optics, semiconductor lasers, inverse scattering theory, and numerical methods applied to electromagnetic problems and communication networks.

Dr. Tamil is a member of the IEEE Antennas and Propagation Society, Sigma Xi, the Optical Society of America, and the Electromagnetics Academy, and is a elected member of Commission B and D of the International Union of Radio Science.

Appendix E

**L. S. Tamil and M. A. Hooshyar, "Inverse Scattering Theory
and the Design of Planar Optical Waveguides With
Same Propagation Constants for Different Frequencies"**

Inverse Problems, Vol. 9, pp. 69–80, 1993.

Inverse scattering theory and the design of planar optical waveguides with the same propagation constants for different frequencies

M A Hooshyar† and Lakshman S Tamil‡

† Programs in Mathematical Sciences, The University of Texas at Dallas, Box 830688, Richardson, TX 75083-0688, USA
‡ Erik Jonsson School of Engineering and Computer Science, The University of Texas at Dallas, Box 830688, Richardson, TX 75083-0688, USA

Abstract. Application of inverse scattering theory for designing planar optical waveguides possessing prescribed propagation constants for light with a given frequency is well known. However, waveguides designed using such a method, in general, will not be able to transmit light at other frequencies with the same propagation constant. In order to overcome this difficulty, the design problem for TE modes is transformed and reformulated to an equivalent inverse problem for Schrödinger's equation. Then using inverse scattering theory, the potential as a function of a modified spatial variable is recovered. Next the important problem of finding an explicit relation between the actual spatial variable and the modified spatial variable is solved and a systematic procedure is developed for designing waveguides which have the same propagation constant for different light frequencies. Existence and uniqueness questions are studied and some model calculations are presented.

1. Introduction

Proper values of propagation constants are very important in the design of waveguides, since they govern the spatial and temporal characteristics of the signals transmitted in waveguides. Systematic procedures for designing waveguides with prescribed propagation constants appeal to the existing inverse scattering theories [1–5], which were originally developed for the inverse problems in quantum mechanics. In standard applications of inverse scattering theories for designing optical waveguides [6–9], we make use of the fact that at a fixed frequency Maxwell's equations governing the light propagation in a waveguide can be transformed to Schrödinger's equation with an energy–independent potential. In this equivalent quantum mechanical inverse problem, the bound states energies are associated with the prescribed propagation constants, and the potential is related to the refractive index of the designed waveguide.

The systematic procedures for designing waveguides as outlined above [6–9] are applicable as long as we are interested in light propagation with a prescribed propagation constant at a single frequency through the designed waveguide. However, such a waveguide in general will not have the designed propagation constants for light with frequencies other than the specific frequency used in the design of the waveguide. Waveguides, which have the same propagation constants for different light frequencies,

have important applications in optics, such as in harmonic generation, wave mixing, parametric amplification, and multiplexing [10–12].

The need for developing a systematic method to design waveguides having the same propagation constant for different light frequencies has motivated us, in this preliminary study, to design planar optical waveguides that have the same propagation constant for TE modes at different frequencies. We achieve this objective by showing that Maxwell's equations can be related to Schrödinger's equation with an energy-dependent potential and that the requirement for the waveguide to have the same propagation constant for *m* different frequencies is shown to be equivalent to the corresponding energy-dependent potential supporting *m* bound states of specified values. Having reduced the problem to an inverse Schrödinger problem for energy-dependent potentials, we then subject this Schrödinger equation to a transformation [13–19] which reduces the inversion to a Schrödinger inverse problem for an energy-independent potential. The modified inversion problem is then solved by using the existing Schrödinger inverse scattering methods in one dimension [1–5]. However, since the equivalent inverse Schrödinger problem is formulated with respect to a modified spatial variable and not the actual spatial variable, the energy independent potential found will not be of any use unless the connection between the actual spatial variable and the modified spatial variable is established. We study this important problem in detail and find an explicit relation between the actual and the modified variable, which then enables us to make use of the energy independent potential and develop a systematic and practical procedure to design waveguides which have the same propagation constant for different light frequencies.

In section 2 we review the problem of electromagnetic wave propagation in a planar waveguide. Section 3 deals with transforming Maxwell's equations to Schrödinger's equation with an energy-independent potential and developing a systematic method to design a waveguide which has the same propagation constant for different frequencies. In section 4 examples of practical interest in waveguide design are presented. We find that the proposed method enables us to design waveguides which have the same propagation constant for any finite number of different light frequencies. The procedure leads to solutions which depend on infinitely many arbitrary parameters. Of course, this non-uniqueness can be further manipulated, enabling the designed waveguide to have other desirable properties.

2. Statement of the problem

Propagation of electromagnetic waves in a planar optical waveguide, with refractive index varying continuously only in one direction say x, is analyzed by assuming that the electric, E, and magnetic, H, fields have the following forms [6]:

$$E_\alpha(x, y, z, t) = E_\alpha(x)e^{i(\omega t - \beta z)} \tag{2.1}$$

$$H_\alpha(x, y, z, t) = H_\alpha(x)e^{i(\omega t - \beta z)} \tag{2.2}$$

where x, y, and z are the cartesian coordinates with z along the axis of the waveguide, t is time, α represents the components of a vector in the x, y, or z directions, ω is the light frequency, and β is the propagation constant. Subsitution of (2.1) and (2.2) in Maxwell's equations lead to the following equation [6].

$$\frac{d^2}{dx^2}\psi(x) + [n^2(x, k_0)k_0^2 - \beta^2]\psi(x) = 0 \tag{2.3}$$

for the TE modes. In (2.3) the positive function $n(x, k_0)$ is the refractive index, $k_0 = \omega/c$, with c being the speed of light in vacuum, and $\psi(x)$ is the field function associated with the electromagnetic fields under consideration. The field function $\psi(x)$ is to decay fast enough, as $|x|$ increases, so that the field function is associated with finite energy which is mostly confined to the inside of the waveguide.

It is well known that the differential equatio (2.3) with the above condition can have solution only for certain values of β, which are called the eigenvalues of the differential equation, and for the problem at hand correspond to different possible propagation constants of the waveguide. Therefore in the waveguide design problem at a fixed frequency, one only need to find $n(x, k_0)$ which is associated with the desired propagation constants β for the specified frequency. A standard procedure to solve this design problem is to appeal to the theory of inverse scattering which was first developed in quantum mechanics, where one has to find the potential from the spectral data of the associated Schrödinger equation [1–5]. In order to be able to make use of the well developed methods of inverse scattering theory in quantum mechanics [1–5], one transforms (2.3) into a Schrödinger differential equation form

$$\frac{\mathrm{d}^2}{\mathrm{d}x^2}\psi(x) + [k^2 - k_0^2 V(x, k_0)]\psi(x) = 0 \tag{2.4}$$

where

$$k^2 = n_\infty^2(k_0)k_0^2 - \beta^2 \tag{2.5}$$

$$V(x, k_0) = n_\infty^2(k_0) - n^2(x, k_0) \tag{2.6}$$

with $n_\infty(k_0)$ being the refraction index for $|x| \to \infty$.

Having transformed the Helmholtz equation (2.3) into a Schrödinger equation (2.4), one notes that the design problem of optical waveguide, that is finding the index of refraction $n(x, k_0)$ which gives us the desired propagation constant β for the specified k_0, is reduced to an inverse scattering problem in quantum mechanics, where the potential $k_0^2 V(x, k_0)$ is to be deduced from the information on the bound states and the reflection coefficients. In this quantum mechanical formulation of the problem, one refers to k^2 as the energy of the system and the eigenvalues as the bound state energies, which we will denote by $-\gamma^2$. Of course as can be seen from (2.5) these binding energies, γ^2, are related to the desired propagation constants through the relation

$$\gamma^2 = \beta^2 - n_\infty^2(k_0)k_0^2. \tag{2.7}$$

From (2.7) it follows that specification of the propagation constant β and frequency ω, will give us the needed bound state energy information for the analogue quantum mechanical problem. Having established the connection between the optical waveguide and the inverse quantum mechanical problem, it is then straightforward to use existing methods [5–7] to find the desired potential $k_0^2 V(x, k_0)$ associated with the bound states and the reflection coefficients and then find the required refractive index $n(x, k_0)$ from $V(x, k_0)$ using (2.6). However, this standard approach is useful for designing waveguides associated with only one fixed frequency. That is, since the inversion potential $k_0^2 V(x, k_0)$ depends on the frequency ω, if we change ω, the potential will change resulting in change of the binding energy γ^2. In other words the waveguide designed will not have the desired propagation constant β at other frequencies. Therefore if we are interested in designing waveguides which have the same propagation constant for different frequencies, the method as stated above is not able to provide us with the desired profile. We will show

in the next section that it is still possible to use the results of inverse scattering theory [1–5] to design waveguides which can have the same propagation constant for different light frequencies.

Before concluding this section, let use note that the refractive index $n(x, k_0)$ in general is a function of both the spatial variable x and also the wavenumber k_0. The dependence of the refractive index on k_0 or the frequency of the light propagating through the waveguide is a very interesting and important topic. However, in this preliminary study, for the sake of simplicity in presentation, we restrict the study to refractive indexes which are twice differentiable with respect to x and have the following type of dependence on k_0 and x:

$$n(x, k_0) = n_\infty(k_0)\eta(x) \tag{2.8}$$

where $\eta(x)$ is a function of x only and, which tends to 1 as $|x|$ tends to infinity. Since $n_\infty(k_0)$ is associated with the refractive index of the cladding, it will be assumed that $n_\infty(k_0)$ is an arbitrary but known function of k_0. In other words, in this study we make the assumption that the refractive index is made up of a known positive function $n_\infty(k_0)$, multiplied by a positive function $\eta(x)$ which is a function of x only. In this study we also need to restrict $\eta(x)$ to class of function which satisfy the following inequality:

$$\int_{-\infty}^{+\infty} |\eta(x) - 1|\, dx < \infty. \tag{2.9}$$

The design problem to be presented in section 3 is to develop a systematic procedure for finding the frequency-independent function $\eta(x)$ corresponding to a refractive index which will allow different light frequencies to propagate through the waveguide with the same propagation constant β.

3. The inversion procedure

As was shown in the previous section, our design problem is to develop a systematic procedure to design waveguides which have the same propagation constant β for all different light frequencies of interest. In order to be able to restate this design specification in the equivalent inverse quantum mechanical problem in a more transparent fashion, let us rewrite the differential equation (2.4) in the following manner:

$$\frac{d^2}{dx^2}\psi(x) + [k^2 - k^2 V_1(x) - V_2(x)]\psi(x) = 0 \tag{3.1}$$

where

$$V_1(x) = V(x, k_0)/n_\infty^2(k_0) = 1 - \eta^2(x) \tag{3.2}$$

$$V_2(x) = \beta^2 V_1(x). \tag{3.3}$$

It should be remembered that throughout the discussion, the propagation constant β is fixed but the frequency ω can take different values, ω_i with $i = 1, 2 \ldots, m$. Since (3.1) is the same as (2.3), the eigenvalues of (3.1) will be the same as those of (2.3) and will be related to frequency ω and propagation constant β through (2.5). However, the advantage of writing (2.3) in the form of (3.1) is the fact that (3.1) clearly shows that our design problem is equivalent to an energy-dependent Schrödinger inverse problem and we are interested in finding $V_1(x)$ and $V_2(x)$ when binding energies of (3.1) are specified

according to following equation:

$$\gamma_i^2 = \beta^2 - n_\infty^2(k_{0i})k_{0i}^2 \qquad i = 1,2,\ldots,m \qquad (3.4)$$

where $k_{0i} = \omega_i/c$. Equation (3.4) is nothing but (2.7), and it is only written to emphasize the fact that in the problem of interest we are not given a single bound state energy, as may be inadvertently deduced from the fact that we only have one propagation constant, but in fact we are given m bound states energies. These binding energies can be easily computed from (3.4) by substituting the desired different values of frequency ω_i which we would like to propagate through the waveguide with the same propagation constant β.

Equation (3.1) as it stands is not in the standard Schrödinger equation form and therefore existing inversion methods for energy-independent potentials cannot be directly applied. However, similar equations have been dealt with when one tries to solve inverse problems for angular-momentum-dependent potentials [13–14] and wave equations in one dimension [15–19]. Motivated by these results, let us then transform our independent variable x to ρ, through the following relation:

$$\rho(x) = \int_0^x dt \sqrt{1 - V_1(t)} = \int_0^x \eta(t)\,dt. \qquad (3.5)$$

In view of the fact that $\eta(x)$ is a positive function, the above-defined mapping is one-to-one and the inverse mapping exists. This allows us to write the quantities of interest as either functions of x or as functions of ρ, depending on which representation is more suitable for solving the inversion problem. With this observation in mind let us define a modified field function through the relation

$$\phi(x) = \psi(x)/\alpha(x) \qquad (3.6)$$

with

$$\alpha(x) = \sqrt{1/\eta(x)}. \qquad (3.7)$$

Changing variable in (3.1) from x to ρ and making use of (3.6) one can rewrite (3.1) in the following form:

$$\frac{d^2}{d\rho^2}\tilde\phi(\rho) + [k^2 - W(\rho)]\tilde\phi(\rho) = 0 \qquad (3.8)$$

where

$$W(\rho) = \left[\frac{d^2}{d\rho^2}\tilde\eta(\rho)\right][2\tilde\eta(\rho)]^{-1} - \left[\frac{d}{d\rho}\tilde\eta(\rho)\right]^2 [2\tilde\eta(\rho)]^{-2} - \beta^2[1 - 1/\tilde\eta(\rho)^2]. \qquad (3.9)$$

In (3.9) $\tilde\phi(\rho)$ and $\tilde\eta(\rho)$ are the field function $\phi(x)$ and the refractive index $\eta(x)$, written as functions of ρ, respectively.

The advantage of working with (3.8) instead of (3.1) is clear. Equation (3.8) is the Schrödinger equation for the energy-independent potentials, whose inverse problem is well studied. Furthermore, let us note that if $\tilde\phi$ is an eigenfunction of (3.8), then the associated field function ψ is also an eigenfunction of (3.1). In other words the eigenvalues of the two equations are the same and therefore the design problem is reduced to finding $W(\rho)$ with bound state energies specified by (3.4). This is the classical inverse quantum mechanical problem and the solution to it is well known [1–6]. The only point

that we need to emphasize is that the solution is not unique and even if we specify not only the bound state energies but also the reflection coefficients, still the inversion result we depend on m arbitrary parameters, which in the design problem could be used to our advantage. However, for the moment let us assume that a potential $W(\rho)$ associated with the given bound states has been obtained and the refractive index $\tilde{\eta}(\rho)$ solution of the nonlinear differential equation (3.9) with the boundary conditions

$$\lim_{|\rho| \to \infty} \tilde{\eta}(\rho) = 1 \tag{3.10}$$

has been found as a function of the intermediate variable ρ. Then the only remaining problem is to find the refractive index as a function of the spatial variable x, when the refractive index as a function of ρ is known. In order to achieve this objective we make use of (3.5) to deduce the following relation:

$$x = F(\rho) = \int_0^\rho \frac{dt}{\tilde{\eta}(t)}. \tag{3.11}$$

Now since $\tilde{\eta}(\rho)$ is a known function, equation (3.11) can be used to find x as function of ρ. In other words the one-to-one function $F(\rho)$ can be computed and its inverse $F^{-1}(x)$ can also be found. Noting that $\rho = F^{-1}(x)$, we are then in a position to find $\eta(x) = \tilde{\eta}(F^{-1}(x))$. By construction the so-designed waveguide will have the same propagation constant β for all light frequencies ω_i, with $i = 1, 2, \ldots, m$.

In principle the above procedure enables us to design waveguides with the same propagation constants β for different frequencies provided that we can find $\tilde{\eta}(\rho)$. In order to show the existence of the solution to (3.9) and develop a practical method for finding the solutions, we note that Berryman and Greene [18], in dealing with inverse problems for elastic waves, have shown that the impedance can be either recovered directly by solving a linear second-order differential equation, which can be regarded as the analogue of (3.9), or indirectly by working with the wavefunction associated with zero frequency. Motivated by this result [18], let us study the wavefunctions, solutions to (3.1) and (3.8), at zero frequency which corresponds to $k^2 = -\beta^2$. We note that when $\omega = 0$ equation (3.1) simplifies to the following equation:

$$\frac{d^2}{dx^2} \psi(x) - \beta^2 \psi(x) = 0 \tag{3.12}$$

with $e^{\pm \beta x}$ being its two fundamental solutions. Let us also denote $\tilde{\phi}_\pm(\rho)$ as the solutions to (3.8) for $k^2 = -\beta^2$ with asymptotic behaviours of the form $e^{\pm \beta \rho}$ for ρ tending to $\mp \infty$, respectively. We should note that $\tilde{\phi}_\pm(\rho)$ are linearly independent. Otherwise, we are forced to accept that $-\beta^2$ is an eigenvalue of (3.8). However, this is not the case since we are assuming that the potential $W(\rho)$ is chosen in such a way that (3.8) has eigenvalues $-\gamma_i^2$ as given by (3.9). Also we assume $W(\rho)$ is such that the solution $\tilde{\phi}_\pm(\rho)$ to (3.8) exist for all real values of ρ, and the associated function $\eta(x)$ satisfies (2.9). Having defined the desired solutions to (3.1) and (3.8) for $k^2 = -\beta^2$, we then make use of the relation (3.6) to find

$$\tilde{\phi}_\pm(\rho) = \sqrt{\tilde{\eta}(\rho)}\, A_\pm e^{\pm \beta x} \tag{3.13}$$

where $A_\pm = \exp(\pm \beta \int_0^{\mp \infty} [\eta(x) - 1] dx)$. It should be noticed that (3.13) is the analogue of equation (40) of Berryman and Greene [18], however, in order for (3.13) to be of practical use we need to eliminate its dependence on x by taking the derivative of (3.13) with

respect to ρ. Making use of the existing relation between ρ and x as given by (3.11), we obtain

$$\frac{d}{d\rho}\,\tilde{\phi}_\pm(\rho) = \left[\frac{d}{d\rho}\,\tilde{\eta}(\rho) \pm 2\beta\right]\tilde{\phi}_\pm(\rho)\,[2\tilde{\eta}(\rho)]^{-1} \tag{3.14}$$

which can be viewed as two linear first-order differential equations satisfied by $\tilde{\eta}(\rho)$. The solution to (3.14) can be written as

$$\tilde{\eta}(\rho) = 2\beta\tilde{\phi}_+^2(\rho) \int_\rho^\infty \tilde{\phi}_+^{-2}(t)\,dt \tag{3.15}$$

or

$$\tilde{\eta}(\rho) = 2\beta\tilde{\phi}_-^2(\rho) \int_{-\infty}^\rho \tilde{\phi}_-^{-2}(t)\,dt. \tag{3.16}$$

It should be noted that if $\tilde{\eta}(\rho)$ defined by (3.15) becomes different from $\tilde{\eta}(\rho)$ as defined by (3.16), then from equations (3.13) and (3.14) one is forced to accept that the linear second-order differential equation (3.8) has more than two linearly independent solutions. Of course this not being the case, proves that the refractive index $\tilde{\eta}(\rho)$ as defined by (3.15) or (3.16) are identical and one can use either representation to compute the refractive index. Also, since we are finding the refractive index in such a roundabout way, one is justified in asking whether this refractive index actually satisfies (3.9). Performing the necessary operations, it is very easy to verify that indeed $\tilde{\eta}(\rho)$ as defined by (3.15) or (3.16) satisfies (3.9). Furthermore, using a similar proof to that developed to show (3.15) and (3.16) lead to the same refractive index, we can conclude that the solution to (3.9), satisfying the boundary conditions specified by (3.10), is unique and is given by (3.15) or (3.16).

Positivity of $\tilde{\eta}(\rho)$ can be deduced from (3.13), (3.15) or (3.16). Equations (3.15) and (3.16) show that $\tilde{\eta}(\rho)$ is non-negative. To show positivity of $\tilde{\eta}(\rho)$, let us assume that there exist a point ρ_0 such that $\tilde{\eta}(\rho_0) = 0$. Then (3.13) will imply that $\tilde{\phi}_\pm(\rho_0) = 0$. From this information we can deduce that the Wronskian of $\tilde{\phi}_+(\rho)$ and $\tilde{\phi}_-(\rho)$ is equal to zero. In other words the solutions $\tilde{\phi}_\pm(\rho)$ of (3.8) are linearly dependent. Then we appeal to the fact that $\tilde{\phi}_\pm(\rho)$ are linearly independent and conclude that the point ρ_0 such that $\tilde{\eta}(\rho_0) = 0$ does not exist and $\tilde{\eta}(\rho)$ is a positive function.

The proposed method for finding the refractive index $\tilde{\eta}(\rho)$, seems to have replaced the need for finding the solution to the nonlinear boundary value problem as given by (3.9) by the need to find the solution to the linear equation (3.8) for a special value of the energy k^2. Although this by itself is a great simplification, it should be noted that the gain is even greater when we remember that any standard inversion procedure which we use to find $W(\rho)$ will also be able to give as the wavefunction for different k^2 values without having to directly solve the associated Schrödinger equation. In other words the functions $\tilde{\phi}_\pm(\rho)$ needed for calculation of $\tilde{\eta}(\rho)$ can be easily found and we will not need to appeal to numerical methods to solve the linear differential equation (3.8) for $k^2 = -\beta^2$. Furthermore, the solution given in the form of (3.15) and (3.16) enable us to easily integrate (3.11) and find the dependence of the spatial variable x on the intermediate variable ρ:

$$x = \frac{-1}{2\beta}\ln\left\{\left[\int_\rho^\infty \tilde{\phi}_+^{-2}(t)\,dt\right]\left[\int_0^\infty \tilde{\phi}_+^{-2}(t)\,dt\right]^{-1}\right\} \tag{3.17}$$

or

$$x = \frac{1}{2\beta} \ln \left\{ \left[\int_{-\infty}^{\rho} \tilde{\phi}_{-}^{-2}(t)\,dt \right] \left[\int_{-\infty}^{0} \tilde{\phi}_{-}^{-2}(t)\,dt \right]^{-1} \right\}. \tag{3.18}$$

Again the two representations of x as given by (3.17) and (3.18) are equivalent, and can be used to relate the spatial variable x to the intermediate variable ρ.

We conclude this section by noting that the proposed procedure is able to give us a practical method for designing waveguides which have the same propagation constant for different light frequencies. The procedure does not lead to a unique solution and this of course is of practical importance since it enables us to design waveguides having further desirable properties. The sources of non-uniqueness are due to the fact that in this design problem the reflection coefficients are not specified and can be chosen arbitrarily and, furthermore, for each required bound state we also have a normalization parameter which is arbitrary. In order to illustrate the procedure in more detail and see some of the effects of the existing arbitrariness in the procedure, in section 4 we present examples which are also of practical interest in waveguide design.

4. Examples

In this section we study the design of a waveguide which allows two frequencies ω_1 and ω_2 to propagate with the same propagation constant β. Following the procedure developed in section 3 we first use (3.4) to define the bound state energies associated with this problem.

$$\gamma_1^2 = \beta^2 - n_{\infty}^2(k_{01})k_{01}^2 \tag{4.1}$$

$$\gamma_2^2 = \beta^2 - n_{\infty}^2(k_{02})k_{02}^2 \tag{4.2}$$

where $n_{\infty}(k_{01})$ and $n_{\infty}(k_{02})$ are the refractive index of the cladding at the frequencies ω_1 and ω_2, and $k_{01} = \omega_1/c$ and $k_{02} = \omega_2/c$. Having defined the desired bound state energies, we are now ready to appeal to the well-known results of Kay and Moses [20] to find the bound state wavefunctions $\tilde{\phi}_1(\rho)$ and $\tilde{\phi}_2(\rho)$ and the associated potential $W(\rho)$:

$$\tilde{\phi}_1(\rho) = -\frac{A_1 e^{\gamma_1 \rho}}{\Delta(\rho)} - \frac{A_1 A_2 (\gamma_1 - \gamma_2) e^{(2\gamma_2 + \gamma_1)\rho}}{2\gamma_2(\gamma_1 + \gamma_2)\Delta(\rho)} \tag{4.3}$$

$$\tilde{\phi}_2(\rho) = -\frac{A_2 e^{\gamma_2 \rho}}{\Delta(\rho)} - \frac{A_1 A_2 (\gamma_1 - \gamma_2) e^{(2\gamma_1 + \gamma_2)\rho}}{2\gamma_1(\gamma_1 + \gamma_2)\Delta(\rho)} \tag{4.4}$$

and

$$W(\rho) = 2\frac{d}{d\rho}[\tilde{\phi}_1(\rho)e^{\gamma_1 \rho} + \tilde{\phi}_2(\rho)e^{\gamma_2 \rho}] \tag{4.5}$$

where

$$\Delta(\rho) = 1 + \frac{A_1 e^{2\gamma_1 \rho}}{2\gamma_1} + \frac{A_2 e^{2\gamma_2 \rho}}{2\gamma_2} + \frac{A_1 A_2 (\gamma_1 - \gamma_2)^2 e^{2(\gamma_1 + \gamma_2)\rho}}{4\gamma_1 \gamma_2(\gamma_1 + \gamma_2)^2} \tag{4.6}$$
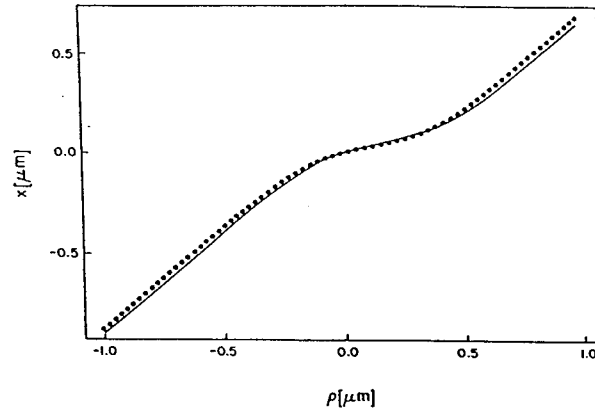
and A_1 and A_2 are arbitrary positive constants.

Figure 1. Plot of $x = F(\rho)$ as defined by (3.11). The solid line corresponds to $A_1 = A_2 = 2$ and the doted line is associated with $A_1 = 4$ and $A_2 = 8$. In all cases $\beta = 6.0611\,\mu m^{-1}$, $n_\infty(k_0) = n_\infty = 1.4850$, $k_{01} = 2.0270\,\mu m^{-1}$ and $k_{02} = 4.0537\,\mu m^{-1}$.

Having found the potential and the bound state wavefunctions we are then in a position to use equation (2.1) of Kay and Moses [20] to find the needed wavefunctions $\tilde{\phi}_\pm(\rho)$ for $k^2 = -\beta^2$ without having to solve the differential equation (3.8) directly:

$$\tilde{\phi}_+(\rho) = \left[1 + \frac{\tilde{\phi}_1(\rho)e^{\gamma_1\rho}}{\gamma_1 + \beta} + \frac{\tilde{\phi}_2(\rho)e^{\gamma_2\rho}}{\gamma_2 + \beta} \right] e^{\beta\rho} \tag{4.7}$$

and

$$\tilde{\phi}_-(\rho) = \left[1 + \frac{\tilde{\phi}_1(\rho)e^{\gamma_1\rho}}{\gamma_1 - \beta} + \frac{\tilde{\phi}_2(\rho)e^{\gamma_2\rho}}{\gamma_2 - \beta} \right] e^{-\beta\rho}. \tag{4.8}$$

It's easy to verify that the so-defined $\tilde{\phi}_\pm(\rho)$ have the desired asymptotic behaviours and are solutions to (3.8). Therefore they can be used in (3.15) or (3.16) and (3.17) or (3.18) to find the refractive index and the spatial variable x as a function of the intermediate varaible ρ numerically. Having found $\tilde{\eta}(\rho)$ and $x = F(\rho)$, the procedure is then complete and the refractive index $\eta(x)$ can be numerically obtained. The result of the numerical computations are presented for different values of A_1, A_2 and different light frequencies in figures 1–4. In these examples we have assumed that the refractive index $n(x, k_0)$ as defined by (2.8) is independent of wavenumber k_0 and can be written as $\eta(x)n_\infty$.

It should be emphasized that the examples presented here are only for the sake of demonstrating the proposed method. Practical implementation of this technique and actual fabrication of such waveguides need further study. Also, for the sake of simplicity in presentation, we have only used reflectionless potentials in these examples. However,
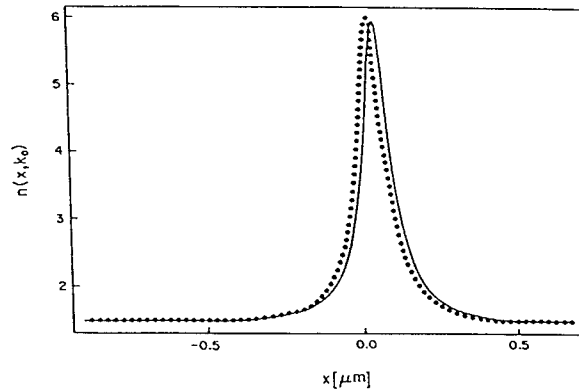

Figure 2. Graph of the refractive index $n(x, k_0) = \eta(x)n_\infty$ as defined by (2.8) and (3.15). Symbols and the constants are the same as in figure 1.
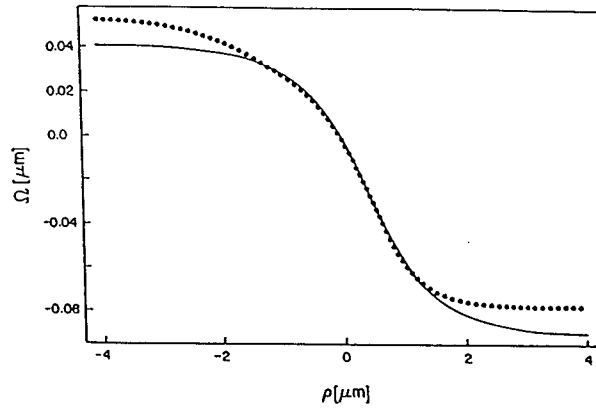
Figure 3. Plot of $\Omega = x - \rho = F(\rho) - \rho$. The solid line corresponds to $A_1 = A_2 = 2$ and the dotted line is associated with $A_1 = 4$ and $A_2 = 8$. In all cases $\beta = 6.0611\,\mu m^{-1}$, $n_\infty(k_0) = n_\infty = 1.4850$, $k_{01} = 3.9270\,\mu m^{-1}$ and $k_{02} = 4.0537\,\mu m^{-1}$.

in actual applications of the method, we should remember that any potential which has the proper bound state energies, including those which are not reflectionless, can be used. Such potentials can be found by appealing to the Faddeev–Marchenko method [5, 21].

$$W(\rho) = 2\,\frac{\mathrm{d}}{\mathrm{d}\rho}\,K(\rho,\rho) \tag{4.9}$$

where

$$K(\rho + \zeta) + M(\rho,\zeta) + \int_{-\infty}^{\rho} K(\rho,\xi)M(\xi + \zeta)\,\mathrm{d}\xi = 0 \qquad \zeta < \rho \tag{4.10}$$

and

$$M(\rho) = (1/2\pi)\int_{-\infty}^{\infty} \mathrm{d}k\, R(k)\mathrm{e}^{-\mathrm{i}k\rho} + \sum_{i=1}^{m} A_i\, \mathrm{e}^{\gamma_i\rho} \tag{4.11}$$

with $R(k)$ being the reflection coefficient. Having found $W(\rho)$, one can apply the proposed method to find the refractive index associated with potentials which are not reflectionless. Use of potentials with $R(k) \neq 0$ may be preferable, if such potentials lead to waveguides with refractive indexes which are easier to fabricate.

The above equations show that in order to find $W(\rho)$ uniquely, we not only need the bound state information and the normalization constants A_i, but also we need to know the reflection coefficients $R(k)$ for all real values of k. In view of the fact that in fibre optics design usually only the value of propagation constants are specified and $R(k)$ is
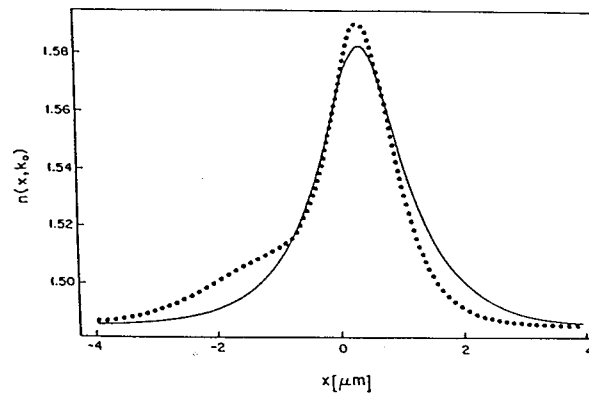

Figure 4. Graph of the refractive index $n(x, k_0) = \eta(x)n_\infty$. Symbols and the constants are the same as in figure 3.

not given, it then follows that such a design problem involves a great degree of non-uniqueness. A very interesting question that was raised by the referees is with regard to the nature of this non-uniqueness and its physical implications. Let us study this question by noting that in order to remove this non-uniqueness, we need to know $R(k)$ for all real values k. In view of the definition of k as given by (2.5), we note that the wavevectors of interest, $k = (k_x, k_z)$, will fall into one of the following two categories. Case (a) is when β is real and $n_\infty^2(k_0)k_0^2 > \beta^2$, resulting in both components of k to be real. That is $k_x = k = \pm [n_\infty^2(k_0)k_0^2 - \beta^2]^{1/2}$ and $k_z = \beta$. Case (b) corresponds to the evanescent waves [22], where $\beta = k_z = -i\bar{\beta}$ is purely imaginary but $k_x = k = \pm [n_\infty^2(k_0)k_0^2 + \bar{\beta}^2]^{1/2}$ is still real. From the above analysis, it also follows that in case (a) for large values of $|x|$ the wave will behave like a free wave and therefore from the point of view of geometric optics it would correspond to refracted rays [22]. This analysis shows that data on $R(k)$ are associated with waves which are significant only in the spatial transient region and their powers are significantly diminished in the spatial steady-state region [22]. The only waves that will have significant power for large values of z, that is in the spatial steady-state region, are the bound waves [22]. Of course propagation constants of such waves, β_i, have played a very important role in our design procedure. This observation clarifies the nature of the existing non-uniqueness in our design problem. It shows that the main difference between the different waveguides which can be deduced from the proposed method is in their radiation properties in the spatial transient region, which is usually a short distance from the source. However, for most of the length of the proposed waveguides, that is in the spatial steady-state region, waves associated with data $R(k)$ will not be significant and only the bound waves will be present. In other words, in the spatial steady-state region, all of the proposed waveguides will perform similarly as far as the bound waves are concerned. It should again be emphasized that although we are mainly interested in the propagation of the bound waves, the existing non-uniqueness can play an important role; such as the ease of fabrication of the waveguide or coupling of energy from the source to the waveguide. Of course such a study is beyond the scope of this paper but it deserves further consideration both for planar waveguides and circular waveguides [6], where the same type of non-uniqueness also exists.

References

[1] Gelfand I M and Levitan B M 1951 On the determination of a differential equation by its spectral function *Dokl. Akad. Nauk.* **77** 557–60
[2] Marchenko V A 1955 The construction of the potential energy from the phases of the scattered waves *Dokl. Akad. Nauk.* **104** 695–8
[3] Agronovich Z S and Marchenko V A 1963 *The Inverse Problem of Scattering Theory* (New York: Gordon and Breach) (Engl. transl.)
[4] Newton R G 1982 Scattering of Waves and Particles (Berlin: Springer) 2nd edn
[5] Chadan K and Sabatier P C 1989 *Inverse Problems in Quantum Scattering Theory* (Berlin: Springer) 2nd edn
[6] Yukon S P and Bendow B 1980 Design of waveguides with prescribed propagation constants *J. Opt. Soc. Am.* **70** 172–9
[7] Jordan A K and Lakshmanasamy S 1989 Inverse scattering theory applied to the design on single-mode planar optical waveguides *J. Opt. Soc. Am.* A **6** 1206–12
[8] Tamil L S and Jordan A K 1991 An inverse scattering model for an all-optical logic gate *J. Appl. Phys.* **70** 1882–4
[9] Hooshyar M A and Tamil L S 1992 Inverse scattering theory at fixed energy and the design of circular optical waveguides *J. Math. Phys.* **33** 663–9
[10] Yariv A 1991 *Optical Electronics* (Chicago, IL: Saunders College Publishing)

[11] Sohler W, Hampel R, Regener R, Ricken R, Suche H and Volk R 1986 Integrated optical parametric devices *J. Lightwave Technol.* **4** 772–97

[12] Stegman G I, Seaton C T and Karaguleff C 1986 Degenerate four-wave mixing with guided waves *IEEE J. Quantum. Electron.* **22** 1344–8

[13] Hooshyar M A 1972 The inverse scattering problem at fixed energy for L^2-dependent potentials *J. Math. Phys.* **13** 1931–33

[14] Hooshyar M A 1980 Construction of L^2-dependent potentials *J. Math. Phys.* **21** 1695–7

[15] Ware J A and Aki A 1969 Continuous and discrete inverse-scattering problems in a stratified elastic medium. I. plane waves at normal incidence *J. Acoust. Soc. Am.* **45** 911–21

[16] Coen S 1981 On the elastic profiles of a layered medium from reflection data. Part I. plane-wave sources *J. Acoust. Soc. Am.* **70** 172–5

[17] Newton R G 1981 Inversion of reflection data for layered media: a review of exact methods *Geophys. J. R. Astron. Soc.* **65** 191–215

[18] Berryman J G and Greene R R 1980 Discrete inverse methods for elastic waves in layered media *Geophysics* **45** 213–33

[19] Hooshyar M A 1990 Goupillaud layers and construction of wave speed and density of a layered acoustic medium *J. Acoust. Soc. Am.* **87** 2310–3

[20] Kay I and Moses H E 1956 Reflectionless transmission through dielectrics and scattering potentials *J. Appl. Phys.* **27** 1503–8

[21] Faddeev L D 1964 Properties of the S-matrix of the one-dimensional Schrödinger equation *Amer. Math. Soc. Trans.* **65** 139–66

[22] Snyder A W and Love J D 1983 *Optical Waveguide Theory* (New York: Chapman and Hall)

Appendix F

L. S. Tamil and G. H. Aicklen, "Analysis of Optical Fibers with Arbitrary Refractive Index profiles: Accuracy, Convergence, and Effects of Finite Cladding,"

Optics Communications, Vol. 99, pp. 393–404, 1993.

Full length article

Analysis of optical fibers with arbitrary refractive index profiles: accuracy, convergence, and effects of finite cladding

Lakshman S. Tamil

Erik Jonsson School of Engineering And Computer Science and Center for Applied Optics, The University of Texas at Dallas, Richardson, TX 75080, USA

and

Gregory H. Aicklen

Erik Jonsson School of Engineering And Computer Science, The University of Texas at Dallas, Richardson, TX 75080, USA

We have formulated a matrix eigenvalue problem for cylindrical optical fibers from a set of finite difference equations. Numerical solution of this problem yields the propagation constants for propagating modes. The method can be used for arbitrary index profiles, does not require the explicit evaluation of Bessel or modified Bessel functions, and does not use iterative methods to search for the propagation constants as was the case in earlier proposed methods using finite differences. The method is accurate, fast, and simple. We have established the convergence and stability of this method, and explored the effects of finite cladding width on the dispersion characteristics.

1. Introduction

Wave propagation in optical fibers has been analyzed using various methods. We will be using a finite difference method. Other methods proposed to find the propagation constants of guided modes in optical fibers with arbitrary refractive index profiles include the WKBJ method, variational method, power series expansion method, staircase approximation method, and finite element method.

The WKBJ method [1,2] is a geometrical optics approximation that works whenever the refractive index of fiber varies only slightly over distances of the order of the optical wavelength and are applicable only to thick fibers in which many modes can propagate. For those fibers in which only a few modes propagate, the error of the WKBJ method increases intolerably and this method is not applicable to modes near cutoff. Besides, the effect of an index valley at the core-cladding boundary, which plays an important role in reducing multimode dispersion, cannot be treated by the ordinary WKBJ method. In

the variational method the scalar wave equation is converted into a variational problem subject to the given boundary conditions. The variational problem is solved either by using the Rayleigh–Ritz method [3] or perturbation method [4]. In the Rayleigh–Ritz method the eigenfunction is expressed in terms of a set of orthogonal functions and the variational function is minimized. The disadvantage is that we need to assume a trial function [5]. In the perturbation method of analysis, the computation of the propagation characteristics for an arbitrary profile is done by correcting the solution for a uniform core fiber considering the difference in the profile as the perturbation term.

The power series expansion method [6] consists of expressing the refractive index for the field term by term. This method is useful only for cases in which the refractive index profile can be expressed by a relatively simple power series. In some cases the series do not converge and this method is not applicable [7]. In the staircase approximation method [8,9] the refractive index is approximated by an appro-

priate staircase function. The wave equation is solved in each stratified layer and the solutions are then connected at the cylindrical boundaries between these layers to obtain the proper solution representing the propagation characteristics. The number of layers should be infinite in order that the refractive index profile approaches that of actual fiber profiles. Thus, the results of the propagation constant will differ from the actual values when a finite number of layers is used. A large number of layers requires considerable computer time and hence in this method the accuracy and computer time are traded off.

The fiber problem has been analyzed by Okamato and Okoshi [10] using a finite element method formulated in the axial fields. The problem with this method is that it suffers from spurious modes when the finite elements are not carefully chosen [11]. Lenahan [12] has formulated a matrix eigenvalue problem from a finite element analysis using the Galerkin weighted residual method. To achieve computational efficiency, a piecewise linear approximation to the solution function must be used.

In this paper we present an efficient finite difference method to find the propagation constants of optical fibers with arbitrary refractive index profiles. The method does not involve a search procedure to find the propagation constants, nor does it require explicitly evaluating Bessel and modified Bessel functions, as was the case in the earlier works on finite difference analysis of optical fibers [13,14]. We construct a matrix equation from a set of simultaneous finite difference equations governing the propagation in an optical fiber and solve for the eigenvalues to obtain the propagation constants. In sect. 2 we give the mathematical formulation of the discretized differential equation at various grid points in the radial direction and the construction of a matrix equation incorporating the boundary conditions at the core-cladding interface and the jacket. Extending our method, which is formulated for α-index fibers, to arbitrary refractive index profiles is covered in sect. 3. In sect. 4 we discuss the numerical evaluation of propagation constants and present results. This includes a discussion of the convergence and stability of the method along with the effect of the number of grid points on the computation, and the effects of finite cladding width on dispersion

characteristics. Our conclusions are given in sect. 5.

2. Mathematical formulation

The optical fibers considered here are inhomogeneous dielectric cylinders of radius a called the "core" surrounded by a homogeneous refractive index medium called the "cladding". The cladding, in turn, is encased in a highly lossy material called the jacket. A representative fiber cross-section is shown in fig. 1.

The refractive index profile of the fiber, called an α-index profile, is given by

$$n^2(r) = n_1^2[1 - 2\rho\Delta(r/a)^\alpha], \quad \text{for } 0 \leqslant r \leqslant a,$$
$$= n_1^2[1 - 2\Delta], \quad \text{for } r > a. \quad (1)$$

Here, n_1 is the maximum refractive index of the core, Δ is the relative refractive index difference between the core axis and cladding, ρ a parameter representing the refractive index step or valley at the core-cladding boundary. A smooth continuation at the core-cladding boundary, the presence of a step, and that of a valley are expressed by $\rho = 1$, $\rho < 1$, and $\rho > 1$, respectively. $\{\alpha | \alpha \in \mathbb{R}\}$ is a profile parameter. Some examples of α-index profiles are shown in fig. 2.

The propagation characteristics of an optical fiber are governed by the scalar Helmholtz differential equation [15]
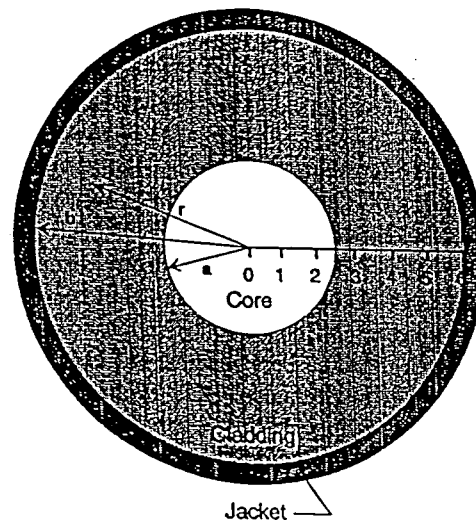

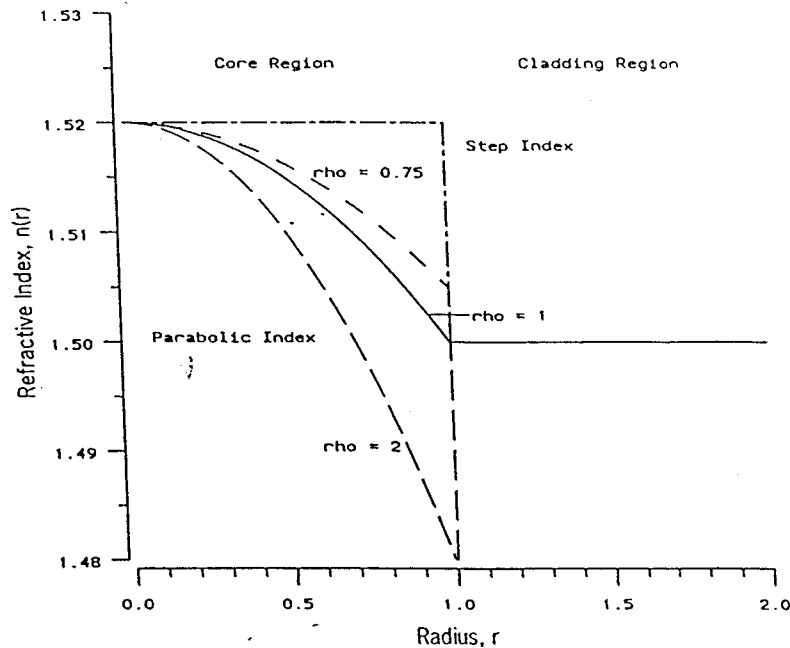Fig. 1. Optical fiber showing grid points used in the example.

394

Fig. 2. Examples of α-index profiles. $\alpha=\infty$ yields a step index, while $\alpha=2$ yields the parabolic index. Values of ρ control the characteristics of the interface between the core and the cladding; $\rho<1$ results in a step at the interface, $\rho>1$ yields a valley.

$$\frac{d^2\psi}{dr^2} + \frac{1}{r}\frac{d\psi}{dr} + \left(n^2(r)k^2 - \beta^2 - \frac{m^2}{r^2}\right)\psi = 0 . \qquad (2)$$

This scalar wave equation is the simplification of the exact vector wave equation under the assumption that $\nabla n/n$ is small, which includes the "small index gradient" and "weakly guiding approximations" [16,17]. In the above equation $\psi(r)$ is the transverse field function which may denote either the dielectric field or the magnetic field, r is the radial coordinate, $n(r)$ is the radial refractive index profile, k is the vacuum wave number, β is the propagation constant which is to be computed, and m is a mode parameter given by

$m=1$,   for TE and TM modes $(n=0)$,

   $=n+1$,   for EH modes $(n\in\mathbb{N})$,

   $=n-1$,   for HE modes $(n\in\mathbb{N})$.   (3)

We need to solve the differential equation in order to compute the propagation constants. From the rotational properties of ψ the associated boundary condition at the center of the core $(r=0)$ is

$$\left(\frac{d\psi}{dr}\right)_{r=0} = 0 , \quad \text{for } m=0 ,$$

$$\psi(0) = 0 , \qquad \text{for } m \neq 0 . \qquad (4)$$

The other boundary condition applied is the extinction of field at the jacket written as

$$\psi_{\text{jacket}} = \psi_{r=b} = 0 , \qquad (5)$$

where b is the radius of core and cladding together.

2.1. Transformation to nondimensional form

We need to nondimensionalize the differential equation for easy computation. This is achieved by setting

$$u = \psi/\psi_0 , \quad x = r/a , \qquad (6)$$

where ψ_0 is the maximum field amplitude and a is the radius of the core. Substituting eq. (6) into eq. (2) we obtain

$$\frac{d^2u}{dx^2} + \frac{1}{x}\frac{du}{dx} + a^2\left(k^2n^2(xa) - \beta^2 - \frac{m^2}{x^2a^2}\right)u = 0 . \quad (7)$$

395

By including the refractive index distribution given by eq. (1), the above equation can be rewritten as

$$\frac{d^2u}{dx^2} + \frac{1}{x}\frac{du}{dx} + a^2\left(k^2 n_1^2[1-f(xa)] - \beta^2 - \frac{m^2}{x^2 a^2}\right)u = 0,$$
(8)

where

$$f(r) = 2\rho\Delta(r/a)^\alpha, \quad 0 \leqslant r \leqslant a,$$
$$= 2\Delta, \qquad a \leqslant r.$$

Defining the parameters U and W as

$$U = a(k^2 n_1^2 - \beta^2)^{1/2}, \quad W = a(\beta^2 - k^2 n_2^2)^{1/2},$$

we can define V, the normalized frequency, as [17]

$$V^2 = U^2 + W^2 = k^2 a^2(n_1^2 - n_2^2),$$
(9)

and the modified propagation constant, $\tilde{\beta}$, as

$$\tilde{\beta} = U^2 = \frac{V^2 n_1^2}{n_1^2 - n_2^2}\left(1 - \frac{\beta^2}{n_1^2 k^2}\right) = a^2(k^2 n_1^2 - \beta^2).$$
(10)

Then eq. (8) becomes

$$\frac{d^2u}{dx^2} + \frac{1}{x}\frac{du}{dx} + \left(\tilde{\beta} - \frac{V^2 n_1^2}{n_1^2 - n_2^2}f(ax) - \frac{m^2}{x^2}\right)u = 0,$$
(11)

with

$$f(x) = 2\rho\Delta x^\alpha, \quad 0 \leqslant x < 1,$$
$$= 2\Delta, \qquad x > 1.$$
(12)

2.2. Discretizing the differential equation

When the function u and is derivative are single valued, finite and continuous functions of x, the first and the second differentials can be approximated by third order difference formulas as follows [18]:

$$\frac{du}{dx} \approx \frac{u_{i+1} - u_{i-1}}{2h},$$
(13)

$$\frac{d^2u}{dx^2} \approx \frac{u_{i+1} - 2u_i + u_{i-1}}{h^2}.$$
(14)

Here

$$u_i = u(x), \quad u_{i+1} = u(x+h), \quad u_{i-1} = u(x-h),$$

h is the width between the grid points and $x = ih$, $\{i = 0, 1, 2, ...\}$. Substituting eqs. (13) and (14) into (11), and defining

$$\tilde{V} = \frac{V^2 n_1^2}{n_1^2 - n_2^2},$$
(15)

we get

$$\frac{u_{i+1} - 2u_i + u_{i-1}}{h^2} + \frac{1}{ih}\frac{u_{i+1} - u_{i-1}}{2h}$$
$$+ \left(\tilde{\beta} - \tilde{V}f(iha) - \frac{m^2}{(ih)^2}\right)u_i = 0,$$
(16)

and on rearranging, the equation becomes

$$u_{i-1}\left[-\frac{1}{h^2}\left(1 - \frac{1}{2i}\right)\right]$$
$$+ u_i\left[\frac{1}{h^2}\left(2 + \frac{m^2}{i^2}\right) + \tilde{V}f(iha) - \tilde{\beta}\right]$$
$$+ u_{i+1}\left[-\frac{1}{h^2}\left(1 + \frac{1}{2i}\right)\right] = 0.$$
(17)

For the purpose of illustration, we have chosen six grid points along the radial direction as shown in fig. 1. In general, the number of grid points can be any number not less than four, the minimum necessary to take care of the boundary conditions. Depending on whether $m = 0$ or $m \neq 0$, the field or its derivative vanishes at the center of the core. When the derivative of the field vanishes, $u_0 = u_1$.

Writing finite difference equations at the grid points, we obtain the following set of equations. At $i = 1$,

$$u_1\left(\frac{4 + 2m^2 - \delta}{2h^2} + \tilde{V}f(1ha) - \tilde{\beta}\right) + u_2\left(\frac{-3}{2h^2}\right) = 0,$$
(18)

where

$$\delta = 1, \quad m = 0,$$
$$= 0, \quad m \neq 0.$$

At $i = 2$,

$$u_1\left(\frac{-3}{4h^2}\right) + u_2\left(\frac{8 + m^2}{4h^2} + \tilde{V}f(2ha) - \tilde{\beta}\right) + u_3\left(\frac{-5}{4h^2}\right)$$
$$= 0.$$
(19)

396

91

At $i=3$,

$$u_2\left(\frac{-5}{6h^2}\right)+u_3\left(\frac{18+m^2}{9h^2}+\tilde{V}f(3ha)-\tilde{\beta}\right)+u_4\left(\frac{-7}{6h^2}\right)$$

$$=0. \tag{20}$$

At $i=4$,

$$u_3\left(\frac{-7}{8h^2}\right)+u_4\left(\frac{32+m^2}{16h^2}+\tilde{V}f(4ha)-\tilde{\beta}\right)+u_5\left(\frac{-9}{8h^2}\right)$$

$$=0. \tag{21}$$

At $i=5$, since the field goes to zero at the jacket,

$$u_4\left(\frac{-9}{10h^2}\right)+u_5\left(\frac{50+m^2}{25h^2}+\tilde{V}f(5ha)-\tilde{\beta}\right)=0. \tag{22}$$

Finally, at $i=6$, again using the boundary condition that the field goes to zero at the jacket,

$$u_6=0. \tag{23}$$

Since the boundary condition in eq. (23) is incorporated in eq. (22), we have a system of five equations.

2.3. Matrix equation formulation

Formulating a matrix equation from the above set of equations for the convenience of generalization and easy computation, we obtain

$$\mathbf{A}u=\begin{pmatrix} a_{11}-\tilde{\beta} & a_{12} & & & \\ a_{21} & a_{22}-\tilde{\beta} & a_{23} & & \\ & a_{32} & a_{33}-\tilde{\beta} & a_{34} & \\ & & a_{43} & a_{44}-\tilde{\beta} & a_{45} \\ & & & a_{54} & a_{55}-\tilde{\beta} \end{pmatrix}\begin{pmatrix} u_1 \\ u_2 \\ u_3 \\ u_4 \\ u_5 \end{pmatrix}$$

$$=0, \tag{24}$$

where the matrix elements are defined by

$$a_{i,i-1}=\frac{-(2i-1)}{2ih^2},$$

$$a_{i,i}=\frac{2i^2+2m^2-\delta}{2i^2h^2}+\tilde{V}f(iha), \quad i=1,$$

$$=\frac{2i^2+m^2}{i^2h^2}+\tilde{V}f(iha), \quad i\neq1,$$

$$a_{i,i+1}=\frac{-(2i+1)}{2ih^2}. \tag{25}$$

In order to convert the problem into an eigenvalue problem, we rewrite eq. (24) as

$$(\mathbf{T}-\tilde{\beta}\mathbf{I})u=0, \tag{26}$$

where $\mathbf{I}$ is the identity matrix, and $\mathbf{T}$ is a tri-diagonal matrix.

Equation (26) defines an eigenvalue problem. This means that eq. (26) has a nontrivial solution if and only if $\tilde{\beta}$ is an eigenvalue [19]. Hence, the required normalized propagation constants contained in $\tilde{\beta}$ are obtained by finding the eigenvalues of the tri-diagonal matrix $\mathbf{T}$. This mathematical formulation can be generalized to $\{n|n|\in\mathbb{N}\}$ grid points in the radial direction of the fiber without difficulty.

3. Arbitrary profiles, multiple layers, and field distributions

We have developed this method of analyzing optical fibers using the α-index profile. This is because the α-index profile is commonly used in the literature and can represent a large variety of real refractive index profiles, including the very important step and parabolic profiles. But our formulation is not limited to α-index profiles.

To see how to extend the method to arbitrary profiles without rederiving a system of finite difference equations, consider eq. (11). The refractive index profile is included in this equation through the function $f(x)$, which is defined in eq. (12). Using $f(x)$, the refractive index profile of the fiber can be rewritten as

$$n^2(x)=n_1^2[1-f(x)]. \tag{27}$$

Solving for $f(x)$ yields

$$f(x)=1-n^2(x)/n_1^2. \tag{28}$$

By generating the discretized $f_i=f(x_i=ih)$ from samples of an arbitrary refractive index profile $n(x_i)$, the method we have outlined in this paper can be used directly on arbitrary profiles, as long as the "weakly guiding" approximation holds.

Multiple layer waveguides of any number of layers may be considered special cases of arbitrary refrac-

tive index profiles. Since we have normalized the fiber core radius, a, to unity, we must explicitly define which layers comprise the core before using our method and scale all quantities accordingly.

Since the propagation constant for a mode i, β_i, is uniquely associated with a $\tilde{\beta}$, the field distributions for a propagating mode can be determined from the eigenvectors u of matrix T (see eq. (26)). Many eigenvalue routines will return eigenvectors as well, but at the cost of greatly increasing the number of computations.

Useful approximations to the eigenvectors for propagating modes can be computed by constructing the tri-diagonal matrix T, subtracting a specific $\tilde{\beta}$ from each element of the main diagonal, and solving for the elements of u using standard techniques from linear algebra. From the observation that for propagating modes the field will approach zero at the cladding/jacket boundary, we can set u_N, the rightmost element of u, to a very small value (not zero), and use a simple backsubstitution process to solve for the rest of the u_i. This procedure yields a good approximation to the field distribution multiplied by an arbitrary constant.

4. Numerical evaluation, results, and discussion

Although the mathematical formulation of our method for determining the propagation characteristics of an optical fiber is couched in terms of matrix equations, there are special structures that lead to very efficient numerical implementations. First, since T is a tri-diagonal matrix, we can use sparse matrix techniques to reduce storage requirements for T. Second, since T is a quasi-symmetric tri-diagonal matrix, we can use a similarity transformation to convert T into a real, symmetric matrix [20]. Finally, the eigenvalues of a real, symmetric matrix may be computed using an efficient $O(N^2)$ algorithm (in our case, the tqli.c routine from ref. [21], which has an operation count of approximately $30N^2$).

Using eqs. (25), we have implemented a pair of C language programs which compute the normalized propagation constants for fibers with arbitrary refractive index profiles. We define the normalized propagation constant as

$$\chi = \frac{U^2}{V^2} = \frac{k^2 n_1^2 - \beta^2}{k^2 n_1^2 - k^2 n_2^2}. \tag{29}$$

Note that some authors (e.g. Gloge [22]) define a normalized propagation constant as

$$b = 1 - U^2/V^2 = 1 - \chi. \tag{30}$$

One program computes χ for all propagating modes at a specific value of m in eq. (2) over a range of normalized frequencies V. Another program searches for the cutoff frequency (V_c) of a specific linearly polarized (LP) mode. Both programs allow all of the parameters in eq. (1) to be varied, as well as the values of b and N_c, which are the fiber radius (see fig. 1) and number of grid points in the fiber core, respectively.

In verifying the performance of our method, we have computed the propagation characteristics of step index and parabolic index fibers over a normalized frequency range of 0 to 20. These index profiles have analytical solutions and have been studied analytically and numerically by other authors [14,23–26]. Our results agree well with previously published results, as shown in table 1. Note that for propagating modes, χ must lie between 0 and 1 (i.e. $0 \leqslant \chi \leqslant 1$).

For comparison with a known case, fig. 3 shows the dispersion characteristics we have computed for the step index profile. The plot agrees well with the analytic results for fibers with infinite cladding. The small differences between the computed and analytic cutoff frequencies for each mode are due to the finite cladding width used in our computations, and the finite number of grid points across the fiber. The fundamental mode, which has zero cutoff in the infinite cladding case, is extremely sensitive to the cladding width.

Figures 4, 5, and 6 show our dispersion calculations for the parabolic index fiber with cladding width 10 times the core width and $\rho = 1.0$, 2.0, and 0.75. These compare favorably with published results (see, for example, refs. [14,23,26]).

Two factors have a major influence on the results of our computations: the number of grid points used across the fiber (which we specify in terms of the number of points in the core of the fiber), and the width of the cladding. Figure 7 shows the results of applying our method to a step index fiber for two LP modes. For each mode we have calculated the cutoff

Table 1

Comparison of the cutoff frequencies obtained by the finite difference method with analytical and previous numerical results. R_{fiber} is the fiber radius, R_{core} is the core radius, and δ is the percentage difference from the infinite cladding result. 256 points were used in the fiber core.

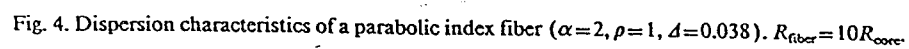| α	Mode (m,l)	Infinite cladding	Normalized cutoff frequency			
			$R_{fiber}=10R_{core}$	δ (%)	$R_{fiber}=20R_{core}$	δ (%)
1	1,1	4.381	4.391	0.23	4.384	0.07
2	1,1	3.518	3.526	0.23	3.520	0.06
	1,2	7.451	7.457	0.08	7.453	0.03
	2,1	5.744	5.744	$<10^{-2}$	5.744	$<10^{-2}$
	2,2	9.645	9.645	$<10^{-2}$	9.645	$<10^{-2}$
	3,1	7.848	7.848	$<10^{-2}$	7.848	$<10^{-2}$
	4,1	9.904	9.904	$<10^{-2}$	9.904	$<10^{-2}$
3	1,1	3.181	3.189	0.3	3.183	0.06
4	1,1	3.000	3.007	0.2	3.002	0.07
5	1,1	2.886	2.894	0.28	2.888	0.07
10	1,1	2.649	2.657	0.30	2.651	0.08
20	1,1	2.527	2.535	0.32	2.529	0.08
∞	1,1	2.405	2.413	0.33	2.407	0.08
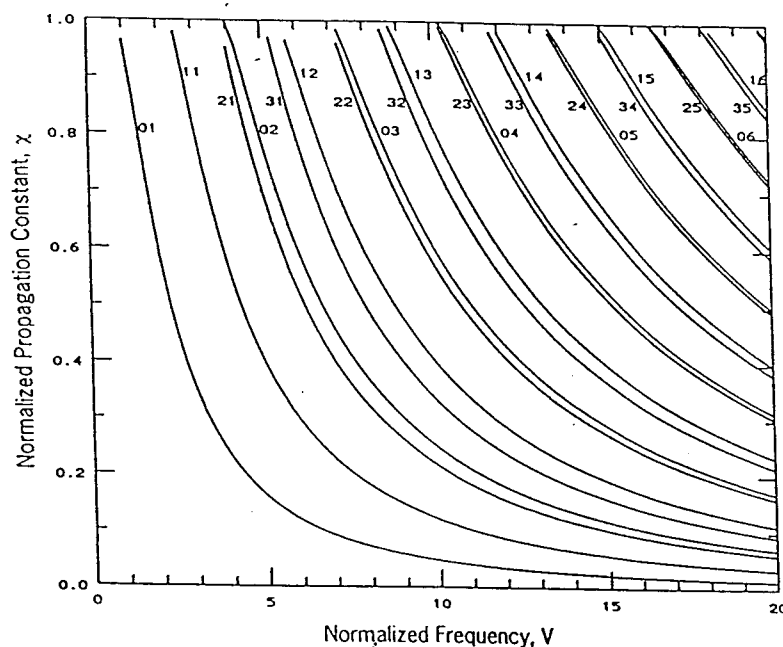
Fig. 3. Dispersion characteristics of a step index fiber ($\alpha=\infty$, $\Delta=0.038$). $R_{fiber}=10R_{core}$.

frequency using from 4 to 256 points in the core, and for fiber radii from 5 to 20 times the core radius. From this figure we can see the expected convergence on a final result as the number of points in the core increases. The effect of cladding width is also apparent.

The effect of the number of grid points in the core is two fold. As the number of grid points is increased the distance between samples of the refractive index
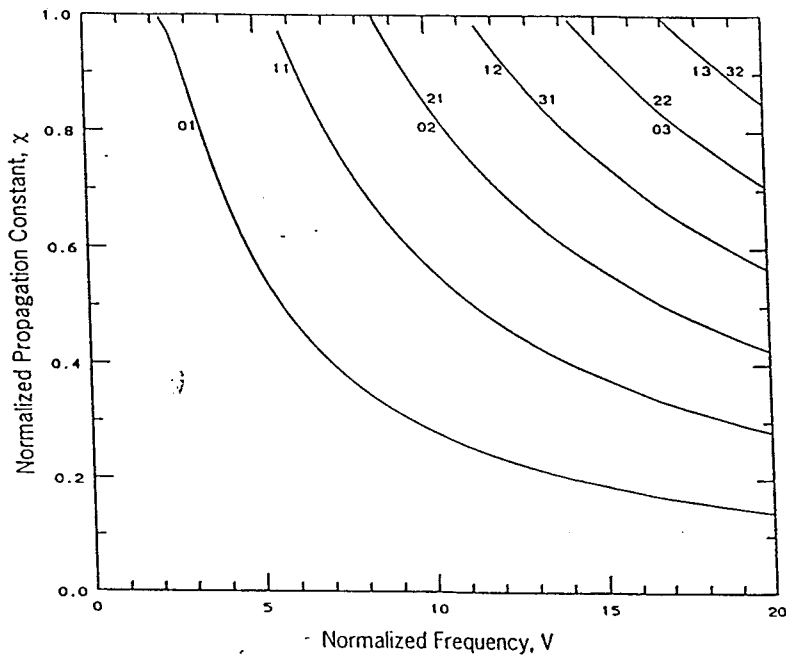
399

Fig. 4. Dispersion characteristics of a parabolic index fiber ($\alpha=2$, $p=1$, $\Delta=0.038$). $R_{fiber}=10R_{core}$.
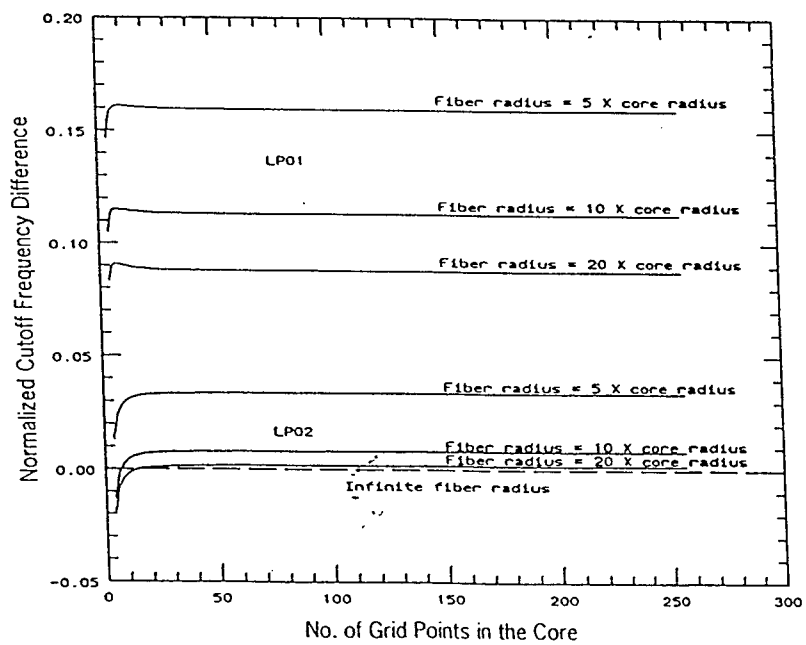

Fig. 5. Dispersion characteristics of a parabolic index fiber ($\alpha=2$, $p=0.75$, $\Delta=0.038$). $R_{fiber}=10R_{core}$.

400

Fig. 6. Dispersion characteristics of a parabolic index fiber ($\alpha=2, \rho=2, \Delta=0.038$). $R_{fiber}=10R_{core}$.

Fig. 7. Convergence behavior of computed cutoff frequency with the number of grid points in the fiber core for the LP_{11} and LP_{02} modes of a step index fiber.

401

profile is decreased, resulting in a better approximation of the actual profile. This is especially apparent in profiles with sharp transitions at the core–cladding interface, such as for $\alpha \gg 1$. Cases where $\rho \neq 1$ (see eq. (1)) are also likely to be poorly modeled by a small number of core sample points. The effect of reducing the number of sample points in the core is to apply a "low pass" spatial filter to the refractive index profile.

Setting the number of points in the core also effectively applies a filter to the spatial frequency content of the field distributions calculated for each mode in the fiber. When computing propagation constants at higher normalized frequencies, using a small number of samples may induce errors due to a form of "aliasing". These two effects are responsible for the poor results when the number of grid points in the core is below approximately 10 for the modes we have examined.

Using the step index fiber as an example, fig. 8 demonstrates the effects of the number of grid points by plotting the computed cutoff frequency for modes LP_{01}, LP_{11}, and LP_{02} for several different grid sizes. In this figure, each curve is normalized to the value of the cutoff frequency for that mode calculated with 256 points in the core. We can see that for mode LP_{01} the cutoff frequency calculated with 8 points in the core is less than 1.0015 times that computed using 256 points in the core, while for mode LP_{11} (with a higher cutoff frequency) we need at least 12 points in the core for similar results. In general, as the normalized frequency increases, the number of points in the core must be increased to maintain the accuracy of the method.

For modes with relatively low cutoff frequencies, variations in cladding width produce large changes in the calculated cutoff frequency, V_c. Cutoff frequency increases as the cladding width decreases. This is the expected behavior. Analyses assuming infinite cladding width, while adequate for many purposes, fail to account for the increasing importance of finite cladding width as the normalized frequency becomes smaller. The fundamental mode, which has no cutoff frequency when the cladding is infinite, shows a definite cutoff in real fiber.

Figure 9 shows the effects of cladding width on the cutoff frequencies of two LP modes in a step index fiber. In this plot, the curves for each mode are nor-
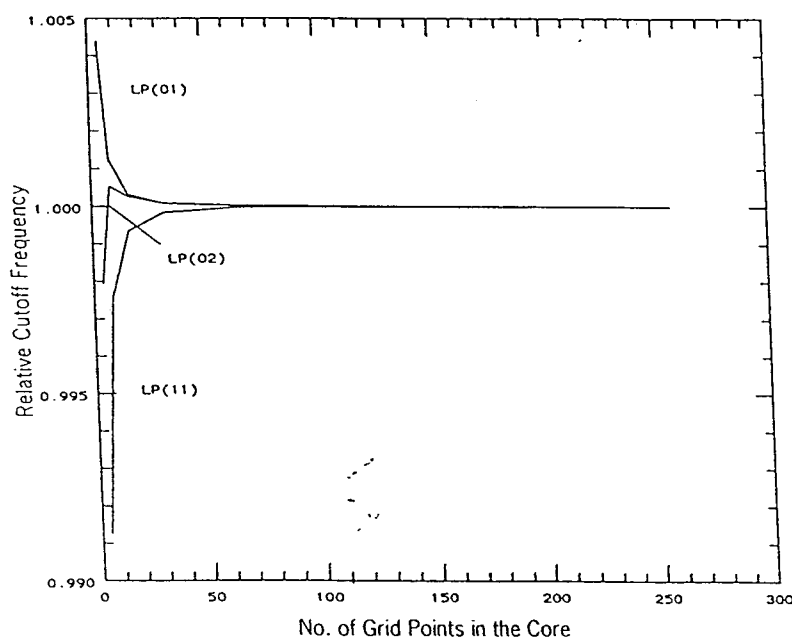

Fig. 8. Effect of the number of grid points on the computed cutoff frequencies of propagating modes of a step index fiber (LP_{01}, LP_{11}, and LP_{02}).
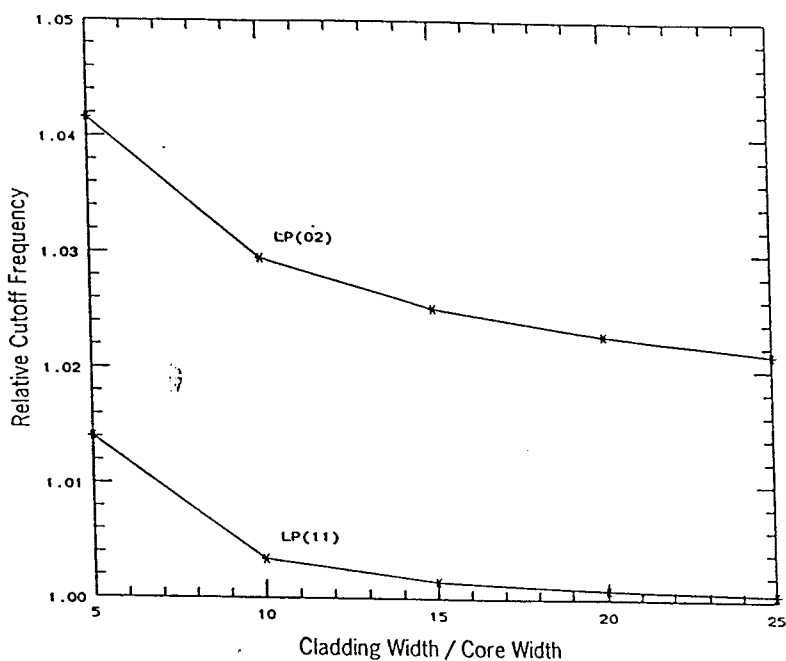
402

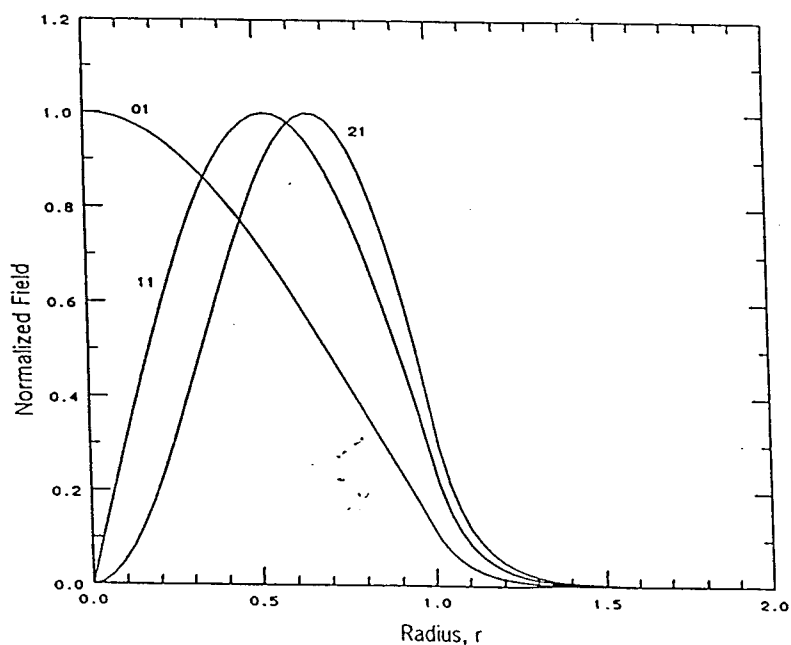Fig. 9. Effect of cladding width on cutoff frequency for a step index fiber.

Fig. 10. Field patterns for the LP_{01}, LP_{11}, and LP_{21} modes of a step index fiber with $\Delta = 0.038$. These patterns were computed using $R_{fiber} = 10 R_{core}$, $V = 10$, and 32 points in the core.

403

malized to the cutoff frequency for that mode in the infinite cladding case. As an example, consider mode LP_{11}. We can see that the cutoff frequency when the fiber radius is 10 times the core radius is only about 1.003 times (0.3%) greater than the cutoff frequency when the fiber radius is 25 times the core radius. However, when the fiber radius is only 5 times the core radius then the cutoff frequency increases to 1.014 times (1.4%) greater than the cutoff frequency when the fiber radius is 25 times the core radius.

Using the approach outlined in sect. 3, we have computed the field distributions for three LP modes in a step index fiber. Figure 10 shows the results, with the field patterns normalized so that the maximum value in each pattern is one. These results agree well with the results reported in ref. [15].

5. Conclusions

We know that when Δ is small in an optical fiber, the scalar approximation yields results that are very close to the exact vector formulation. Even for large differences between the core and cladding refractive indexes, optimum single-mode fiber parameters obtained from the scalar approximation differ negligibly from those obtained using the exact formulation [27].

We have developed a method to evaluate the propagation constants by transforming the scalar wave equation into a set of finite difference equations and then converting into a matrix eigenvalue problem. The method does not involve a search procedure to find the propagation constants, or the explicit evaluation of Bessel and modified Bessel functions, which is time consuming, as was the case in earlier works.

We have demonstrated the convergence of the method and the dependence of the rate of convergence on the number of grid points. The method is elegant, stable, straight forward, is applicable to arbitrary index profiles, and is accurate. We have also explored and established the effects of finite cladding width on the dispersion characteristics of optical fiber.

Acknowledgements

## References

[1] D. Gloge and E.A.J. Marcatili, Bell Syst. Tech. J. 52 (1973) 1563.
[2] A. Gedeon, Optics Comm. 12 (1974) 329.
[3] M. Matsuhara, J. Opt. Soc. Am. 63 (1973) 1514.
[4] A.W. Snyder, Electron. Lett. 6 (1970) 561.
[5] T. Okoshi and K. Okamoto, IEEE Trans. Microwave Theory Tech. MMT-22 (1974) 938.
[6] K. Oyameda and T. Okoshi, IEEE Trans. Microwave Theory Tech. MTT-28 (1980) 1113.
[7] S.G. Gedam and S.S. Mitra, J. Lightwave Tech. LT-3 (1985) 706.
[8] T. Tanaka and Suematsu, Trans. Inst. Electronics Comm. Eng. Jpn. E 59 (1976) 1.
[9] C. Yeh and G. Lindgren, Appl. Optics 16 (1977) 483.
[10] K. Okamoto and T. Okoshi, IEEE Trans. Microwave Theory Tech. MTT-26 (1978) 109.
[11] C.C. Su, Electron. Lett. 21 (1985) 858.
[12] T.A. Lenahan, Bell Syst. Tech. J. 62 (1983) 2663.
[13] J.D. Decontignie, O. Parriaux and F. Gardiol. J. Opt. Comm. 3 (1982) 8.
[14] C.C. Su and C.H. Shen, IEEE Trans. Microwave Theory Tech. MTT-34 (1986) 328.
[15] T. Okoshi, Optical Fibers (Academic Press, New York, 1977).
[16] A.W. Snyder, IEEE Trans. Microwave Theory Tech. MTT-17 (1969) 1130.
[17] D. Gloge, Appl. Optics 10 (1971) 2252.
[18] G.D. Smith, Numerical solution of partial differential equations: finite difference methods (Clarendon Press, Oxford, 1979).
[19] G. Strang, Linear algebra and its applications (Academic Press, New York, 1976).
[20] J.H. Wilkinson, The algebraic eigenvalue problem (Oxford University Press, 1965).
[21] W.H. Press, B.P. Flannery, S.A. Teukolsky and W.T. Vetterling, Numerical recipes in C (Cambridge University Press, New York, 1988).
[22] D. Gloge, Appl. Optics 10 (1971) 2442.
[23] K. Okamoto and T. Okoshi, IEEE Trans. Microwave Theory Tech. MTT-24 (1976) 416.
[24] T.I. Lukowski and F.P. Kapron, J. Opt. Soc. Am. 67 (1977) 1185.
[25] E.K. Sharma, I.C. Goyal and A.K. Ghatak, IEEE J. Quantum Electron. QE-17 (1970) 2317.
[26] C.C. Su, IEEE J. Quantum Electron. QE-21 (1985) 1554.
[27] S.I. Hosain, I.C. Goyal and A.K. Ghatak, Optics Comm. 47 (1973) 313.

Appendix G

G. H. Aicklen and L. S. Tamil, " Interactive Analysis of Propagation in Optical Fibers"
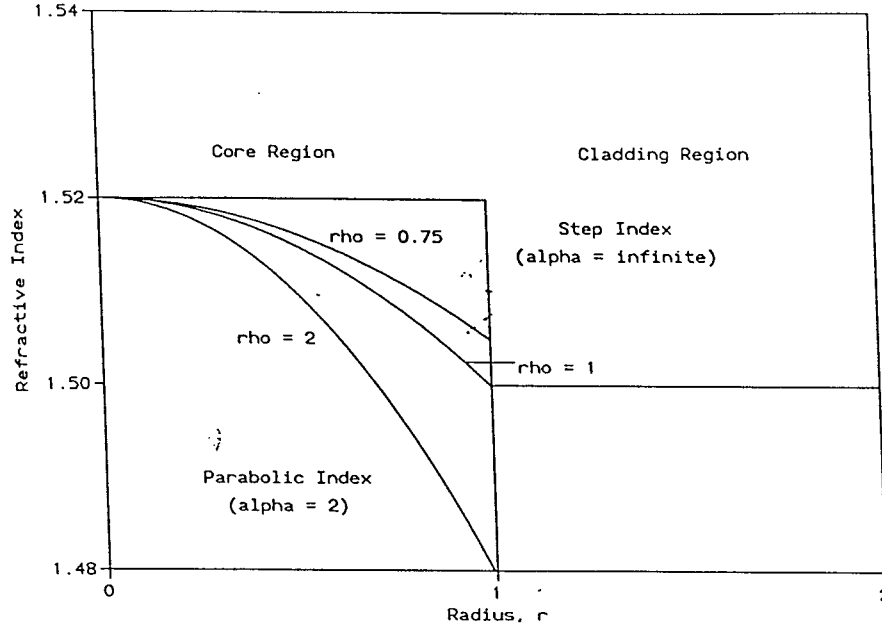
Figure 1   Examples of α-index profiles.

The propagation characteristics of an optical fiber are governed by the scalar Helmholtz differential equation [1]

$$\frac{d^2\psi}{dr^2} + \frac{1}{r}\frac{d\psi}{dr} + \left[n^2(r)k^2 - \beta^2 - \frac{m^2}{r^2}\right]\psi = 0 \quad (2)$$

This scalar wave equation is the simplification of the exact vector wave equation under the "small index gradient" and "weakly guiding" approximations [1]. When $\Delta \ll 1$ in an optical fiber, the scalar approximation yields results that are very close to the exact vector formulation, and even for larger differences between the core and cladding refractive indexes, optimum single-mode fiber parameters obtained from the scalar approximation differ negligibly from those obtained using the exact formulation [2]. For fibers used in communication applications, $\Delta < 0.03$ is common [3].

In Eq. (2), $\psi(r)$ is the transverse field function (either the electric field or the magnetic field), r is the radial coordinate, $n(r)$ is the radial refractive index profile, k is the vacuum wave number, β is the propagation constant which is to be computed, and m is a mode parameter given by

$$m = \begin{cases} 1 & \text{for TE}_{0l} \text{ and TM}_{0l} \text{ modes } (p = 0) \\ p + 1 & \text{for EH}_{pl} \text{ modes } (p \in N) \\ p - 1 & \text{for HE}_{pl} \text{ modes } (p \in N) \end{cases}$$

$$(3)$$

Here, N is the set of natural numbers.

Modes with the same propagation constants are grouped under a linearly polarized (LP) mode classification. Each propagating mode is identified by an LP$_{ml}$ designation where m is defined in Eq. (3) and l is identical to the value in the traditional HE$_{pl}$, EH$_{pl}$, TE$_{pl}$, and TM$_{pl}$ mode designation [3].

We need to solve the differential equation to compute the propagation constants. From the rotational properties of ψ the associated boundary condition at the center of the core ($r = 0$) is

$$\left[\frac{d\psi}{dr}\right]_{r=0} = 0 \quad \text{for} \quad m = 0$$

$$\psi(0) = 0 \quad \text{for} \quad m \neq 0$$

$$(4)$$

The other boundary condition applied is the extinction of field at the jacket, written as

$$\psi_{\text{jacket}} = \psi_{r=b} = 0 \quad (5)$$

where b is the radius of core and cladding together.

The issue of boundary conditions is complex but very important in all numerical work. A more appropriate boundary condition in the jacket is an absorbing boundary condition, but for a large cladding width, as assumed here, our boundary condition is appropriate [1]. For an excellent discussion of radiation boundary conditions, see Moore et al. [4].

We need to rewrite the differential equation to eliminate dependence on units; this is a more general formulation that is also easier for computation. We do this by setting

$$u = \frac{\psi}{\psi_0}$$

and

$$x = \frac{r}{a} \tag{6}$$

where ψ_0 is the maximum field amplitude and a is the radius of the core. Substituting Eq. (6) into Eq. (2) we obtain

$$\frac{d^2 u}{dx^2} + \frac{1}{x}\frac{du}{dx}$$
$$+ a^2 \left[k^2 n^2(xa) - \beta^2 - \frac{m^2}{x^2 a^2} \right] u = 0 \tag{7}$$

By including the refractive index distribution given by Eq. (1), and normalizing all waveguide dimensions to the core radius, the above equation can be rewritten as

$$\frac{d^2 u}{dx^2} + \frac{1}{x}\frac{du}{dx}$$
$$+ \left[k^2 n_1^2 (1 - f(x)) - \beta^2 - \frac{m^2}{x^2} \right] u = 0 \tag{8}$$

Defining, V, the normalized frequency, as

$$V^2 = k^2[n_1^2 - n_2^2] \tag{9}$$

and the modified propagation constant, $\tilde{\beta}$, as

$$\tilde{\beta} = \frac{V^2 n_1^2}{(n_1^2 - n_2^2)} \left[1 - \frac{\beta^2}{n_1^2 k^2} \right] = k^2 n_1^2 - \beta^2 \tag{10}$$

Eq. (8) becomes

$$\frac{d^2 u}{dx^2} + \frac{1}{x}\frac{du}{dx}$$
$$+ \left[\tilde{\beta} - \frac{V^2 n_1^2}{(n_1^2 - n_2^2)} f(x) - \frac{m^2}{x^2} \right] u = 0 \tag{11}$$

with

$$f(x) = \begin{cases} 2\rho \Delta x^\alpha & 0 \leq x \leq 1 \\ 2\Delta & x > 1 \end{cases} \tag{12}$$

When the function u and its derivative are single valued, finite and continuous functions of x, the first and the second differentials can be approximated by second order difference formulas. Using the finite difference approximation, and defining

$$\tilde{V} = \frac{V^2 n_1^2}{(n_1^2 - n_2^2)} \tag{13}$$

we arrive at the discretized wave equation

$$u_{i-1}\left[-\frac{1}{h^2}\left[1 - \frac{1}{2i} \right] \right]$$
$$+ u_i\left[\frac{1}{h^2}\left[2 + \frac{m^2}{i^2} \right] + \tilde{V}f(iha) - \tilde{\beta} \right]$$
$$+ u_{i+1}\left[-\frac{1}{h^2}\left[1 + \frac{1}{2i} \right] \right] = 0 \tag{14}$$

where h is the distance between grid points and $x = ih$, $\{i = 0, 1, 2 \cdots\}$.

Writing finite difference equations at the grid points, we obtain a set of equations that may be written as a matrix equation:

$$\mathbf{Au} = \mathbf{0} \tag{15}$$

To convert the problem into an eigenvalue problem, we rewrite Eq. (15) as

$$[\mathbf{T} - \tilde{\beta}\mathbf{I}]\mathbf{u} = \mathbf{0} \tag{16}$$

where $\mathbf{I}$ is the identity matrix, and $\mathbf{T}$ is a tri-diagonal matrix. Equation (16) has a nontrivial solution if and only if $\tilde{\beta}$ is an eigenvalue [5]. Hence, the required normalized propagation constants contained in $\tilde{\beta}$ are obtained by finding the eigenvalues of the tridiagonal matrix $\mathbf{T}$.

EXAMPLES

To construct a system of computer codes that will run well on IBM-PC compatible computers, we have taken advantage of the special properties of our matrix formulation. Most importantly, since $\mathbf{T}$ is a quasi-symmetric tri-diagonal matrix, we can use a

Fiber User Interface
Version 2.14

Fiber Parameter Selection   **Numerical Procedures**

Profile Type: Computation:
  Step: X   Dispersion: X
  Graded: Field Pattern:
  Arbitrary: Cutoff Frequency:

Profile parameters: Computational Parameters:
  Alpha: Starting V: 00.25
  Delta: 0.038   Ending V: 20.00
  Rho: Step Size for V: 00.25

  Core Refractive Idx: 1.520   Mode Number (m,l):   00
  Clad Refractive Idx:

                                                     Cutoff Lower Bound:
  Core Radius (um):   01.00   Cutoff Upper Bound:
  Fiber Radius (um):   10.00

  Points in Core: 032

Figure 2   Examples of the Fiber User Interface for a step index fiber.

similarity transformation to convert **T** into a real, symmetric matrix [6]. The eigenvalues of a real, symmetric matrix may be computed using an efficient $O(N^2)$ algorithm (in our case, the `tqli` routine from [7], which has an operation count of approximately 30 N^2).

The computational kernel of our pedagogical system consists of a trio of computer codes that compute the normalized propagation constants and field patterns for cylindrical fibers. Arbitrary refractive index profiles (which must meet the criteria for Eq. (2) to be valid) are read from a file on disk,
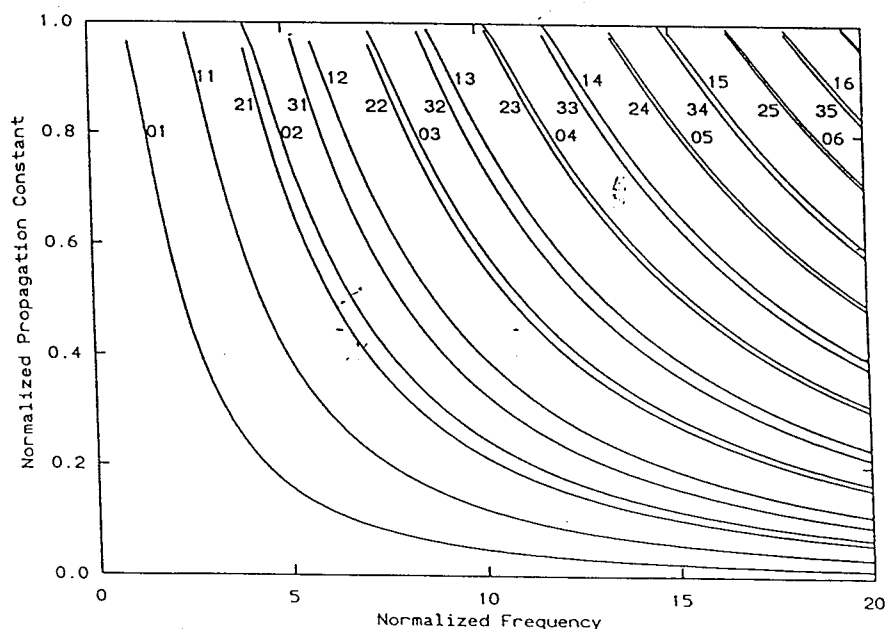

Figure 3   Normalized propagation constant vs. normalized frequency for a step index fiber ($\alpha = \infty$, $\Delta = 0.038$). $R_{fiber} = 10\ R_{core}$ and $N_c = 32$.

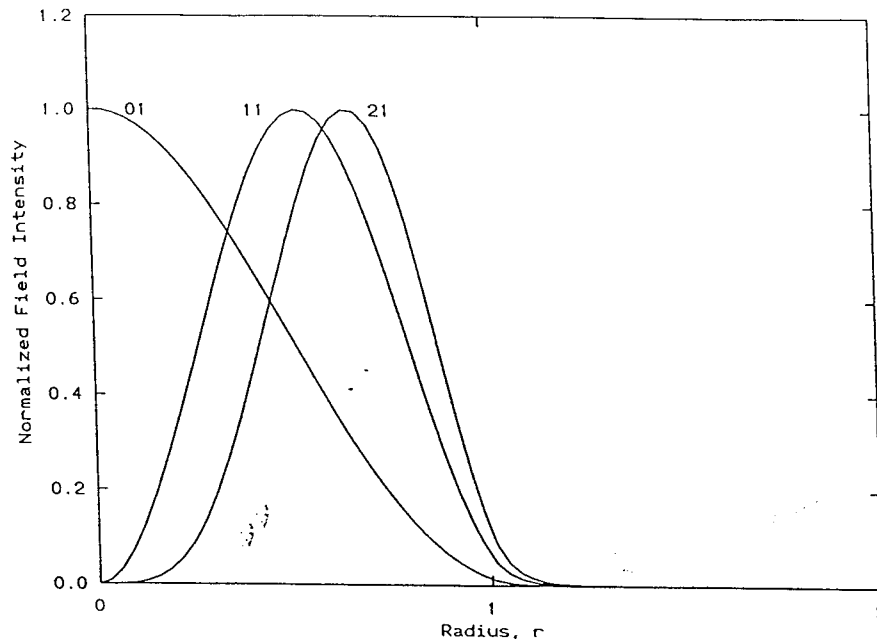**Figure 4**   Field patterns for the modes LP_{01}, LP_{11}, and LP_{21} of a step index fiber ($\alpha = \infty$, $\Delta = 0.038$) at $V = 10$. $R_{fiber} = 10 R_{core}$ and $N_c = 32$.

while α-index profiles are constructed directly within each program. The numerical computer codes call upon a common graphical display program and file I/O routines. A single shell program controls the entire suite of computer codes and coordinates the loading and execution of code segments as required to perform the computations requested by a user.

Common to all computer codes in the suite, the normalized propagation constant is defined by

$$\chi = \frac{k^2 n_1^2 - \beta^2}{k^2 n_1^2 - k^2 n_2^2} \qquad (17)$$

For propagating modes, $k n_2 \leq \beta \leq k n_1$ [3], and so χ must lie between 0 and 1. All computer codes allow the parameters in Eq. (1) to be varied, as well as the values of b and N_c, the fiber radius and number of grid points in the fiber core, respectively.

To illustrate our system, we have computed the propagation characteristics of a step index ($\alpha = \infty$) and a parabolic index fiber ($\alpha = 2$) over a normalized frequency range of 0–20. These refractive index profiles have solutions that have been studied analytically and numerically by other authors [8,9,10,11,12], and our results agree well with previously published results.

The first step in an analysis is to define the fiber profile parameters, and the number of points to use in finite difference approximations. These definitions are made in the shell, as shown in Figure 2 for

the step index case. Then, a user indicates which computation is desired. The shell runs appropriate computer codes to generate the desired data and graphs.

Figure 3 shows the step index fiber dispersion curves generated using $N_c = 32$, and Figure 4 shows the field patterns for the LP_{01}, LP_{11}, and LP_{21} modes. The fiber parameters are as shown in Figure 2. Field intensity patterns for each LP mode are defined by

$$I = \frac{u_i^2}{u_{max}^2}$$

where u_{max} is the maximum field magnitude along the fiber radius for each LP mode.

Dispersion curves for a parabolic index fiber are shown in Figure 5. These curves were generated using $\alpha = 2$ and $\rho = 1$; all other parameters were identical to those for the step index case presented in Figure 3. Figure 6 shows the field pattern for the LP_{01}, LP_{11}, and LP_{21} modes.

Figures 3–6 were prepared using data passed directly to gnuplot, a powerful scientific function and data graphing program available without charge on a variety of platforms, including IBM-PC compatibles. By using gnuplot as our graphical display routine, we allow students to view plots on any IBM-PC with a standard graphics adapter and prepare publication quality graphics on any of the devices supported by gnuplot.
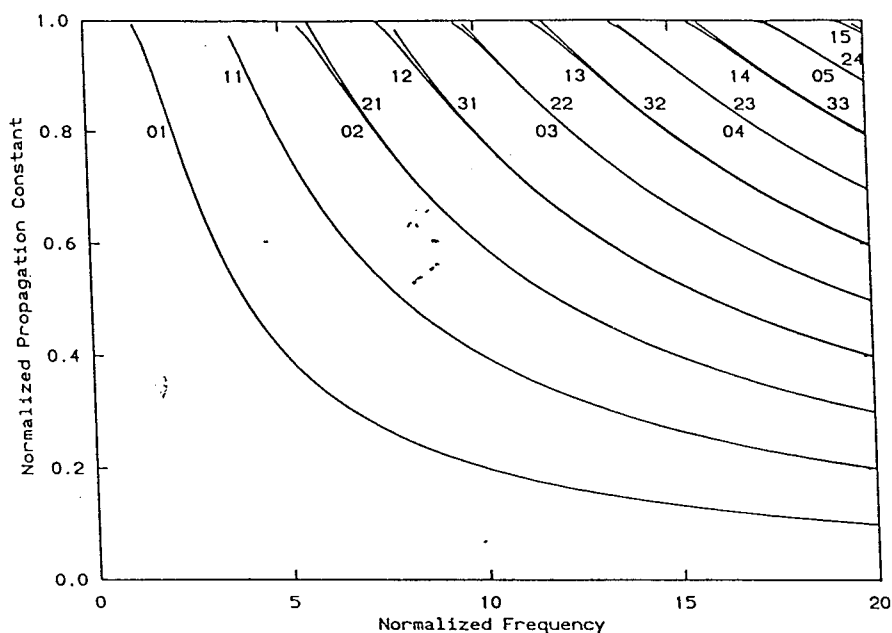
Figure 5   Normalized propagation constant vs. normalized frequency for a parabolic index fiber ($\alpha = 2$, $\rho = 1$, $\Delta = 0.038$). $R_{\text{fiber}} = 10 R_{\text{core}}$ and $N_c = 32$.

Using our suite of computer codes, students can compute dispersion characteristics and field patterns for a variety of refractive index profiles in one session. The computations and graphs can be printed and compared, facilitating an understanding of the effect on propagation of varying fiber parameters.

Due to the nature of solutions that can be computed directly from the scalar Helmholtz wave equation, the field patterns generated by our system are limited to showing the radial variations of each mode. Students may determine the angular variation of a field pattern by relating the LP_{ml} mode desig-
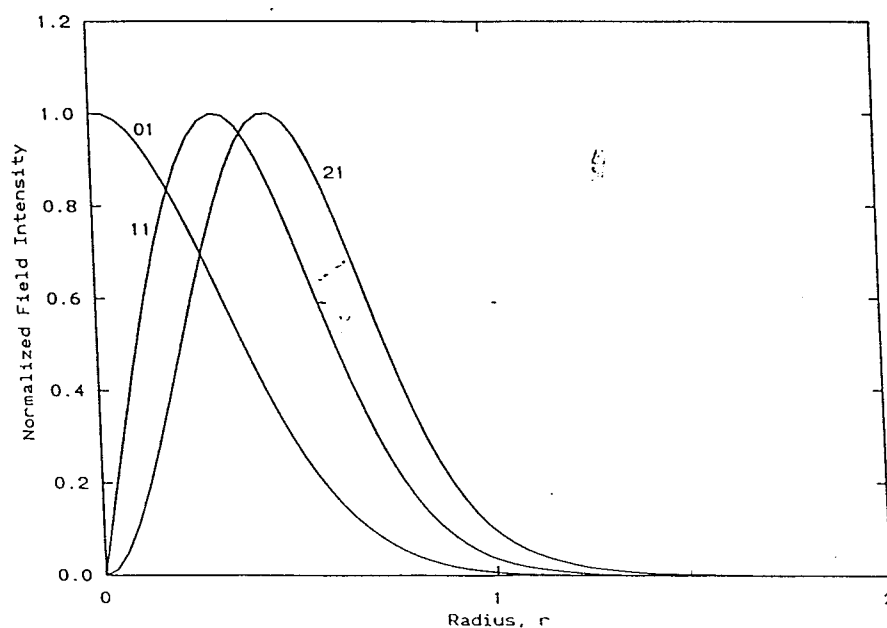

Figure 6   Field patterns for modes LP_{01}, LP_{11}, and LP_{21} of a parabolic index fiber ($\alpha = \infty$, $\rho = 1$, $\Delta = 0.038$) at $V = 10$. $R_{\text{fiber}} = 10 R_{\text{core}}$ and $N_c = 32$.

nations to TE, TM, HE, and EH mode designations as described in the introduction, and noting that there are $2m$ field maxima around the fiber circumference and l field maxima along the fiber radius [3]. A further release of our software will include modules designed to aid in the construction of full 2-D field patterns.

Two factors have a major influence on the results of our computations: the number of grid points used across the fiber (which we specify as the number of points in the core of the fiber), and the width of the cladding. For modes with low cutoff frequencies, variations in cladding width produce large changes in the calculated cutoff frequency, V_c. Cutoff frequency increases as the cladding width decreases. This is the expected behavior. The fundamental mode, which has no cutoff frequency when the cladding is infinite, shows a definite cutoff in real fiber.

The number of grid points across the fiber affects the accuracy of the finite difference approximations used in computing solutions to the wave equation. In general, a coarse grid results in an apparent shift of all propagation constants that increases with frequency. In our experience, 16 points in the core are sufficient for normalized frequencies below 10. N_c = 128 is sufficient for most cases of interest, but will run slowly even on a '486 based computer.

CONCLUSIONS

We have developed an integrated set of computer codes to evaluate propagation constants and field patterns of modes by transforming the scalar wave equation into a set of finite difference equations and then converting into a matrix eigenvalue problem. Our computer codes are fast enough to run on an IBM-PC with a numeric coprocessor, are accurate, and provide a convenient system with which students can explore propagation in optical fibers.

ACKNOWLEDGMENTS

REFERENCES

[1] T. Okoshi, *Optical Fibers*. Academic Press, New York, 1977.

[2] S. I. Hosain, I. C. Goyal, and A. K. Ghatak, "Accuracy of scalar approximation for single-mode fibers," *Optics Commun.*, Vol. 47, 1973, pp. 313–316.

[3] J. Senior, *Optical Fiber Communications: Principles and Practice*. Prentice-Hall, London, 1985.

[4] T. Moore, J. Blaschak, A. Taflove, and G. Kriegsmann, "Theory and application of radiation boundary operators," *IEEE Trans. Ant. Prop.*, Vol. AP-36, 1988, pp. 1797–1811.

[5] G. Strang, *Linear Algebra and Its Applications*. Academic Press, New York, 1976.

[6] J. H. Wilkinson, *The Algebraic Eigenvalue Problem*. Oxford University Press, 1965.

[7] W. H. Press, B. P. Flannery, S. A. Teukolsky, and W. T. Vetterling, *Numerical Recipes in C*. Cambridge University Press, New York, 1988.

[8] C. C. Su and C. H. Shen, "Calculation of propagation constants and cutoff frequencies of radially inhomogeneous optical fibers," *IEEE Trans. Microwave Theory Tech.*, Vol. MTT-34, 1986, pp. 328–332.

[9] K. Okamoto and T. Okoshi, "Analysis of wave propagation in optical fibers having core with alpha-power refractive-index distribution and uniform cladding," *IEEE Trans. Microwave Theory Tech.*, Vol. MTT-24, 1976, pp. 416–421.

[10] T. I. Lukowski and F. P. Kapron, "Parabolic fiber cutoffs: A comparison of theories," *J. Opt. Soc. Amer.*, Vol. 67, 1977, pp. 1185–1187.

[11] E. K. Sharma, I. C. Goyal, and A. K. Ghatak, "Calculation of cutoff frequencies in optical fibers for arbitrary profiles using the matrix method," *IEEE J. Quantum Electron.*, Vol. QE-17, 1970, pp. 2317–2321.

[12] C. C. Su, "Eigenproblems of radially inhomogeneous optical fibers from the scalar formulation," *IEEE J. Quant. Electron.*, Vol. QE-21, 1985, pp. 1554–1557.

BIOGRAPHIES

Gregory H. Aicklen (Member, IEEE) was born in 1958 in Baton Rouge, Louisiana. He received the B.S. degree in electrical engineering and the B.S. degree in computer science from Tulane University in New Orleans, Louisiana, in 1980. In 1991, he received the M.S. degree in electrical engineering from The University of Texas at Dallas in Richardson. Mr. Aicklen is currently in the Ph.D. program in the Erik Jonsson School of Engineering and Computer Science at The University of Texas at Dallas.

Prior to returning to graduate study in 1987, Mr. Aicklen had industrial experience with the Defense Systems and Electronics Group at Texas Instruments in Dallas. In 1985, he left Texas Instruments to pursue a private venture. In 1987 he joined the staff of The University of Texas at Dallas as a research associate in the Erik Jonsson School of Engineering and Computer Science.

Mr. Aicklen's research interests include fiber optics, nonlinear guided wave optics, integrated optical devices, and numerical methods in optics.

Lakshman S. Tamil (Member, IEEE) was born on July 24, 1960, in Tamilnadu, India. He received the B.E. degree in electronics and communication engineering from the Madurai Kamaraj University, Madurai, India, in 1981, and the M. Tech degree in microwave and optical communication engineering from the Indian Institute of Technology, Kharagpur, India, in 1983. He also received the M.S. degree in mathematics and the Ph.D. degree in electrical engineering from the University of Rhode Island, Kingston, in 1988. Since 1988 he has been with the University of Texas at Dallas in Richardson as an assistant professor of electrical engineering. He is also a member of the Center for Applied Optics in the same university. His research interests include fiber optics, photonic integrated devices and circuits, nonlinear guided wave optics, semiconductor lasers, inverse scattering theory, and numerical methods applied to electromagnetic problems.

Dr. Tamil is a member of Sigma Xi, Optical Society of America, Electromagnetics Academy, and is a elected member of Commission B and D of the International Union of Radio Science.